DISSERTATION

MULTI-OMIC APPROACHES TO INVESTIGATE MEAT QUALITY VARIATION

Submitted by

Chaoyu Zhai

Department of Animal Sciences

In partial fulfillment of the requirements

For the Degree of Doctor of Philosophy

Colorado State University

Fort Collins, Colorado

Summer 2022

Doctoral Committee:

Advisor: Mahesh N. Nair

Jessica E. Prenni
Adam J. Chicco
Keith E. Belk

ABSTRACT

MULTI-OMIC APPROACHES TO INVESTIGATE MEAT QUALITY VARIATION

Variation in the proteome profile of *longissimus lumborum* (LL) and *psoas major* (PM) post-rigor influences meat quality attributes such as tenderness and color stability during retail display. Tandem mass tag (TMT) labeling is a chemical labeling approach using isobaric mass tags for accurate mass spectrometry-based quantification and identification of biological macromolecules. The objective of first study was to use TMT labeling to examine proteome profile variation between beef LL and PM during the early postmortem period (45 min, 12 h, and 36 h). We identified a total of 629 proteins, of which 71 were differentially abundant (fold change > 1.5, $P < .05$) from three comparisons between the muscles (PM vs. LL at 45 min, 12 h and 36 h). These proteins were mainly involved in oxidative phosphorylation and ATP-related transport, tricarboxylic acid cycle, NADPH regeneration, fatty acid degradation, muscle contraction, calcium signaling, chaperone activity, oxygen transport, as well as degradation of the extracellular matrix. At early postmortem, more abundant antiapoptotic proteins in LL could cause high metabolic stability, enhanced autophagy, and delayed apoptosis, while overabundant metabolic enzymes and pro-apoptotic proteins in PM could accelerate the generation of reactive oxygen species and initiation of cell death.

Pulmonary hypertension is a noninfectious disease of cattle at altitudes > 1524 m (5,000 ft). Mean pulmonary arterial pressures (PAP) are used as an indicator for pulmonary hypertension in cattle. High PAP cattle (≥50 mmHg) entering the feedlot at moderate elevations have lower feed efficiency as compared to low PAP cattle (< 50 mmHg). In second study, the impact of

pulmonary arterial pressure on mitochondrial function, oxidative phosphorylation (OXPHOS) protein abundance, and meat color was examined using LL from high (98 ± 13 mmHg; n = 5) and low (41 ± 3 mmHg; n = 6) PAP fattened Angus steers (live weight of 588 ± 38 kg) during early postmortem period (2 and 48 h) and retail display (days 1 to 9), respectively. High PAP muscle had greater (P = 0.013) OXPHOS-linked respiration and proton leak-associated respiration than low PAP muscles at 2 h postmortem but rapidly declined to be similar (P = 0.145) to low PAP muscle by 48 h postmortem. OXPHOS protein expression was higher (P = 0.045) in low PAP than high PAP muscle. During retail display, redness, chroma, hue, ratio of reflectance at 630 and 580 nm, and metmyoglobin reducing activity decreased faster (P < 0.05) in high PAP steaks than low PAP. Lipid oxidation significantly increased (P < 0.05) in high PAP steaks but not (P > 0.05) in low PAP. The results indicated that high PAP caused a lower OXPHOS efficiency and greater fuel oxidation rates under conditions of low ATP demand in premortem beef LL muscle; this could explain the lower feed efficiency in high PAP feedlot cattle compared to low PAP counterparts. Mitochondrial integral function (membrane integrity or/and protein function) declined faster in high PAP than low PAP muscle at early postmortem. LL steaks from high PAP animals had lower color stability than those from the low PAP animals during simulated retail display, which could be partially attributed to the loss of muscle mitochondrial function at early postmortem by ROS damage in high PAP muscle.

Rapid Evaporative Ionization Mass Spectrometry (REIMS) is a type of ambient ionization mass spectrometry, which enables real-time evaluation of several complex traits from a single measurement. The objectives of third study were (1) to investigate the capability of REIMS to accurately identify and predict cooked sheep meat flavor and carcass characteristics based on consumer response utilizing metabolomic data acquired from different types of raw sample by I-

Knife and (2) to compare the data generated by these two electrodes (Meat Probe vs. I-Knife) in their ability to differentiate carcass background and sheep meat flavor. Current study demonstrated that REIMS analysis of raw meat samples can be used to accurately predict and classify cooked sheep meat flavor and carcass characteristics (based on consumer response). Specifically, the lean and fat tissue collected at 45 min postmortem can be used to predict carcass characteristics and post rigor meat flavor. Models for diet, flavor intensity acceptance, off flavors presence, overall acceptance, age, and flavor acceptance achieved prediction accuracies higher than 80%. In addition, data generated using the Meat Probe resulted in models with better or similar prediction accuracies of carcass background (age, diet, and gender) and consumer preference (intensity acceptance, flavor acceptance, off flavors presence, and overall acceptance) as compared to models based on data generated using the I-Knife. The Meat Probe was more user-friendly, faster, and cleaner than I-Knife for REIMS analysis. Further investigations are necessary to evaluate the use of the Meat Probe for REIMS analysis in other applications.

ACKNOWLEDGEMENTS

Many people helped, supported, mentored, and advised me to complete my Ph.D. program. I feel lucky to have these people in my life, and I want to thank these individuals in this acknowledgment section.

I firstly thank my committee members, Dr. Adam Chicco, Dr. Jessica Prenni, Dr. Keith Belk, and my advisor, Dr. Mahesh Nair. I thank my committee members for agreeing to advise me through my Ph.D. program. They supported me with their patience, sincerity, knowledge, and resource. They always trusted me as a person, and they challenged me to be a better scientist. I enjoy every single conversion with them because they always inspire me. My committee members showed me how to complete an interdisciplinary collaboration project with team spirit and individual expertise. I feel fortunate to be advised by these distinguished researchers. I also thank my Ph.D. advisor, Dr. Mahesh Nair, for taking me as his first student and advising me to grow from a graduate student to an independent researcher. During this four-year program, he gave me time to learn, chances to try, space to grow, and freedom to create. His awesome personality and excellent research philosophy benefit me with fantastic opportunities to lead projects and work with other brilliant researchers. To me, Mahesh is the best advisor in this world. I am proud to be his first student. As my friend, he treated me with respect, humor, equality, and honesty. I believe we will play an important role in each other's careers and support each other to be successful.

In addition, I thank my M.S. advisors and mentors in my seven-year graduate school life. I thank Dr. Xin Luo for accepting me as a M.S. student at Shandong Agricultural University and bringing me into meat science. He is the person who educated me and helped me mold my creativity in the scientific world. Dr. Luo always encourages his students to challenge the

conventional theories and supports them in developing leadership. His international research collaborations expanded my vision and allowed my subsequent study abroad. I also thank Dr. Surendranath Suman for accepting me as a visiting student in his lab. Dr. Suman systemically trained me with lab and writing skills, and I failed in love with proteomic research due to my research experience in his lab. His patience and encouragement shaped my decision to pursue further education to become a meat scientist. Likewise, I thank Dr. Steven Lonergan, Dr. Elisabeth Huff-Lonergan, and Dr. Ranjith Ramanathan for being my great mentors in both the professional and academic worlds. As a younger meat scientist who grew up reading their publications, I feel incredibly honored to work with and learn from them. Their mentorship encourages me to explore unknown knowledge and create novel research hypotheses. Furthermore, I thank Dr. Gina Geornaras, Dr. Robert Delmore, and Dr. Brad Morgan for teaching me how to work outside the chemistry lab, training me on how to present scientific research to general audiences, and directing me on how to answer a research question from a practical standpoint. Their guidance has helped me prepare myself with the comprehensive skills needed for my future career.

Further, I must thank my family for their tremendous love and support throughout my life. My wife, Mingyue Zhang, has always been my biggest supporter since the day we fell in love with each other. We have always been helping each other to be better people and better scientists every day. Being with her and having her in my life is the highest achievement I can ever complete. My parents instilled in me the meaning of hard work, determination, honesty, and humility. I pride myself on achieving such attributes in everything I do. I am proud of being the son of them throughout my life.

Finally, I must thank my dear friends at Colorado State University. I thank Tyler Thompson, Sara Gonzalez, Nathan Frazier, Tianqing (Sunny) Liu, Ashley Corona, Michael Hernandez, Caleb

Swing, Colton Smith, David Velazco, Aeriel Belk, Maggie Weinroth, Arquimides Reyes, Mo Jia, Haley Davis, and Hayden Blumberg for supporting me with our friendship. Having these wonderful human beings as my friends is a great treasure in my life. I also thank my lovely officemates, Paxton Sullivan, Melissa Davis, Lily Keogh, Hailey Simpson, Corley Rogers, Emma Briggs, Miguel Sanchez, Kaysie Jennings, Caleb Hurst, Jarrett Douglas, Chris Poppy, and Hannah Cochran for sharing coffee and pleasant chat with me. There are also a lot of other graduate students who helped me with my research projects, and I appreciate their help.

All the people mentioned above contributed to my Ph.D. competence, and I thank them for their hard work and kind help!

TABLE OF CONTENTS

LIST OF TABLES

LIST OF FIGURES

CHAPTER 1 – REVIEW OF LITERATURE

1.1 Application of proteomic tools in meat quality evaluation

1.1.1 Introduction

Meat quality attributes such as color, tenderness, and juiciness are highly variable and are often dictated by the functionality of proteins present in meat. Quality defects and inconsistencies in quality are major challenges for the meat industry. Although extensively researched, some of the fundamental mechanisms contributing to these quality differences are not completely understood, and developing a clear understanding of these processes at a biochemical and molecular level is critical to improving meat quality consistently.

Proteins constitute around 20% of meat and serve as a connection between the genetic profile of the animals and meat quality. In general, meat proteins could be categorized into three broad categories based on their solubility, namely (1) sarcoplasmic, (2) myofibrillar, and (3) stromal (connective tissue) proteins. Among these groups, sarcoplasmic proteins are located in the sarcoplasm (cytoplasm) of the muscle cells and constitute about 25%-30% of the total muscle proteins. These proteins are water-soluble and are generally globular proteins. There are hundreds of proteins present in the sarcoplasm, and their functionalities can influence the meat quality. For example, the glycolytic enzymes present in the sarcoplasm can influence postmortem metabolism, which in turn can influence meat quality. Myoglobin is another sarcoplasmic protein that critically influences meat quality, especially meat color. Although the physiological function of myoglobin is to store oxygen for muscle metabolism, the redox chemistry of myoglobin postmortem determines meat color.

Myofibrillar proteins constitute around 50%-60% of total meat proteins and are salt soluble. They are largely responsible for textural and structural properties of meat and meat products. Myosin (thick filament) and actin (thin filament) are two major myofibrillar proteins that play a critical role in the process of muscle contraction and postmortem rigor. These proteins dictate functionalities such as gelation and emulsification during meat processing. Stromal proteins are typically insoluble in water and require a strong acid/alkali solution for solubilizing them (e.g., collagen, elastin, reticulin). They are part of the extracellular matrix that provides structure and organization to the muscles. However, stromal proteins can critically influence meat quality parameters, particularly meat tenderness. Among the stromal proteins, collagen has been studied extensively in relation to meat tenderness. The large number and varied nature of the meat proteins make it challenging to examine the interactions between them using traditional meat quality analysis approaches. Moreover, the protein profile could be very dynamic in comparison to the static genome. Hence the application of novel tools such as proteomics has gathered a lot of interest from the meat scientific community in the past decade. This section will focus on some of the commonly used proteomic tools and their applications for meat quality evaluation.

1.1.2 Proteomics

The term "proteome" is defined as the protein complement of the genome comprising the total amount of proteins expressed at a certain time point in an animal (Wilkins et al., 1996). Proteomics is the systematic analyses of the proteome, which could include protein identification, quantification, and functional characterization (Liebler, 2002). When compared to the static genome, the proteome is dynamic and influenced by various factors related to protein synthesis or degradation. In eukaryotes, the alternative splicing of genes and various posttranslational

modifications (PTMs) that a protein undergoes, like acetylation, phosphorylation, and glycosylation, result in the proteome being larger than the genome.

From a meat science perspective the proteome can be considered as the molecular linkage between the genome and meat quality traits (Hollung et al., 2007). Although cutting-edge tools in mass spectrometry and proteomics have been extensively utilized in many disciplines within agricultural sciences, the application of proteomics in meat research grew significantly only in the last decade as it enables researchers to investigate postmortem protein changes at a molecular level. Chromatography-based techniques such as ion-exchange chromatography, size exclusion chromatography, and affinity chromatography are conventionally used in the purification of proteins, whereas techniques such as enzyme-linked immunosorbent assay and Western blotting are used for the analysis of selective proteins (not discussed in this section). These techniques are restricted to the analysis of few individual proteins and might be poor in defining protein expression levels. However, proteomics enables the characterization of hundreds of proteins in a single analysis by identifying cleavage sites and protein modifications such as protein oxidation and phosphorylation. Since proteins are effectors of biological function whose levels are not only dependent on corresponding mRNA levels but also on host translational control and regulation, proteomics could be considered as the most relevant data set to characterize a biological system (Huang and Lametsch, 2013).

The proteomic approaches can be broadly classified into two categories: (1) gel-based approaches, and (2) gel-free approaches. Each of these approaches will be discussed briefly in this section, whereas Baggerman et al., (2005) have comprehensively reviewed the topic.

1.1.2.1 Gel-based approaches

Sodium dodecyl sulfate-polyacrylamide gel electrophoresis (SDS-PAGE), often referred to simply as one-dimensional electrophoresis (1-DE), is a technique for the separation of proteins according to their size, which enables approximation of the molecular weight. Proteins are neutrally charged at their isoelectric point (pI). When an electric field is applied in a medium having pH different from their pI, the proteins migrate on the gels (usually on polyacrylamide gels) and form bands, which are then visualized through staining techniques. The rate/velocity of migration depends on the ratio between the protein's charge and mass. However, the addition of sodium dodecyl sulfate denatures the proteins and therefore separates them absolutely according to molecular weight (Aslam et al., 2017). Although 1-DE is very useful for the separation of proteins at a higher level, the resolution of the gels is very low, with the possibility of multiple proteins with similar molecular weight appearing in a single protein band.

The two-dimensional PAGE often referred to simply as two-dimensional electrophoresis (2-DE), enables the separation of proteins by their mass and charge. The 2-DE is capable of resolving ~5000 different proteins successively, depending on the size of the gel. In this technique, proteins are separated by charge (pI) by isoelectric focusing in the first dimension, and then according to their molecular weight in the second dimension. Since these two parameters are unrelated, an almost uniform distribution of protein spots can be obtained across a two-dimensional gel, and the resulting map of protein spots can be considered as the protein fingerprint of that sample. As in SDS-PAGE gels, the protein spots are visualized through staining methods. The most popular protein staining method is using Coomassie blue, as it is inexpensive, easy to use, and has a wide linear range that makes relative quantification easy. Moreover, Coomassie staining is compatible with downstream analysis by mass spectrometry. However, due to its

medium sensitivity, not all proteins can be visualized by Coomassie blue. Another option is to use silver staining which has a 20-50 times higher detection limit (highest sensitivity). The disadvantage of silver staining is that it is not very compatible with mass spectrometry and extensive destaining methods have to be used before the identification of the protein spot. Moreover, due to its limited dynamic range, the reproducibility of the spot intensities is low while using silver staining. This problem can be somewhat circumvented by differentially labeling different protein samples and separating them on the same gel.

One such method is the two-dimensional differential gel electrophoresis (2D-DIGE), which is performed by covalently tagging two protein samples (control and treatment) with two distinct N-hydroxysuccinamide derivatives with different fluorescent emission spectra, but identical masses and electrophoretic mobility. The labeled extracts are pooled and separated by 2-DE. An imager then scans the gel at the two Cy-dye emission wavelengths, and the image analysis software can identify spots of different intensity by superimposing the images. The major advantage of the 2D-DIGE is that it allows the comparison of two protein samples on the same gel. However, in larger studies where multiple conditions have to be compared, there could be issues with gel-to-gel variation. A novel approach of using a third dye was suggested by Alban et al. (2003) to solve this problem. These researchers used a third dye to label a third sample that will function as an internal standard. The standard sample comprises equal amounts of each sample to be compared. This standard is then mixed with two of the protein samples that have to be compared and subjected to 2-DE, which will enable the relative quantification easier.

However, 2-DE gels cannot visualize all proteins in a complex sample due to different technical limitations. A typical 2-DE gel can visualize only 30%-50% of the entire proteome (depending on the type of tissue), although some prefractionation methods can be used to

overcome this drawback to some extent. Especially, proteins present in extremely low concentrations or proteins that cannot be separated on 2-DE gels due to their physicochemical properties (molecular weight, pI, hydrophobicity) will not be typically detected in 2-DE gels. Proteins with high (> 150 kDa) and low (< 10 kDa) molecular weight, and proteins with extreme pIs are usually outside the detection limit in a standard 2-DE. Additionally, the hydrophobic proteins are not soluble in the typical buffers used for sample preparation or could precipitate during the electrophoretic process (Lescuyer et al., 2004). This means that the membrane proteins and small proteins (peptides) cannot be examined in most proteomic studies. Strong detergents that will disrupt the double layer of phospholipids and release the embedded hydrophobic protein can be used for extraction of the membrane proteins. However, these detergents are not compatible with the first dimension separation (isoelectric focusing) in 2-DE. Briefly, the 2-DE process is time-consuming, labor-intensive, and requires significant technical expertise to generate reproducible gels (Rabilloud, 2002). To overcome some of these challenges, several gel-free high-throughput technologies for proteome analysis have been developed in recent years.

1.1.2.2 Gel-free approaches

Instead of using gel-based approaches, multidimensional capillary liquid chromatography (LC) coupled to tandem mass spectrometry (MS/MS) can be used to separate and identify the peptides obtained from the enzymatic digest of an entire protein extract. This bottom-up (shotgun) proteomics technique (multidimensional protein identification technology; MudPIT) allows analysis of hydrophobic proteins as well as peptides. Basically, complex protein mixtures are digested to peptides using proteolytic enzymes, fractionated using chromatographic columns according to different chemical properties, and subsequently analyzed by MS/MS resulting in protein identification. Several drawbacks associated with 2-DE such as underrepresentation of

extreme acid/basic proteins and the poor sensitivity for lowly expressed proteins can be avoided through gel-free approaches. Moreover, the MudPIT method simplifies sample handling, avoids sample loss in the gel matrix and increases throughput and data acquisition (Bantscheff et al., 2007; Lewis et al., 2012). However, it is important to realize that proteins are not examined in their intact state, but instead as peptides obtained through proteolytic cleavage. Since it is easier to separate peptides by LC compared to proteins, a peptide-based proteomic analysis can be performed much faster and more cheaply than a gel-based analysis. Although the MudPIT technology is fast and sensitive with good reproducibility, it lacks the ability to provide quantification.

In gel-free proteomic approaches, there are two basic possibilities of quantification: (1) a relative quantification of proteins in compared samples (e.g., control vs. treatment) or (2) an absolute quantification (Yates et al., 2009). One of the most popular methods for relative quantification is stable isotope labeling of proteins in samples before analysis. Proteins are labeled with heavy isotopologues of C, H, N, or O through chemical derivatization processes before mass spectrometric (MS) analysis. Isotope-coded affinity tags (ICATs), dimethyl labeling, and isobaric mass tags are some of the common labeling techniques for protein quantification. Except for isobaric mass tags, stable isotope derivatization methods introduce a small mass difference to identical peptides from two or more samples which can be distinguished in the MS1 spectrum. The relative abundance ratios of peptides are measured by comparing heavy/light peptide pairs, and then protein levels are inferred from a statistical evaluation of the peptide ratios.

The ICAT reagents generally comprise an affinity tag for the isolation of labeled peptides, an isotopically coded linker, and a reactive group (Shiio and Aebersold, 2006). In an ICAT experiment, either light or heavy ICAT reagents are used to label protein samples. The mixtures of labeled proteins are then digested by trypsin and separated through a multistep chromatographic

separation, which can be then identified with MS/MS. Integrated LC peak areas of the heavy and light versions of the ICAT-labeled peptides can be then used to infer the relative quantities of the peptide. Stable isotopic labeling with amino acids in cell culture (SILAC) is another gel-free mass spectrometry-based approach for quantitative proteomics. The whole proteome of different cells grown in cell culture are labeled with light or heavy forms of amino acids (metabolic labeling) and are differentiated through mass spectrometry. The SILAC was primarily developed as a technique to study the regulation of gene expression, cell signaling, and PTMs, but is not widely used for meat science applications.

Isobaric tag for relative and absolute quantitation (iTRAQ) is also a gel-free multiplex protein labeling technique for protein quantification based on tandem mass spectrometry. In iTRAQ, each sample is derivatized with a different isotopic variant of an isobaric mass tag, and then the samples are pooled and analyzed simultaneously in the mass spectrometer. The N-terminus and side chain amine groups of proteins are usually labeled and are fractionated through LC columns before mass spectrometric analysis. The iTRAQ method has several advantages such as the ability to multiplex several samples, easier quantification, simplified analysis, and increased analytical precision and accuracy (Aggarwal et al., 2006; Zieske, 2006; Lund et al., 2007). Since the tags are isobaric, the differentially labeled peptides appear as a single composite peak at the same m/z value in the MS1 scan. When the iTRAQ tagged peptides are subjected to MS/MS it generates two types of product ions: (1) reporter ion peaks and (2) peptide fragment ion peaks. The reporter ions provide relative quantitative information of proteins, whereas the original peptide fragments are used to obtain the identity of the proteins. The quantification is accomplished by directly correlating the relative intensity of reporter ions to that of the peptide selected for MS/MS fragmentation. Since every tryptic peptide can be labeled in an isobaric labeling method, more

than one peptide representing the same protein could be identified, which in turn increases the confidence in both the identification and quantification of the protein (Rauniyar and Yates, 2014). Additionally, techniques such as Edman degradation can be used to determine the amino acid sequence of a particular protein (Smith, 2001). X-ray crystallography and nuclear magnetic resonance spectroscopy are also major high-throughput techniques that provide three-dimensional structure of a protein that might be helpful to understand its biological function (Smyth and Martin, 2000).

1.1.3 Proteomic approaches to meat quality

Proteomic tools can be applied to investigate preharvest as well as postharvest aspects of meat production (Bendixen, 2005; Mullen et al., 2006). Preharvest applications explain the biochemistry of food animal growth (Doherty et al., 2004) and muscle biology (Okumura et al., 2005), whereas postharvest aspects primarily focus on the fundamental aspects of meat quality, such as color (Nair et al., 2017), tenderness (Picard and Gagaoua, 2017), and water-holding capacity (WHC; Di Luca et al., 2011)

1.1.3.1 Meat color

Meat color is an important quality attribute that critically influences consumer purchase decisions. As mentioned earlier in this section, sarcoplasmic proteins in meat play a critical role in meat color, especially through the interactions with myoglobin. The changes in the skeletal muscle proteome continue during the postmortem period (Hollung et al., 2007) and can critically influence meat color (Nair et al., 2018a, 2018b). Earlier meat color research using proteomic tools focused on the interaction between myoglobin and small biomolecules, especially the effect of lipid oxidation products on myoglobin redox chemistry using 4-hydroxy-2-nonenal (HNE) as a model aldehyde. This research demonstrated that the covalent modification of histidine residues (via

Michael addition) in myoglobins of horse (Faustman et al., 1999), pork (Lee et al., 2003), beef (Alderton et al., 2003), emu (Nair et al., 2014), and ostrich (Nair et al., 2014) by reactive aldehydes is responsible for lipid oxidation-induced meat discoloration. Further, Yin et al. (2011) compared lipid oxidation-induced oxidation in various livestock and poultry myoglobins. These authors reported that the effect of HNE on myoglobin oxidation was correlated with a number of histidine residues in myoglobins, with a greater oxidation rate observed in myoglobins containing a greater number of histidine residues.

Suman et al. (2006) reported mono- and di-adducts between HNE and beef myoglobin, whereas only monoadducts were present in pork myoglobin at typical meat conditions (pH 5.6, 4 °C). While tandem mass spectrometry revealed four histidine adduction sites (36, 81, 88, and 152) in beef myoglobin, only two histidines (24 and 36) were found to be adducted in pork myoglobin, which indicated that the effect of lipid oxidation on myoglobin redox stability and meat color are species-specific. Further studies (Suman et al., 2007) revealed that histidine 36 was preferentially adducted in pork myoglobin, whereas histidine 81 and 88 were the major sites of early HNE adduction in beef myoglobin. These authors also concluded that the preferential adduction of HNE at proximal histidine (93) observed exclusively in beef myoglobin was responsible for increased lipid oxidation-induced oxidation in beef myoglobin compared to pork myoglobin. These studies (Suman et al., 2006, 2007) also explained why vitamin E is effective in stabilizing color in beef, but not in pork.

Proteomic tools are also used to examine the fundamental basis of muscle-specificity in meat color. Joseph et al. (2012) compared the sarcoplasmic proteome of color-stable *longissimus lumborum* and color-labile *psoas major* using 2-DE and tandem mass spectrometry and reported differential abundance of several proteins, including metabolic enzymes, antioxidant proteins, and

chaperones. Further, Wu et al. (2015, 2016) reported differentially abundant sarcoplasmic proteins in *longissimus lumborum*, *psoas major*, and *semitendinosus* muscle from Luxi yellow cattle during postmortem storage for 0, 5, 10, and 15 days, indicating that the variation in the sarcoplasmic proteins contributes to the muscle-specificity in meat color. Clerens et al. (2016) performed proteomic and peptidomic analysis of four muscles (*semitendinosus*, *longissimus thoracis et lumborum*, *psoas major*, and *infraspinatus*) from New Zealand-raised Angus steers. Although the muscles exhibited similar 2-DE profile, there was significant intensity difference between many proteins, including hemoglobin subunit beta, carbonic anhydrase 3, triosephosphate isomerase, phosphoglycerate mutase 2, serum albumin, and β-enolase. Clerens et al. (2016) performed comprehensive proteome analysis of differentially color-stable beef muscles, *longissimus lumborum*, *psoas major*, *semitendinosus*, and *semimembranosus* during postmortem aging and reported significant changes in proteins associated with glycolysis and energy metabolism in relation to meat color. Yu et al. (2017) utilized label-free mass spectrometry to characterize the effect of postmortem storage time (0, 4, and 9 days) on the proteome changes of *semitendinosus* muscle in Holstein cattle, and correlations between differentially abundant proteins and meat color traits. A total of 118 proteins with significant changes (fold change > 1.5; $P < 0.05$) were identified by comparisons of day 4 versus day 0, day 9 versus day 0, and day 9 versus day 4. Bioinformatics analyses revealed that most of these proteins were involved in glycolysis and energy metabolism, electron-transfer processes, and antioxidative function, which implied an underlying connection between meat discoloration and these biological processes.

Beef *semimembranosus* is a large muscle in beef hindquarter that exhibits intramuscular differences in color stability and could be separated into the color-stable outside (OSM) and color-labile inside (ISM) regions. The variations in temperature decline and pH drop during carcass

chilling are considered to be partly responsible for this intramuscular color difference. Nair et al. (2016) investigated the proteome basis of the color difference between OSM and ISM steaks using 2-DE and tandem mass spectrometry which revealed that ISM steaks had a greater abundance of glycolytic enzymes (fructose-bisphosphate aldolase A, phosphoglycerate mutase 2, and β-enolase) than their OSM counterparts. A combination of rapid pH decline (due to possible rapid glycolysis as a result of increased enzyme levels) and the high temperature (due to the location within the carcass) in ISM during the immediate postmortem period could have an adverse effect on myoglobin redox stability (Faustman et al., 2010; Suman and Joseph, 2013), thus compromising the meat color stability.

Li et al. (2018) used TMT labeling in combination with TiO2 phosphopeptide enrichment to perform a quantitative analysis of protein phosphorylation in ovine *longissimus* muscles with different color stability. These researchers performed informatics analysis and reported that among the differentially phosphorylated proteins, 27 phosphoproteins were key color-related proteins, including glycolytic enzymes and myoglobin. Sayd et al. (2006) characterized the sarcoplasmic proteome of pale versus dark pork meat (*semimembranosus* muscle) using 2-DE and tandem mass spectrometry, along with the correlation of protein expression to color-related attributes. These researchers reported an overexpression of oxidative enzymes related to mitochondrial metabolism, hemoglobin, and chaperone/regulatory proteins in darker meat. On the other hand, the pale meat revealed greater expression of glycolytic enzymes and glutathione S-transferase. The authors correlated such differential abundance in porcine meat with faster postmortem metabolism, possibly with accelerated ATP depletion and subsequent pH decline, which could lead to protein denaturation and thereby resulting in discoloration.

1.1.3.2 Tenderness

Tenderness is an important quality attribute of meat, which is considered to be critical for consumer eating satisfaction and repurchase decisions. Postmortem degradation of several structural proteins has been implicated in the development of meat tenderness. However, the fundamental mechanisms for meat tenderization and biochemical basis of variation in tenderness are yet to be completely understood (Huff-Lonergan et al., 2010). Most proteomic studies on tenderness have been conducted by comparing extreme groups (tender vs. tough) using different proteomic methods.

Zapata et al. (2009) used SDS-PAGE and functional proteomics to associate electrophoretic bands from the myofibrillar proteins to meat tenderness to understand the mechanisms of beef tenderness. Six significant electrophoretic bands were identified by electrophoretic and statistical analysis and were sequenced by nano-LC-MS/MS. These authors reported that the shear values were associated with the structural proteins, myosin heavy chains, myosin light chains, actin, desmin, and tubulin or their fragments. Marino et al. (2015) investigated postmortem proteolysis in *psoas major*, *longissimus dorsi*, and *semitendinosus* muscle from Podolian young bulls aged 1, 7, 14, and 21 days using SDS-PAGE, Western blotting, and 2-DE. Throughout postmortem aging, some structural proteins changed in intensity in all the muscles analyzed. The blotting profile highlighted that desmin and troponin-T bands were affected by both muscle and aging effects. Moreover, postmortem aging of *semitendinosus* muscle did not result in the same improvement in tenderness observed in *longissimus* and *psoas muscles* during aging, which was supported by proteolysis analysis, particularly troponin-T degradation.

Proteome analysis of troponin-T degradation in beef *longissimus* muscle, utilizing 2-DE demonstrated that several troponin-T isoforms were fragmented by 14 days postmortem (Muroya

et al., 2007a). Further mass spectrometric analyses of peptides revealed that all the isoforms were cleaved exclusively at the glutamic acid-rich amino terminal region, and the troponin-T fragments yielded a conventional 30 kDa band in the gel which could be utilized as biomarkers for monitoring postmortem beef tenderization. Morzel et al. (2008) examined the proteome of *longissimus thoracis* of Blonde d'Aquitaine beef animals to identify early predictors of tenderness using 2-DE and LC-ESI-MS. Although succinate dehydrogenase was suggested as an excellent candidate protein for predicting initial and overall tenderness, HSP-27 (Heat Shock Protein-27 kDa) and its fragments correlated well with the sensory scores, indicating the possibility of HSP-27-related cellular mechanisms influencing tenderness as well as the suitability of HSP-27 as a potential marker for beef tenderness. Variations in tenderness of *longissimus thoracis* within Charolais young bulls were examined by Laville et al. (2009) utilizing proteome analyses of tough and tender muscles. Mass spectrometric analyses revealed the presence of a greater quantity of actin fragments and proteins from inner and outer mitochondrial membranes in the tender group on day 0 postmortem. Mitochondrial fragmentation occurs during apoptosis, and the findings of this study suggested a possible role for cell apoptotic process in meat tenderization. Muroya et al. (2007b) and Jia et al. (2009) utilized the 2D-DIGE approach to assess the changes in the myosin light chains of *longissimus* myofibril proteins during postmortem aging and for identification of protein markers of meat tenderness in *longissimus* muscle respectively.

iTRAQ and 2-DE were utilized by Bjarnadóttir et al. (2012) to find potential biomarkers for meat tenderness in bovine *longissimus thoracis* muscle and to compare the two methods. Although the overlap among significantly changed proteins was relatively low between iTRAQ and 2-DE analysis, certain proteins predicted to have the same function were found in both analyses and showed similar changes between the groups, such as structural proteins and proteins

related to apoptosis and energy metabolism. The iTRAQ approach was also utilized by Mao et al. (2016) for the identification of the differentially expressed proteins involved in intramuscular fat deposition.

The molecular basis of meat tenderization in pork during the first 72 hours postmortem was investigated by Lametsch et al. (2003) through proteome analyses using 2-DE. The researchers identified 27 proteins with pronounced changes, including fragments of actin, myosin heavy chain, titin, myosin light chain I, myosin light chain II, Cap Z, and cofilin. Statistical analysis revealed a significant correlation between myosin light chain II, and several actin and myosin heavy chain fragments with shear force (objective measurement of tenderness), indicating that postmortem degradation of actin and myosin heavy chain is critical in meat tenderization. Further research by Lametsch et al. (2004) characterized the proteolytic changes in pork myofibrils after incubation with μ-calpain at 4 C for 4 days using electrophoresis and mass spectrometry. In contrast to the previous reports, these authors suggested actin and myosin heavy chain as substrates for μ-calpain. Also, several proteins including desmin, troponin-T, tropomyosin α-1, thioredoxin, and Cap Z were degraded by μ-calpain.

One of the limitations of proteomic approaches for studying meat tenderness is the difficulty of extracting proteins from extracellular matrices that are not solubilized by typical buffers. Hence connective tissue proteins known to be important for meat tenderness are typically not considered in these studies. However, these approaches provide opportunities to study PTMs such as phosphorylation, glycosylation/glycation, oxidation, and ubiquitination. These PTMs play major roles in the postmortem process in muscle/meat science (Huang et al., 2011; D'Alessandro and Zolla, 2013). For example, phosphorylation is a reversible protein modification that can affect the protein structure and activity of many enzymes in vivo, and hence have a potential role in meat

tenderization through regulation of the activities of glycolytic enzymes. Muroya et al. (2007b) reported that myosin light chain (MyLC2) was doubly phosphorylated during rigor mortis in bovine *longissimus* muscle. Furthermore, the appearance of the doubly phosphorylated protein after 8 hours postmortem correlated with the fast phase of rigor mortis, suggesting its potential influence on muscle shortening.

1.1.3.3 Water-holding capacity

WHC refers to the ability of meat to hold on to water during the postmortem period and processing. It is not only important for visual and sensory acceptability and economic reasons, but also because of its role in molding muscle structure and the consequent effects on quality (Hughes et al., 2014).

Marcos and Mullen (2014) utilized 2-DE to examine the relationship between pressure-induced changes on individual proteins and quality parameters of bovine *longissimus thoracis* and reported that the solubilization of myofibrillar proteins and insolubilization of sarcoplasmic proteins due to pressure resulted in paler meat with decreased WHC. These results indicated that the sarcoplasmic proteins play a critical role in determining the WHC of meat. Similarly, other authors have highlighted the role of sarcoplasmic proteins such as aldehyde dehydrogenase, glycerol-3-P-dehydrogenase, protein DJ-1, serotransferrin, β-enolase, creatine kinase M-type, and heat shock protein 70 kDa on meat color (*L**; lightness) and drip loss (Hwang et al., 2004; Sayd et al., 2006; van de Wiel and Zhang, 2007; Kwasiborski et al., 2008).

Zuo et al. (2016) used proteomic tools to identify differentially expressed proteins during postmortem aging of yak *longissimus lumborum* muscle which was classified into high and low drip loss groups. Heat shock protein, myosin light chain, and triosephosphate isomerase were identified as differentially expressed between the groups. Further research by Zuo et al. (2018)

compared proteome profile of *longissimus thoracis* of yak classified into low cooking loss and high cooking loss (HCL) groups. The results showed that cooking loss could be attributed to structural proteins, metabolic enzymes, stress-related proteins, and transport protein. There was a greater expression in the level of desmin, troponin-T, and L-lactate dehydrogenase in the HCL group.

Di Luca et al. (2011) compared protein abundance of diverse WHC phenotypes in pork using SDS-PAGE across time-points postmortem and identified several significant associations between the protein/fragment band volumes and WHC. Their results indicated that proteins such as HSP-70 could have the potential for inclusion in biomarker panels for the early prediction of meat quality in an industrial setting. Further, Di Luca et al. (2016) used 2-D DIGE and mass spectrometry to investigate the changes in metabolic proteins that occur over 7 days (day 1, 3, and 7) of postmortem aging using centrifugal exudate from pigs with divergent WHC. These researchers used a machine-learning algorithm (L1-regularized logistic regression), to derive a model with the ability to discriminate between high and low drip phenotypes using a subset of 25 proteins with an accuracy of 63%.

Phongpa-Ngan et al. (2011) compared the *pectoralis* proteome of chicken with different growth rates and WHC within the same genotype. The differentially expressed proteins included creatine kinase, pyruvate kinase, triosephosphate isomerase, ubiquitin, heat shock proteins, as well as several structural and contractile proteins. Many of these proteins were proposed as markers of WHC and growth rate, demonstrating the potential of proteomics for the selection of quality and production traits. Further, Zhang et al. (2019b) used label-free quantitative mass spectrometry to understand the mechanisms underlying drip loss and to identify the protein markers associated with WHC of goose meat. They identified 21 differentially abundant proteins between high and

low drip loss groups, which generally fell into the structural proteins, metabolic enzymes, antioxidant enzymes, and stress response proteins.

Desai et al. (2016) examined the whole muscle proteome of normal and pale, soft, exudative (PSE) broiler breast meat and identified 15 differentially abundant proteins. Actin alpha, myosin heavy chain, phosphoglycerate kinase, creatine kinase M-type, β-enolase, carbonic anhydrase 2, proteasome subunit alpha, pyruvate kinase, and malate dehydrogenase were overabundant in PSE broiler breast, whereas phosphoglycerate mutase-1, α-enolase, ATP-dependent 6-phosphofructokinase, and fructose 1,6-bisphosphatase were overabundant in normal meat. These results indicated that the overabundance of proteins involved in glycolytic pathways, muscle contraction, proteolysis, ATP regeneration, and energy metabolism in PSE breast could be related to the quality differences between normal and PSE meat.

Woody breast is a quality defect in poultry breast that is characterized by hardened areas and pale ridge-like bulges at both the caudal and cranial regions of the breast, and can be classified as slight, moderate, and severe (Tijare et al., 2016). Proteomic tools were utilized to understand the biochemical basis of this quality defect (Cai et al., 2018). Whole muscle proteome analysis using 2-DE reported that eight proteins were differentially expressed between normal and woody breast meat samples, and indicated increased oxidative stress in woody breast meat when compared to normal meat.

In summary, Proteomic investigations have expanded the understanding of the cellular and biochemical mechanisms governing the quality of fresh muscle foods, and results of these studies will aid the food industry's efforts to engineer novel processing strategies to improve the quality of muscle foods. Furthermore, proteomics studies have implicated that biological functions such as apoptosis, oxidative stress, and autophagy play a critical role in postmortem metabolism and in

turn on meat quality. The technological advances in the field of mass spectrometry and the development of novel proteomic tools will further facilitate the application of these tools to address meat quality issues.

1.2 Application of metabolomic tools in meat quality evaluation

1.2.1 Introduction

The metabolome refers to the complete set of small-molecule (<1.5 kDa) metabolites (such as metabolic intermediates, hormones and other signaling molecules, and secondary metabolites) found within a biological sample, such as a single organism. Each type of cell and tissue has a unique metabolic 'fingerprint' that can reflect organ or tissue-specific information. Skeletal muscle characteristics are designed by a functionally cooperative set of genes specific to the spatiotemporal requirement in each muscle. The gene expression is further modulated at levels of transcription, post-transcription, translation, and protein modification during development, growth, and maturation stages of the muscle. Accordingly, muscle metabolites determine the physiological muscle characteristics and meat quality traits as the major phenotypic components. Likewise, metabolites in postmortem muscle can impact the meat quality attributes, such as meat color, tenderness, water-holding capacity, and flavor.

1.2.2 Metabolomics

Metabolomics is the analytical approach used to comprehensivly profile the total metabolites in a given organism or biological sample (Fiehn, 2002). As a relatively new omics technique, the methodology includes metabolite separation, detection, quantification, data analysis, and interpretation. The quantification of metabolites provides a real-time snapshot of reactions in a biological system. Metabolites can be identified by using a targeted and nontargeted approach. Currently, two major types of platforms, mass spectrometry (MS)-based (Junot et al., 2014) and

non-MS-based techniques such as nuclear magnetic resonance (Consonni and Cagliani, 2019), have been applied for metabolomic studies. This section will focus on MS-based metabolomic tools and their applications for meat quality evaluation and prediction.

The most common analytical platform used in metabolomics is liquid chromatography coupled to mass spectrometry (LC-MS). The type of LC separation can be optimized for the detection of different metabolite classes. For example, a non-polarC18 reverse-phase column is commonly used in liquid chromatography (LC) for separation of hydrophobic molecules, while a polar stationary phase, such as silica and amide, is used for separation of hydrophilic molecules. Separation can be further improved by using ultra-high-performance liquid chromatography (UPLC) systems. To enable detection by the MS, molecules must be ionized generally by electrospray ionization or atmospheric pressure chemical ionization following LC separation. There are many types of MS systems that vary in their sensitivity, accuracy and resolution. Time-of-flight (ToF) MS is a common platform used in metabolomics due to higher sensitivity, accuracy, rate of measurement, and mass and dynamic range for the acquisition of more metabolite information (Junot et al., 2014).

Gas chromatography coupled to mass spectrometry (GC–MS) has also been widely used for decades due to its established high-separation efficiency, selective and sensitive mass detection, and a optimal separation and detection of small polar and moderately non-polar compounds such as fatty acids and sugars. Volatile compounds can be analyzed directly by GC-MS while non-volatile compounds require derivatization of sample molecules to increase their volatility and thermal stability for analysis. Derivatization artifacts may be generated by decomposition of thermolabile molecules in GC. The molecules are ionized generally by electron ionization or chemical ionization following GC separation. Most MS systems coupled with GC are low

resolution single quadrupole mass spectrometers, although GC can be coupled to high resolution MS system such as time-of-flight or orbitrap.

The use of GC–MS and LC-MS for the assessment of meat quality and integrity has been established (Muroya et al., 2020; Zhang et al., 2021c). However, sample preparation is normally extensive and therefore requires more labor, which limits the applicability of these techniques outside of the laboratory environment. Furthermore, the chromatographic separation takes significant time which limits the throughput of these approaches. As a novel sample introduction method for mass spectrometry analysis that was originally designed for cancer surgery, Rapid Evaporative Ionization Mass Spectrometry (REIMS) has the potential for rapid on-line measurement of several complex traits from a single measurement. REIMS is an ambient pressure ionization technique that allows direct sampling of an unprocessed sample and detection of the mass spectral fingerprint of that sample within a few seconds. A sample aerosol is created by point heating of a sample (called a 'burn'), often using an electronic surgical knife or other ways of creating an aerosol such as a soldering iron or laser. The aerosol is pulled through tubing using a Venturi pump where part of the sample gas flow is diverted into a mass spectrometer via an impact heater. Current mass spectrometers that can have a REIMS interface include quadrupole-time of flight high resolution mass spectrometers and quadrupole-ion mobility-time of flight high resolution mass spectrometers.

In the case of measuring meat with REIMS, a small sample can be analyzed several times to get replicate measurements. The resulting smoke is introduced into the mass spectrometer where ionization occurs and results in a large 'peak' containing the molecular information detected. These 'molecular features' are a combination of both native compounds released during burning, products of heating, and adducts (molecular species combining during the ionization process). In

a typical meat sample, the number of molecular features is often between 2000 and 4000 depending on the instrument and operational parameters. These molecular features are acquired with high mass resolution which can be used to tentatively assign an identification based on accurate mass matching, though actual identification requires confirmation with other methodologies. Measurement time is as fast as 5 s/burn, during which the aerosol is generated, transferred into the mass spectrometer, detected, and signal returns to baseline before the next measurement.

1.2.3 Metabolomic approaches to meat quality

Metabolomic tools can be applied to investigate preharvest as well as postharvest aspects of meat production (Muroya et al., 2020; Ross et al., 2021; Zhang et al., 2021c). The studies using MS-based metabolomic tools to understand meat quality, such as meat color, tenderness, water-holding capacity, and flavor, are reviewed in this section.

1.2.3.1 Meat color

Subbaraj et al. (2016) used a hydrophilic interaction LC-MS to identify and compare polar metabolites between ovine meat samples that were exposed to different durations of aging, storage conditions, and display times to understand metabolome change during the discoloration process. The results indicated that compounds with known antioxidant properties (e.g., NADH, malic acid-borate complex, guanosine, and taurine) were found in higher levels in color stable samples.

Ma et al. (2017) compared the metabolome profile of differentially color-stable beef muscles, LL, PM, and SM muscle, during postmortem via LC-MS. The study reported that fatty-acetyl carnitines, carnosine and anserine were at a higher level in LL compared to SM and PM muscles. Similarly, Yu et al. (2019) utilized LC-MS/MS to detect energy metabolites in beef LL and PM muscles, and the differentially abundant metabolites between muscles were found to be

majorly involved in tricarboxylic acid (TCA) cycle, which distinguished metabolic patterns between these two muscles.

Ramanathan et al. (2020a) examined metabolomic difference between DFD and normal beef via GC-MS and reported a downregulation of glycolytic metabolites, such as glucose-6-phosphate, fructose-6-phosphate, and glucose-1-phosphate. This could explain the lower lactic acid formation during anaerobic metabolism and resultant high pH of dark-cutting beef. The TCA metabolites such as fumaric acid, citric acid, and malic acid were upregulated in dark-cutting beef, which in turn can promote mitochondrial activity and limit myoglobin oxygenation.

1.2.3.2 Tenderness and water holding capacity

D'Alessandro et al. (2012a) utilized LC-MS to investigate the metabolome profile in Chianina beef with different tenderness. Phosphocreatine/creatine and oxidized glutathione/reduced glutathione ratios were significantly higher in tender meat compared to tough meat. Glycolysis metabolic intermediates were also observed to accumulate more in tender than in tough meat. In particular, glyceraldehyde-3-phosphate (a product of GAPDH) showed a 2-fold increase in tender compared to tough meat. Likewise, a companion study conducted on meat with differing tenderness from Maremmana cattle, reported that phosphoenolpyruvate, glycerol 3-phosphate, lactate, NADH, NAD^+, and guanosine monophosphate (GMP) accumulated more in tender meat than in tough meat (D'Alessandro et al., 2012b).

Abasht et al. (2016) studied metabolome profile of chicken breast muscle affected with the Woody Breast, a myopathy having meat quality defects in tenderness, via GC/MS and LC-MS/MS. Affected muscle showed elevated levels of hypoxanthine, xanthine, and urate molecules, generation of which can contribute to altered redox homeostasis.

Boerboom et al., (2018) used both GC-MS and LC-MS to analyze the metabolomic profile of chicken breast muscle affected with white striping, a quality defect with lower water holding capacity, and their results indicated that C14:1 carnitine, taurine, sorbitol, taurine, alanine, and long-chain fatty acid were more abundant in the affected chicken breast. Based on these results, authors speculated that birds suffering from white striping have a vascular support system in muscle that is borderline adequate to support growth but inadequate to support muscle health under stress. Therefore, local hypoxia could happen and damage breast muscle tissue.

Przybylski et al. (2022) applied metabolomics analysis of exudate from chicken breast muscle to explain differences in drip loss. The results showed an increase in energy transformation metabolism in muscle tissue after slaughter in the group with higher drip loss. Also, the differences between groups were mainly related to carbohydrate metabolism (glycolysis, gluconeogenesis, pentose phosphate pathway), adenine and adenosine salvage, adenosine nucleotides degradation, arsenate detoxification, methylglyoxal degradation. More methylglyoxal (as a by-product of carbohydrate metabolism) was produced in the high drip loss group which may lead to changes in muscle proteins properties and contribute to an increase in the drip loss.

1.2.3.3 Flavor

Lee et al. (2011) examined volatile metabolites related to beef flavor by GC-MS. The relationship between volatile compounds and the sensory attributes of glutathione-Maillard reaction products prepared under different reaction conditions were examined. Specifically, 2-methylfuran-3-thiol, 3-sulfanylpentan-2-one, furan-2-ylmethanethiol, 2-propylpyrazine, 1-furan-2-ylpropan-2-one, 1H-pyrrole, 2-methylthiophene, and 2-(furan-2-ylmethyldisulfanylmethyl)furan were identified as potential compounds contributing to beef-related flavor. Similarly, Takakura et al. (2014) identified aroma-active compounds in the flavor

dilution factor range of 32–128 from commercial beef extract. Moreover, the study found that 2,3,5-trimethyl pyrazine, 1-octen-3-ol, 3-methylbutanoic acid, and 4-hydroxy-2,5-dimethyl-3(2H)-furanone were the main active compounds contributing to the aroma of commercial beef extract. In addition, Jiang and Bratcher (2016) utilized LC-MS to investigate the metabolites in ground beef associated with beef flavor or off-flavor. Twenty-two compounds, including 2,4-decadiynoic acid, 8,10-hexadecadienoic acid, 3α,11β, 21-5α-trihydroxy-pregnane-20-one, dihydroxy-docosapentaenoic acid isomers were selected as the most important ones associated with beef flavor and off-flavor.

Suzuki et al. (2017) investigated the chemical composition of sirloin beef via GC-MS which revealed that sugar content and ATP-related compounds in roasted meat were significantly correlated with 'overall evaluation' of the sensory panel. ATP-related compounds, such as inosinic acid, carnosine and taurine, in roasted and raw meat were positively correlated significantly 'umami intensity' of the sensory panel. These results suggest that the composition of these components is important for an index related to the overall evaluation of beef.

Watanabe et al., (2015) used solid-phase microextraction (SPME) to collect volatiles in the headspace of beef cooked at 180 °C after differing aging period. The volatile compounds collected on the SPME were then analyzed with GC-MS. Using a positive regression model, these researchers found the abundance of toluene, benzeneacetaldehyde, 2-formylfuran, pyrazine, 2,6-dimethylpyrazine, 2,3-dimethylpyrazine, 2-acetylthiazole, and 2-formyl-3-methylthiophene increased with aging time. Similarly, Sawano et al., (2020) used capillary electrophoresis-MS to characterize the pork metabolite changes resulting from cooking. Cooking treatment increased the levels of N-acetylornithine, ribulose 5-phosphate, N-acetyl lysine, N-acetylneuraminic acid, ATP, methionine sulfoxide, methionine, phenylalanine, tryptophan, and tyrosine but decreased the levels

of diethanolamine, iso-glutamic acid, succinic acid, glutamine, reduced glutathione, thiamine phosphate, gamma-aminobutyric acid, ethanolamine, putrescine, and ethanolamine phosphate compared with those in the four uncooked samples.

Tamura et al. (2022) investigated the role of taste-related metabolites in the aroma composition of roasted pork meat during postmortem aging. Metabolomic analyses of taste-related metabolites and volatile organic compounds in aged pork were conducted by GC-MS. Among the detected aroma compounds, benzeneacetaldehyde and 2,5-dimethyl-3-(3-methylbutyl)-pyrazine levels increased with aging period; these compounds potentially contribute to roasty and meaty aromas.

In summary, metabolomic investigations have expanded the understanding of the cellular and biochemical mechanisms governing the quality of fresh muscle foods, and the results of these studies will help the meat industry to improve the muscle food quality. The technological advances in the field of mass spectrometry and the development of novel metabolomic tools will further facilitate the application of these tools to address meat quality issues.

CHAPTER 2 – TANDEM MASS TAG LABELING TO CHARACTERIZE MUSCLE-SPECIFIC POTEOME CHANGES IN BEEF DUING EARLY POSTMORTEM PERIOD

2.1 Introduction

Meat quality attributes such as color, tenderness, and water holding capacity are highly influenced by the postmortem metabolism in muscles (Matarneh et al., 2017). These quality attributes significantly influence consumer purchase and repurchase decisions (Shackelford et al., 2001; Mancini and Hunt, 2005; Suman and Joseph, 2013; Neethling et al., 2017), and are economically significant for the meat industry (Smith et al., 2000; Lusk et al., 2001). Moreover, different muscles from the same animal can demonstrate significant differences in these quality attributes (Carmack et al., 1995; Belew et al., 2003; Melody et al., 2004; McKenna et al., 2005; Gruber et al., 2006; Seyfert et al., 2006). The variation in postmortem metabolism between muscles due to their location, physiological function, and muscle fiber characteristics could be the major factors contributing to their meat quality differences (Lefaucheur, 2010).

Longissimus lumborum (LL) and *psoas major* (PM) are two economically important bovine muscles that have been extensively researched to explore the fundamental and molecular basis of these quality differences (Hunt and Hedrick, 1977; Melody et al., 2004; Hwang et al., 2010). Among these muscles, LL has a higher proportion of type IIB (α-white) muscle fibers (Hunt and Hedrick, 1977; Ozawa et al., 2000; Hwang et al., 2010), whereas PM have more type I (β-red) muscle fibers (Hunt and Hedrick, 1977; Hwang et al., 2010). Type I fiber possesses greater glycolytic ability than type IIB fiber, but the trend is reversed when comparing their oxidative metabolism. Correspondingly, LL and PM show significant differences in tenderness (Carmack et al., 1995; Gruber et al., 2006), color stability (McKenna et al., 2005; Seyfert et al., 2006) and oxidative stability (Canto et al., 2016). Recent research indicated that the differences in

postmortem mitochondrial function (Mancini et al., 2018) and oxidative stress (Ke et al., 2017) could also contribute to the differential quality attributes between these muscles.

Muscle proteome profile analysis can provide the molecular linkage between the genome and phenotypic expression of meat quality traits (Hollung et al., 2007). In the past couple of decades, proteomic investigations have expanded our understanding of the cellular and biochemical mechanisms governing meat color (Nair et al., 2017) and tenderness (Picard and Gagaoua, 2017) as well as the food allergy through molecular characterization of food allergens (Marzano et al., 2020). Muscle specific protein level differences reflective of beef color have been examined via gel-based 2-dimensional electrophoresis (Joseph et al., 2012; Wu et al., 2016; Nair et al., 2018a) and label-free approaches (Yu et al., 2018). Moreover, various proteomic approaches have been utilized to identify biomarkers related to beef tenderness among different muscles (Guillemin et al., 2011a, 2011b; Anderson et al., 2012; Gagaoua et al., 2015a; Picard et al., 2018).

The conversion of muscle to meat occurs during the early postmortem period, primarily due to exsanguination, which is a short but intensive period accompanied by several changes in the muscle metabolism pathways (England et al., 2013; Matarneh et al., 2017). The postmortem period in muscle can also involve cell death processes (Herrera-Mendez et al., 2006; Ouali et al., 2006; Becila et al., 2010; Kemp and Parr, 2012; Sierra and Olivan, 2013; Lomiwes et al., 2014; Lana and Zolla, 2015; Longo et al., 2015; Huang et al., 2016), which, to the best of our knowledge, are controlled by cell metabolism (Green et al., 2014). These changes can play a critical role in the development of meat quality (Laville et al., 2009; Kemp and Parr, 2012; Sierra and Olivan, 2013; Chen et al., 2017). Due to differences in location, physiological function, and muscle fiber characteristics, we hypothesize that proteome changes during the early postmortem period will be muscle specific.

Tandem mass tag (TMT) labeling, a chemical labeling approach used for accurate mass spectrometry-based quantification and identification of biological macromolecules, is commonly applied to enable to investigation of biological pathways and cellular processes at the protein level using a shotgun approach (Churchman et al., 2015; Mertz et al., 2015; Wang et al., 2016b). Recently, the TMT strategy has been used in meat science research to investigate the postmortem process in ovine (Li et al., 2018) and porcine muscle (Liu et al., 2018). Here, we used a TMT labeling approach coupled with high resolution mass spectrometry to examine proteomic variation between beef LL and PM during the early postmortem period to explore the underlying biological pathways during the process of muscle to meat conversion.

2.2 Material and methods

2.2.1 Sample collection

In order to effectively simulate the commercial beef retail marketing conditions in the United States, ten grams of LL and PM muscle tissue from four carcasses (n = 4) were obtained from a commercial packing plant at the following time intervals points postharvest: (1) 45 min, (2) 12 h, and (3) 36 h post exsanguination, resulting in collection of a total of 24 samples (2 muscles of 4 animals at 3 different postmortem time points). The muscle samples were collected using a biopsy punch and were frozen immediately in liquid nitrogen until proteomic analyses.

2.2.2 Sample preparation

2.2.2.1 Protein extraction and quantification

Two hundred mg of frozen muscle tissue per sample was homogenized using the Bullet Blender 5 Storm (Next Advance). To each sample, 6 stainless steel beads and 500 µL lysis buffer (2.5% SDS, 1× HALT protease inhibitor, 75 mM triethyl ammonium bicarbonate; TEAB) were added. Lysis/homogenization were achieved using speed 10 for 3 min followed by speed 12 for 3

min. Two hundred and fifty µL additional lysis buffer was added to each sample followed by transfer to microcentrifuge tube. Bullet Blender tubes were rinsed with 500 µL lysis buffer which was subsequently transferred to the corresponding sample tube. Samples were incubated at 100 °C for 20 min. After cooling on ice, samples were centrifuged at 5000 ×g for 5 min to pellet intact cells and debris. Small aliquots were diluted 1:50 and measured for total protein content using the Pierce BCA Protein Assay Kit (Thermo Fisher Scientific; Waltham, MA) following the manufacturer instructions.

2.2.2.2 Protein reduction-alkylation and digestion

Preparation of all solutions and procedures were as described in the TMT 10-plex kit instructions (Thermo Fisher Scientific; Waltham, MA). A volume corresponding to 100 µg total protein from each sample was aliquoted and then raised to 100 µL total volume using 100 mM TEAB. Tris(2-carboxyethyl)phospine (TCEP) was added to 9.5 mM final concentration and incubated at 55 °C for an hour. Free cysteines were alkylated at room temperature using 17.9 mM final concentration iodoacetamide (IAM) for 30 min in the dark. Six volumes of ice-cold acetone were then added and protein were precipitated overnight at −80 °C. Precipitate was collected after centrifugation (8000 ×g, 4 °C, 10 min). Pellets were allowed to air dry under a sheet of foil, and then were reconstituted in 100 µL TEAB and digested with 2.5 µg Trypsin at 37 °C overnight.

2.2.2.3 Peptide labeling and cleanup

After digestion, absorbance at 205 nm was measured on a NanoDrop (Thermo Fisher Scientific; Waltham, MA). Total peptide concentration was calculated using an extinction coefficient of 31 (Scopes, 1974). 66.31 µg peptide from each sample was aliquoted and raised to 100 µL using TEAB. Samples were randomly assigned to one of 8 TMT labels spanning three TMT lab sets. One of the TMT labels in each set was used for a pooled QC which was generated

by combining equal protein amounts from all samples, and one of the TMT labels in each set was used for blank sample. All TMT label reagents were allowed to equilibrate to room temperature followed by addition of 41 µL LC-MS acetonitrile and occasional vortex over 5 min. 41 µL of TMT label was added to each sample and incubated at room temperature for 1 h. Quenching was achieved by addition of hydroxylamine (0.37% final) and 15 min additional incubation. Subsequently, samples were pooled into the 3 TMT sets. Pooled, labeled peptides were cleaned up using TT1000C18 Top- Tips (PolyLC; Columbia, MD) and centrifugated at 3000 rpm. Different solvents were used for activation (50% Acetonitrile [ACN]), equilibration and wash (5% ACN, 0.5% trifluoracetic acid [TFA]) and elution (70% ACN, 0.1% formic acid [FA]). Eluates were dried using a Savant speedvac and reconstituted in 66 µL 5% ACN, 0.1% FA.

2.2.2.4 Peptide fractionation

Ten µL of each set (90µg total peptide) was subjected to high pH fractionation through a Waters Acquity UPLC BEH C18, 1.7 µm column (held at 45 °C) using a Waters H-class UPLC. Mobile phase A consisted of 10 mM ammonium formate, pH 10, while B contained 90% ACN, 10% 10 mM ammonium formate, pH 10. Fractionation took place at 100 µL/min using the 30 min gradient. During peptide elution, a total of 48 fractions were collected in a linear fashion into four rows of a 96 well plate. Peptides eluting at varied portions of the gradient were pooled into 12 fractions (by pooling all samples in column 1, all samples in column 2, etc). Pooled fractions were dried in the Savant speedvac, reconstituted in 12 µL of 5% ACN, 0.1% FA, and quantified as described above using the NanoDrop.

2.2.3 Mass spectrometry analysis

The 12 fractions from each TMT set were block randomized and injected in a randomized set order. A total of 0.6 µg of peptides were purified and concentrated using an on-line enrichment

column (Waters Symmetry Trap C18 100 Å, 5 µm, 180 µm ID x 20 mm column). Subsequent chromatographic separation was performed at a flow rate of 350 nanoliters/min on a reverse phase nanospray column (Waters, Peptide BEH C18; 1.7 µm, 75 µm ID x 150 mm column, 45 °C) using a 55 min linear gradient from 5%–40% buffer B (100% ACN, 0.1% formic acid) followed by 40–85% buffer B over 7 min. Peptides were eluted into the mass spectrometer (Orbitrap Velos Pro, Thermo Fisher Scientific; Waltham, MA) equipped with a Nanospray Flex ion source and spectra were collected over a m/z range of 400–1500, positive mode ionization, using a dynamic exclusion limit of 1 MS/MS spectra of a given m/z value for 30 s (exclusion duration of 120 s). The instrument was operated in FT profile mode detection (resolution of 30,000) for both MS and MS/MS detection. Fragmentation was via HCD with a normalized collision energy set to 35%. Compound lists of the resulting spectra were generated using Xcalibur 3.0 software (Thermo Scientific) with a S/N threshold of 1.5 and 1 scan/group.

2.2.4 Data processing

Tandem mass spectra were extracted, charge state deconvoluted and deisotoped by ProteoWizard MsConvert (version 3.0). Spectra from all samples were searched using Mascot (Matrix Science, London, UK; version 2.6.0) against the Uniprot_Bovine_rev_020518 database (unknown version, 48,676 entries) assuming the digestion enzyme trypsin. Mascot search was performed with a fragment ion mass tolerance of 0.020 Da and a parent ion tolerance of 20 ppm. Oxidation of methionine, carbamidomethyl of cysteine and TMT6plex of lysine and the N-terminus were specified in Mascot as variable modifications.

Search results from each TMT set were subjected to MuDPIT, imported and combined using the probabilistic protein identification algorithms (Keller et al., 2002) implemented in the Scaffold software (version Scaffold_4.8.4, Proteome Software Inc., Portland, OR) (Searle et al.,

2008). Peptide thresholds were set such that a peptide FDR of 0.04% was achieved based on hits to the reverse database (Käll et al., 2008). Protein identifications were accepted if they could be established at greater than 99.0% probability and contained at least 2 identified peptides. Protein probabilities were assigned by the Protein Prophet algorithm (Nesvizhskii et al., 2003). Proteins that contained similar peptides and could not be differentiated based on MS/MS analysis alone were grouped to satisfy the principles of parsimony.

Channels were corrected using values supplied by Thermo Fisher Scientific (Lot SH255638) according to the algorithm described in Shadforth et al. (2005). Normalization was performed iteratively (across samples and spectra) on intensities, as described in (Oberg et al., 2008). Medians were used for averaging. Reporter ion intensities were log-transformed and then weighted by an adaptive intensity weighting algorithm. Results from peptide spectra that were assigned to multiple proteins as well as spectra missing a reference value were removed from the analysis.

2.2.5 Statistical analysis

Statistical analysis was performed with R 3.4.3 using the limma package (Ritchie et al., 2015). The identified proteins that had missing values for 12 or more (more than half the observations) were removed. A moderated t-test was used for pairwise comparisons between time points and muscles. Benjamini–Hochberg multiple testing adjustment was used to control the false discovery rate and control for multiple testing (Benjamini and Hochberg, 1995) at $P < 0.05$.

2.2.6 Bioinformatic analysis

An analysis of functional interactions between the identified proteins (Figure 2.2) was performed using String 11 (Szklarczyk et al., 2019), a software analyzing protein–protein association networks with timely updates and various bioinformatics information. The network

nodes are the proteins, and the edges represent the predicted functional associations. To group the proteins in the network based on their interactions from STRING, Markov clustering (MCL) was run with an inflation parameter 3.4 (Brohée and van Helden, 2006). The identified proteins were clustered mainly based on their function according to KEGG Pathway database (https://www.genome.jp/kegg/pathway.html) and Reactome Pathway database (https://reactome.org), and the proteins with limited description in the databases were further explored via literature search.

2.3 Results and discussion

Of 89,580 spectra in the experiment at the given thresholds, 67,643 (76%) were included in quantitation. In total, 629 proteins were confidently identified, of which 71 were found to be differentially abundant ($P < 0.05$) across muscle type and postmortem time period (PM 45 min vs. LL 45 min, PM 12 h vs. LL 12 h, and PM 36 h vs. LL 36 h). These proteins are detailed in Table 2.1 including their name, abbreviation (string code), accession number and differential abundance ratio (if it was significant). No differentially abundant proteins ($P > 0.05$) were detected within same muscle during different time points postmortem. Among the 71 differentially abundant proteins, 19 proteins were identified as different irrespective of the time postmortem (Figure 2.1). Specifically, there were 33, 42, and 50 differential proteins among comparisons between LL and PM at 45 min, 12 h, and 36 h respectively. The results of the Markov Cluster Algorithm clustering analysis (inflation parameter set as 3.4) of functional interactions between the identified proteins are shown in Figure 2.2.1, 2.2.2, and 2.2.3. The network nodes are the abbreviations of proteins, and the edges represent functional associations. The distribution of the functional clusters is presented in Figure 2.3.1, 2.3.2, and 2.3.3. The clustered functions were oxidative

phosphorylation/ATP-related transport, tricarboxylic acid (TCA) cycle/NADPH regeneration, fatty acid degradation, muscle contraction/calcium signaling, and a cluster for all other functions.

2.3.1 Proteomic comparison between LL and PM muscles during early postmortem

Among the differentially abundant proteins, those involved in oxidative phosphorylation, ATP-related transport, TCA cycle, NADPH regeneration, fatty acid degradation, oxygen transport, and degradation of the extracellular matrix were primarily more abundant in PM at different postmortem periods (Table 2.1) as compared to LL. A total of 6 proteins involved in muscle contraction and 3 proteins involved in calcium signaling were identified as differential at different postmortem time periods (Table 2.1). Among these, myosin light chain 6B (MYL6B), cysteine and glycine-rich protein 3 (CSRP3), protein S100-A2 (S100A2), ryanodine receptor 3 (RYR3), immunoglobulin-like and fibronectin type III domain containing 1 (IGFN1), and tropomyosin alpha-1 chain (TPM1 or ENSBTAG00000005373) were more abundant in LL, while sarcoplasmic reticulum calcium ATPase 2 (ATP2A2), myosin light chain 3 (MYL3), troponin I1 (slow skeletal type; TNNI1), and troponin T (slow skeletal muscle; TNNT1) were more abundant in PM. Three chaperone proteins showed differential abundances at different postmortem periods (Table 2.1) of which heat shock protein beta-6 (HSPB6) and peptidylprolyl cis-trans isomerase A (PPIA) were more abundant in LL, while mitochondrial 60 kDa heat shock protein (HSPD1) was more abundant in PM. Among proteins with other functions, peptidyl arginine deiminase 2 (PADI2), NADH-cytochrome b5 reductase (CYB5R3), cytoplasmic serine-tRNA ligase (SARS), and beta-enolase (ENO3) were more abundant in LL, while interleukin 31 receptor A (IL31RA), mitochondrial GTP:AMP phosphotransferase AK3 (AK3), mitochondrial ubiquinone biosynthesis protein COQ9 (COQ9), and histone-lysine N-methyltransferase 2D (KMT2D) were more abundant in PM. For

the ease of discussion, we have separated the proteins into different function clusters described below.

2.3.1.1. Oxidative phosphorylation enzymes and mitochondrial carrier proteins

Among the differentially identified proteins, nine proteins (Table 2.1) were components of mitochondrial complex I (NADH dehydrogenase), the first large protein complex of the respiratory chain, which catalyzes the transfer of electrons from NADH to coenzyme Q10 and translocates protons across the inner mitochondrial membrane. Two proteins identified (Table 2.1) at both 12 h and 36 h postmortem were components of mitochondrial complex II (succinate dehydrogenase), the only enzyme that participates in both the TCA cycle and the electron transport chain, which catalyzes the oxidation of succinate to fumarate with the reduction of ubiquinone to ubiquinol. Another four were a part of mitochondrial complex III (cytochrome bc1 complex; Table 2.1), which uses quinol and ferricytochrome c as substrates and produces quinone, ferrocytochrome c, and hydrogen ion. In addition, five differential proteins (Table 2.1) were components of complex IV (cytochrome c oxidase), which receives an electron from each of four cytochrome c molecules and transfers them to one dioxygen molecule, converting the molecular oxygen to two molecules of water. Seven differential proteins (Table 2.1) were components of complex V (ATP synthase). Among them, mitochondrial ATP synthase subunit alpha (ATP5A1) and mitochondrial ATP synthase subunit gamma (ATP5C1) were a part of F1 portion of ATP synthase, which is responsible for hydrolyzing ATP; while the rest of them (Table 2.1) belong to F0 portion containing the membrane proton channel. These results indicated that, overall, oxidative phosphorylation enzymes were more abundant in PM muscle as compared with LL throughout early postmortem. This result is consistent with previous reports that have demonstrated higher rates of mitochondrial oxygen consumption in PM as compared to LL during the postmortem

period (O'Keeffe and Hood, 1982; McKenna et al., 2005). Yu et al. also reported higher abundance of oxidative phosphorylation enzymes in PM (compared to an LL; Yu et al., 2017b, 2018).

Phosphate carrier protein (SLC25A3) and ADP/ATP translocase 1 (SLC25A4) are mitochondrial carriers which catalyze the transport of phosphate ions and ATP/ADP, respectively. Similar to the current study, Yu et al. reported overabundance of SLC25A3 and SLC25A4 in PM compared to LL at early postmortem (Yu et al., 2017b, 2018). As carrier proteins, the higher abundance of these proteins could represent a greater transformation capacity from ADP to ATP in PM, which agrees with the higher abundance of oxidative phosphorylation enzymes in PM as discussed above.

Among the complexes represented by the differential proteins identified in this study, complex I (Turrens and Boveris, 1980; Genova et al., 2001; Kushnareva et al., 2002), complex II (Quinlan et al., 2012) and complex III (Dröse and Brandt, 2008) can produce reactive oxygen species (ROS) during oxidative phosphorylation. These ROS can cause direct damage to complex I through to IV (electron transport chain) (Brown, 1999) and SLC25A4 (Yan and Sohal, 1998), which can further trigger a series of metabolic disorder leading to cell death (Vakifahmetoglu-Norberg et al., 2017). Therefore, ROS producers and ROS targets detected as more abundant in PM as compared to LL supports previous studies that demonstrated greater oxidative stress, cytochrome c release, and faster mitochondria degradation in color-labile PM than LL during early display (Ke et al., 2017; Mancini et al., 2018).

2.3.1.2 Enzymes in TCA cycle and NADPH regeneration

Seven proteins (Table 2.1) associated with the TCA cycle were more abundant in PM which, coupled with the increase in oxidative phosphorylation enzymes discussed above, indicates increased oxidative metabolism in PM. These results are also consistent with previous reports that

demonstrated greater oxygen consumption (O'Keeffe and Hood, 1982; McKenna et al., 2005) and increased abundance of TCA enzymes (Yu et al., 2017b, 2018) in PM as compared to LL during early postmortem. Previous research has indicated that vitamin E supplementation can decrease oxidative phosphorylation and TCA enzymes in beef mitochondria (Zhai et al., 2018) which results in improved color stability. Thus, the increased abundance of oxidative phosphorylation and TCA enzymes in PM observed in the current study along with previous research suggests that these oxidative enzymes could have a negative impact on beef color stability. Among the identified differential proteins in this section, mitochondrial aconitate hydratase (ACO2) can be the source of ROS production (Vásquez-Vivar et al., 2000) and ROS attack (Yan et al., 1997). This also support previously reported greater oxidative stress, and faster mitochondrial damage in PM than LL (Ke et al., 2017; Mancini et al., 2018).

Mitochondrial NAD(P) transhydrogenase (NNT) was more abundant in PM throughout the early postmortem period. This enzyme is responsible for transhydrogenation between NADH and NADP and functions as a proton pump across the mitochondrial membrane. NNT-catalyzed reduction of NADP+ is the most vital source of the mitochondrial NADPH pool (Rydström, 2006). Moreover, the function of NNT is a critical link between the metabolic and H_2O_2 antioxidant function in mitochondria (Lopert and Patel, 2014), which can ultimately influence cell survival/death (Yin et al., 2012). In the present study, mitochondrial isocitrate dehydrogenase (IDH2), another source of mitochondrial NADPH pool (Yin et al., 2012), was also more abundant in PM. Overall, our results indicated that, during the postmortem period, NADPH regeneration enzymes are in higher abundance in PM, supporting previously reported increased oxidative metabolism in PM as compared to LL.

2.3.1.3 Enzymes involved in fatty acid degradation

Nine proteins (Table 2.1) involved in fatty acid degradation were more abundant in PM at different postmortem periods. Fatty acid-binding protein (FABP3) is involved in active fatty acid metabolism where it transports fatty acids from the cell membrane to mitochondria for oxidation. Moreover, previous studies have indicated that the abundance of fatty acid-binding protein correlated with the level of negative energy balance in live animals (Piras et al., 2019). Further, D'Alessandro et al. reported a greater abundance of FABP3 in tender longissimus dorsi (LD) compared to tougher LD counterparts (D'Alessandro et al., 2012b). Mitochondrial electron transfer flavoprotein subunit alpha (ETFA) is a flavoprotein located in the matrix of the inner mitochondrial membrane and is involved in the oxidation of fatty acids (Weidenhaupt et al., 1996). Previous research indicated that the expression of ETFA gene is related to pork quality (Yang et al., 2018). Long-chain-fatty-acid-CoA ligase 1 (ACSL1) is an enzyme of the ligase family that activates the breakdown of complex fatty acids before beta-oxidation (Soupene and Kuypers, 2008) and is associated with intramuscular fat deposition in beef LL (Poleti et al., 2018a).

Mitochondrial long-chain specific acyl-CoA dehydrogenase (ACADVL) and mitochondrial short-chain specific acyl-CoA dehydrogenase (ACADS) are proteins catalyzing the first step of the long-chain and short chain fatty acid beta-oxidation pathway respectively. Previous research showed higher ACADVL abundance in pig LD muscle in breeds with high lipid deposition (Wang et al., 2017b). Yu et al. also reported more abundant ACADVL in beef PM compared to LL (Yu et al., 2017b, 2018). Previous research also reported that ACADS was more abundant in bovine PM compared to LL throughout the early postmortem period (Yu et al., 2018). Additionally, ACADS had higher abundance in Nellore cattle with high estimated genomic breeding values for intramuscular fat (Poleti et al., 2018a).

Mitochondrial hydroxyacyl-CoA dehydrogenase (HADH) is a mitochondrial enzyme involved in production of NADH in beta-oxidation. Higher HADH abundance in pig LD muscle was also associated with greater lipid deposition capability (Wang et al., 2017b). Mitochondrial acetyl-CoA acetyltransferase (ACAT1) is an enzyme that catalyzes the reversible formation of acetoacetyl-CoA from two molecules of acetyl-CoA. Poleti et al. reported that ACAT1 was found in bovine *longissimus thoracis* (LT) muscle with normal ultimate pH (< 5.8), but not in high ultimate pH (> 6.0) (Poleti et al., 2018b).

Taken together, our results indicate a higher abundance of fatty acid degradation enzymes in PM as compared to beef LL during early postmortem, which could be reflective of increased lipid oxidation. In support of this idea, Canto et al. demonstrated that beef PM had more lipid oxidation than LL (Canto et al., 2016). Yu et al. also reported that beef PM had more abundant fatty acid beta-oxidation enzymes compare to LL (Yu et al., 2018). Mitochondrial fatty acid oxidation has been targeted as an important source for ROS generation (Seifert et al., 2010; Schönfeld and Wojtczak, 2012). Among the proteins identified in this function cluster, ETFA can produce ROS when acyl-CoA dehydrogenase is present (Rodrigues and Gomes, 2012) whereas FABP3 can further promote apoptosis (Zhu et al., 2011). Along with our observations of oxidative phosphorylation and TCA cycle enzymes, these results could explain the connection between the higher abundance of ROS-related proteins, increased oxidative stress, mitochondrial degradation, and cytochrome c release in PM compared to LL during early display (Ke et al., 2017; Mancini et al., 2018), and its negative association to color stability and oxidative metabolism.

2.3.1.4 Proteins related to muscle contraction and calcium signaling

Among proteins related to muscle contraction and calcium signaling, myosin light chain 6B (MYL6B), cysteine and glycine-rich protein 3 (CSRP3), immunoglobulin-like and fibronectin

type III domain containing 1 (IGFN1), tropomyosin alpha-1 chain (TPM1) ryanodine receptor 3 (RYR3), and protein S100-A2 (S100A2) were more abundant in LL during postmortem; while myosin light chain 3 (MYL3), troponin I1 (slow skeletal type; TNNI1), troponin T (slow skeletal muscle; TNNT1) and sarcoplasmic reticulum calcium ATPase 2 (ATP2A2) were more abundant in PM (Table 2.1).

Myosin light chain 6B (MYL6B) and myosin light chain 3 (MYL3) were detected as higher and lower abundance in LL as compared to PM in early postmortem, respectively (Table 2.1). In agreement with our results, Yu et al. reported the same trend in early postmortem (Yu et al., 2017b, 2018). MY6LB and MYL3 are regulatory light chains of myosin and are closely associated with beef quality. Zhang et al. reported down-regulation of MYL3 in bovine LD with high intramuscular fat scores (Zhang et al., 2010), whereas Poleti et al. reported a lower abundance of MYL6B in cattle with high estimated genomic breeding value for intramuscular fat content (Poleti et al., 2018a). Moreover, MYL3 and MYL6B showed greater level of oxidative damage in tender meat when compared to either the intermediate or tough meat (Malheiros et al., 2019).

Cysteine and glycine-rich protein 3 (CSRP3), also referred to as muscle LIM protein, an important scaffold protein in the sarcoplasm, related to calcium homeostasis (Esposito et al., 2000; Su et al., 2001; Gupta et al., 2008; Kemecsei et al., 2010), showed greater abundance in LL than PM in early postmortem (Table 2.1). The abundance of CSRP3 was positively associated with Warner-Bratzler shear force (WBSF) of beef aged for 14 days (Zapata et al., 2009). The IGFN1 (Immunoglobulin-like and fibronectin type III domain containing 1), a part of a Z-band protein complex (Baker et al., 2010), related to actin cytoskeleton (Otey et al., 2009), was more abundant in LL in early postmortem (Table 2.1).

Tropomyosin alpha-1 chain (TPM1) was more abundant in LL at 12 h postmortem. Similarly, Oe et al. reported that the content of TPM1 was higher in bovine LT than PM (Oe et al., 2007, 2009). Moreover, there was a greater expression of TPM1 in LL from Nellore cattle compared to that from Angus (Rodrigues et al., 2017). Troponin I1 (slow skeletal type; TNNI1) and Troponin T (slow skeletal muscle; TNNT1) are two regulatory proteins of troponin complex that is integral to muscle contraction. Troponin T binds to tropomyosin, interlocking them to form a troponin-tropomyosin complex, and troponin I binds to actin in thin myofilaments to hold the troponin-tropomyosin complex in place. D'Alessandro et al. demonstrated that TNNT1 was up-regulated in tough bovine LD muscle compared to tender LD (D'Alessandro et al., 2012b), while the oxidation level of TNNT1 showed a positive association with tenderness (Malheiros et al., 2019). In agreement with our result, Yu et al. also reported increased abundances of TNNT1 in PM as compared to LL (Yu et al., 2018).

Sarcoplasmic reticulum calcium ATPase 2 (ATP2A2) and ryanodine receptor 3 (RYR3) represent the entrance and exit of calcium in endoplasmic reticulum (ER) /sarcoplasmic reticulum (SR), respectively. ATP2A2 was more abundant in PM throughout early postmortem, but RYR3 was more abundant in LL at 45 min postmortem. Previous studies on meat showed a significant level of phosphorylation at early postmortem (from 1 to 24 h) in ATP2A1, which may contribute to the regulation of Ca^{2+} pump (Huang et al., 2011). RYR3, a Ca^{2+} permeable channel mediating the majority of Ca^{2+} release from the ER/SR (Lai and Meissner, 1989), can be activated by ROS to release Ca^{2+} (Favero et al., 1995; Aghdasi et al., 1997). Protein S100-A2 (S100A2) was more abundant in LL at 45 min and 12 h postmortem. S100A2 is a homodimeric protein showing a conformational change after binding calcium (Bhattacharya et al., 2004) and is involved in the organization of the cytoskeleton (Gimona et al., 1997).

Among the proteins identified in this function cluster (2.3.1.4), CSRP3 (van den Bosch et al., 2005; Rashid et al., 2015), ATP2A2 (Giorgi et al., 2015; Chemaly et al., 2018), RYR3 (Vervliet, 2018), S100A2 (Mueller et al., 2005; van Dieck et al., 2009; Wolf et al., 2011) and IGFN1 (Mansilla et al., 2008; Li et al., 2017) are associated with metabolic disorder, cell death, or factors related to cell death, such as tumor suppressor p53 (p53) and autophagy, and most of them (except ATP2A2) were more abundant in LL in the current study. Cell death, a critical and active process maintaining tissue homeostasis and eliminating potentially harmful cells by metabolic control, has three major types: apoptosis (type I cell death), autophagic cell death (type II), and necrosis (type III) (Green and Llambi, 2015). The effect of apoptosis on meat tenderization has been highlighted by previous researchers (Herrera-Mendez et al., 2006; Ouali et al., 2006; Kemp and Parr, 2012; Sierra and Olivan, 2013; Lomiwes et al., 2014; Lana and Zolla, 2015; Longo et al., 2015; Lana and Zolla, 2016). Autophagy generally functions as a survival process to delay apoptosis (Lum et al., 2005). Tumor suppressor p53 (p53) is a transcription factor that could be transiently activated to promote survival and permanently engaged to stimulate cell death (Green et al., 2014), and this apoptotic stimulation can be achieved by stimulating mitochondrial Ca^{2+} overload (Giorgi et al., 2015), inhibiting autophagy (Tasdemir et al., 2008), activating proapoptotic proteins, like apoptosis regulator BAX (BAX) and BCL-2 homologous antagonist/killer (BAK) (Chipuk et al., 2004; Leu et al., 2004), and, lastly, leading to mitochondrial outer membrane permeabilization (MOMP) (Chipuk et al., 2004, 2005). In postmortem muscle, the apoptosis is typically reflected by the release of cytochrome c from mitochondria to sarcoplasm, which is also associated with discoloration in beef muscle (Ke et al., 2017).

Although the association between these proteins (ATP2A2, RYR3, and S100A2) and cell death is not yet fully confirmed, most of the proteins discussed in previous sections have confirmed

role in cell death, meat quality variation, and postmortem metabolism. In fact, several of previous proteomic investigations (Hunt and Hedrick, 1977; Ozawa et al., 2000; Melody et al., 2004; McKenna et al., 2005; Seyfert et al., 2006; Hwang et al., 2010; Joseph et al., 2012; Canto et al., 2016; Wu et al., 2016; Ke et al., 2017; Yu et al., 2017b; Mancini et al., 2018; Yu et al., 2018) have reported proteins associated with muscle metabolism and muscle contraction to be differentially abundant between muscles of differing meat quality attributes. However, as demonstrated in the function clusters distribution (Figure 2.3.1, 2.3.2 and 2.3.3), the four main function clusters discussed above cannot explain all the proteome difference between LL and PM at early postmortem. We have attempted to capture these unexplained/unknown proteins and their potential pathways as it relates to cell metabolism and cell death in Figure 2.4, which will be explained in detail in Section 2.3.2.

2.3.1.5. Chaperone proteins

Chaperones are proteins that assist the covalent folding or unfolding and the assembly or disassembly of macromolecular structures, which generally helps alleviate cellular stress. Peptidyl-prolyl cis-trans isomerase A (PPIA), heat shock protein beta-6 (HSPB6) were more abundant in LL, while heat shock protein 60 (HSPD1) was more abundant in PM (Table 2.1). Recently, it was reported that PPIA was more abundant in the inner part of normal pork hams compared to that of PSE-like pork ham (Théron et al., 2019). Heat shock protein beta-6 (HSPB6; also known as hsp20) is a 17-kDa member of the small heat shock proteins and was more abundant in LL at 45 min postmortem. Similarly, a greater abundance of HSPB6 in beef LL (or LT or LD) compared to *semimembranosus* (SM), *semitendinosus* (ST), *triceps brachii* (TB), and PM has been reported previously (Guillemin et al., 2011a; Yu et al., 2017b; Picard et al., 2018; Yu et al., 2018). In addition, HSPB6 abundance was reported to have a negative association with tenderness (Zapata

et al., 2009; Rosa et al., 2018). However, this association depends on muscle and breed (Picard et al., 2014). Moreover, previous studies have shown a negative association between the oxidation level of HSPB6 and tenderness (Malheiros et al., 2019) as well as an increase in phosphorylation with meat aging (Longo et al., 2015). Furthermore, Gagaoua et al. reported that HSPB6 was positively associated with color parameters such as a* (redness) and C* (chroma) values (Gagaoua et al., 2018). Heat shock protein 60 (HSPD1), a mitochondrial chaperone was more abundant in PM than LL at 36 h postmortem, and this is in agreement with previous study (Yu et al., 2018). Other research has also indicated that HSPD1 has a positive correlation with a* value in beef *semitendinosus* (ST) muscle during the extended storage (Yu et al., 2017a).

Peptidyl-prolyl cis-trans isomerase A (PPIA) has been also shown to have a significant protective function in cell survival (Boulos et al., 2007; Obchoei et al., 2009; Cheng et al., 2016). Specifically, it promotes cell survival by alleviating the generation and damage of ROS (Doyle et al., 1999; Lee et al., 2001; Suzuki et al., 2006; Choi et al., 2007), activating signal transducer and activating transcription 3 (STAT3; an antiapoptotic transcription factor) (Bauer et al., 2009), promoting autophagy (Mao et al., 2017), modifying p53 function (Baum et al., 2009), and increasing expression of the antiapoptotic protein B-cell lymphoma 2 (BCL-2) (Seko et al., 2004; Wei et al., 2013). Interestingly, Basigin isoform 2 (BSG), another differential protein identified in this study (Table 2.1), can be the receptor of PPIA, and this interaction between PPIA and BSG can also contribute to anti-apoptosis (Seko et al., 2004; Boulos et al., 2007). Similarly, heat shock protein beta-6 (HSPB6) can also prevent apoptosis (Wang et al., 2009; Cameron et al., 2014; Wang et al., 2016a), and this prevention results from HSPB6's inhibitive effect on the proapoptotic effector, apoptosis regulator Bax (BAX) (Nagasawa et al., 2014; Zhong et al., 2015). Conversely, heat shock protein 60 (HSPD1) is more associated with a proapoptotic process or a process during

apoptosis (Samali et al., 1999; Xanthoudakis et al., 1999; Chandra et al., 2007; Kim et al., 2009). Taken together, these results indicate an increase in antiapoptotic chaperones in LL and an increase in proapoptotic chaperones in PM during early postmortem.

2.3.1.6 Oxygen transport proteins

Hemoglobin (subunit A; HBA and subunit B; HBB) was more abundant in PM as compared to LL, a result that is in agreement with previous study (Yu et al., 2017b). In general, there is not much hemoglobin left in the muscles after exsanguination, and the difference in the hemoglobin levels detected could be reflective of their muscle fiber types, with LL being a glycolytic muscle and PM being an oxidative muscle (Kirchofer et al., 2002). Moreover, HBA and HBB have been shown to be over-expressed in dark SM muscle compared to those in the light group (Sayd et al., 2006; Kim et al., 2018). Also, hemoglobin (more abundant in PM) is very susceptible to autooxidation, which can happen under low temperature or low pO2 (Minetti et al., 1993; Kanias and Acker, 2010; Wither et al., 2016), leading to production of ROS (Misra and Fridovich, 1972), accumulated oxidative stress (Olsson et al., 2010), and peroxidation of fatty acids (Sadrzadeh et al., 1984; Moxness et al., 1996), thereby contributing to greater lipid oxidation and lower color stability in PM (Canto et al., 2016).

2.3.1.7 Proteins related to degradation of the extracellular matrix

Basigin isoform 2 (BSG; also known as extracellular matrix metalloproteinase inducer) and alpha-2-macroglobulin (A2M) were more abundant in PM compared to LL at 36 h postmortem. As mentioned above in PPIA's function, BSG can receive signal from PPIA, which can further stimulate antiapoptotic function (Boulos et al., 2007; Obchoei et al., 2009). Alpha-2-Macroglobulin (A2M) is a large (720 KDa) plasma protein, which can inhibit all four classes of proteases by a unique trapping mechanism. Matrix metalloproteinase plays an important role in

extracellular matrix via proteolysis during postmortem aging of meat, consequently affecting the tenderness (Nishimura, 2015; Christensen and Purslow, 2016). In our results, the increased abundance of A2M and BSG in PM could indicate an earlier and greater degradation of the extracellular matrix, thereby contributing to its superior tenderness.

2.3.1.8 Glycolytic enzymes

Although not captured as a clustered function during the string analysis, glycolytic enzyme beta-enolase (ENO3) was more abundant in LL at 12 h postmortem as compared to PM. ENO3 is a glycolytic enzyme that catalyzes the reversible conversion of 2-phosphoglycerate to phosphoenolpyruvate and is expressed at higher levels in fast-twitch fibers than in slow-twitch fibers (Giallongo et al., 1993). In general, LL is considered a fast-twitch muscle compared to PM. Previous research has also indicated a positive association between ENO3 abundance and tenderness (Bjarnadóttir et al., 2012; Rosa et al., 2018). Moreover, oxidative damage to ENO3 has been shown to be less in tender LL as compared to tough group (Malheiros et al., 2019). Laville et al. also reported an increase of ENO3 fragments in bovine LT muscle after 21d aging (Laville et al., 2009).

Joseph et al. reported a positive association between ENO3 and redness (a* value) of beef LL and PM during retail display (Joseph et al., 2012). It has also been shown that ENO3 was also negatively associated with pH of LT muscle of Blond d'Aquitaine bulls at 3 h postmortem (Gagaoua et al., 2015b), but positively related to ultimate pH in Charolais LT muscle (Gagaoua et al., 2018). Yet another study found that it had a negative relation with redness (a* value) and a positive relation with pH of *semitendinosus* (ST) muscle from Holstein during postmortem (Yu et al., 2017a). Similarly, ENO3 was shown to be negatively correlated with lightness of Aberdeen Angus LT muscle at early postmortem (Gagaoua et al., 2017). These studies collectively suggest

that ENO3 is closely associated with beef color and pH, but those relationships are muscle-specific and breed-specific.

2.3.1.9 Proteins involved in other functions

Several additional proteins that did not fit into the functional categories described above were also identified as differentially abundant between LL and PM at different time points postmortem. Mitochondrial GTP:AMP phosphotransferase AK3 (AK3) was more abundant in PM at 36 h postmortem. AK3 is a mitochondrial GTP:AMP phosphotransferase that catalyzes the interconversion of ADP and AMP. As energy levels change under different metabolic stresses, adenylate kinase can generate AMP; which itself acts as a signaling molecule in further signaling cascades. This generated AMP can stimulate various AMP-dependent receptors such as those involved in glycolytic pathways and 5′ AMP-activated protein kinase (AMPK; Dzeja and Terzic, 2009). By continually monitoring and altering the levels of ATP and the other adenyl phosphates (ADP and AMP levels), adenylate kinase acts as an important regulator of energy expenditure at the cellular level (Dzeja et al., 2011). However, in postmortem muscle, the activity of AMPK has been shown to significantly decrease after 1 h postmortem (Shen et al., 2006a, 2006b), thus the increased abundance of AK3 in PM at 36 h postmortem observed in our study may not be directly contributing to AMPK activity. In support of this hypothesis, recent research reported that the AMP content was higher in LL than PM at 24 h postmortem (Yu et al., 2019), thus, our observed increased abundance of AK3 in PM at 36 h is likely not related to its enzyme functionality but is important as a landmark of the cell death event. It has also been reported that the release of AK3 from mitochondrial matrix to cytoplasm results from mitochondrial permeability transition (MPT; Gogvadze et al., 2001), an event committing cell to death (Lemasters et al., 2009; Rasola and

Bernardi, 2011; Bonora et al., 2015). Therefore, the increased abundance of AK3 at 36 h could be associated with programmed cell death (Figure 2.4).

Peptidyl arginine deiminase 2 (PADI2) was more abundant in LL throughout early postmortem compared to PM. Interleukin 31 receptor A (IL31RA) is a type I cytokine receptor (Ghilardi et al., 2002). IL31RA can be activated by binding interleukin 31 (IL31) through its cytokine binding domain and was detected in increased abundance in PM throughout early postmortem. NADH-cytochrome b5 reductase (CYB5R3), a protein known to play a role in metmyoglobin reduction (Hagler et al., 1979), was increased in abundance in LL (color-stable muscle) at 45 min postmortem. Arihara et al. located NADH-cytochrome b5 reductase in subcellular fractions from bovine muscle, and reported that NADH-cytochrome b5 reductase can reduce metmyoglobin (Arihara et al., 1995) and provide meat color stability. CYB5R3 has also been shown to provide protection against metabolic disorders (Siendones et al., 2014; Martin-Montalvo et al., 2016) and attenuate damage of lipids and proteins (Hyun and Lee, 2015; Figure 2.4). Cytoplasmic serine-tRNA ligase (SARS), a protein than can counteract c-Myc (a transcription factor generally inducing apoptosis by p53) (Hermeking and Eick, 1994; Nieminen et al., 2013), was increased in abundance in LL at 12 h postmortem (Figure 2.4). Histone-lysine N-methyltransferase 2D (KMT2D), a protein associated with activation of p53 (Lee et al., 2009; Xiong et al., 2018) and expression of antiapoptotic proteins, such as B-cell lymphoma 2 (BCL-2) and BCL-2-like 1 protein (BCL-XL; Lv et al., 2018), was increased in abundance in PM at 36 h postmortem (Figure 2.4).

As shown in Figure 2.3, after animal bleeding, the total number of differentially abundant proteins between PM and LL increased from 33 at 45 min to 42 at 12 h and ended with 50 at 36 h, which indicates that over time the biological activity between the two muscle tissues is

increasingly divergent. At 45 min postmortem, the greatest (25%) proteome difference between PM and LL was observed in proteins related to in fatty acid degradation (Figure 2.3). The number of differential proteins in this cluster is constant between 12 h and 36 h, but the percentage decreased due to the increase in total proteome variance. The greatest change of proteomic variance between LL and PM over early postmortem was observed in proteins related to oxidative phosphorylation and ATP-relate transport. The number of differential proteins in this cluster rapidly increased from 6 (18%) at 45 min to 17 at 12 h, ending with 20 at 36 h, which accounted for 41% (largest) and 40% (largest) difference at 12 h and 36 h, respectively. Within the other functional clusters, the proteome variance did not change significantly throughout early postmortem, however the percent changes decreased due to the overall increased in protein variance. Proteins related to degradation of the extracellular matrix showed significant variance between the two muscle types at 36 h, but not at 45 min and 12 h. This could suggest that the extracellular matrix degradation (associated with tenderness) does not start until 36 h postmortem. Interestingly, the number of differentially abundant mitochondrial proteins continued to increase in abundance throughout the postmortem time period in PM tissue.

2.3.2 Overview of association between meat quality and the differentially abundant proteins between PM and LL during early postmortem

The metabolism-related and cell death-related pathways/effectors in our results were summarized and a "metabolism"-"cell death"-"meat quality" network was built and presented in Figure 2.4. After animal bleeding, the muscle tissue cannot access blood-delivered oxygen and nutrients. This ischemia-like situation will influence cell metabolism, changing it from aerobic to anaerobic. This drastic change results in mitochondria that produce less ATP but more ROS. The produced ROS can be reduced to water (H_2O) by the mitochondrial antioxidant system (Yin et al.,

2012). However, due to the limited energy source and ATP production, AMPK will be activated (Herzig and Shaw, 2018; Lin and Hardie, 2018), and the ratio between ROS and antioxidant will become greater and lead to increased oxidative stress. The increased oxidative stress will lead to the activations of p53 (Han et al., 2008). In the cytoplasm, p53 is localized in mitochondria-associated membranes and stimulates apoptosis in a "non-nuclear" manner by directly binding to and activating ATP2A2. This promotes ER Ca^{2+} loading under stress conditions, subsequently increasing Ca^{2+} transfer from the ER to the mitochondria (Giorgi et al., 2015). Moderate amounts of Ca^{2+} entering the intermembrane space can stimulate oxidative metabolism through the modulation of Ca^{2+}-sensitive dehydrogenases and metabolite carriers (Denton et al., 1972; McCormack et al., 1990; Denton, 2009; Bonora et al., 2012), which works to enhance mitochondrial and cytosolic ATP concentrations (Jouaville et al., 1999). However, in beef postmortem muscle, free Ca^{2+} concentration will dramatically and irreversibly increase after slaughtering (Ji and Takahashi, 2006). The increase of Ca^{2+} will also lead to the activations of AMPK (Mungai et al., 2011; Sundararaman et al., 2016), activating glycolysis and fatty acids oxidation (O'Neill and Hardie, 2013; Herzig and Shaw, 2018; Lin and Hardie, 2018) even if the oxidation of fatty acids will cause ROS generation (Seifert et al., 2010; Schönfeld and Wojtczak, 2012). Meanwhile, autophagy also will be activated by AMPK (Egan et al., 2011; Kim et al., 2011), which could remove dysfunctional mitochondria and maintain intracellular homeostasis (Green and Levine, 2014), leading to a delayed apoptotic process (Lum et al., 2005). However, the activation of p53 can inhibit autophagy (Tasdemir et al., 2008) and ultimately lead to mitochondrial outer membrane permeabilization (MOMP) (Chipuk et al., 2004; Chipuk et al., 2005) or mitochondrial permeability transition (MPT; Vaseva et al., 2012), although the MPT can also result from mitochondrial Ca^{2+} overload (Lemasters et al., 2009; Rasola and Bernardi, 2011). Once

MOMP or MPT happen, cell death is inevitable. In postmortem muscle, apoptosis has been associated with factors influencing meat quality attributes, such as tenderization and color stability (Herrera-Mendez et al., 2006; Ouali et al., 2006; Laville et al., 2009; Kemp and Parr, 2012: 2012; Sierra and Olivan, 2013; Lomiwes et al., 2014; Lana and Zolla, 2015; Longo et al., 2015; Lana and Zolla, 2016; Ke et al., 2017; Cramer et al., 2018; Zhang et al., 2019a; Figure 2.4). It is also possible that the observed increased in abundance of mitochondrial proteins in PM compared to LL resulted from more intensive MOMP and MPT over time, which lead to a greater content of mitochondrial proteins, such as cytochrome c (Ke et al., 2017) and HSPD1 (Nair et al., 2018a), in sarcoplasm from PM.

Moreover, previous research has demonstrated relationship between p53, AMPK, STAT3, autophagy, and apoptosis as indicated in Figure 2.4. Specifically, p53 and AMPK have been shown to have interactive functions during metabolic stress (Jones et al., 2005; Budanov and Karin, 2008). p53 can also inhibit autophagy (Tasdemir et al., 2008), while AMPK can activate autophagy (Egan et al., 2011; Kim et al., 2011). Autophagy can functionally delay apoptosis (Lum et al., 2005), whereas p53 can promote apoptosis by increasing expression of proapoptotic proteins, like BAX and BAK (Chipuk et al., 2004; Leu et al., 2004). STAT3 can inhibit apoptosis by increasing synthesis of antiapoptotic proteins, including BCL-2 (Bhattacharya et al., 2005) and BCL-XL (Catlett-Falcone et al., 1999). In beef muscle, free sarcoplasmic calcium concentration has been shown to rapidly increased from 16 μM at 40 min postmortem to 210 μM at 4 days postmortem, and the amount of phospholipid in sarcoplasmic reticulum to decrease during the same window (Ji and Takahashi, 2006). It was hypothesized that the calcium ions leak into the sarcoplasm through channels formed by those phospholipid liberations (Ji and Takahashi, 2006). However, this decrease of phospholipid in sarcoplasmic reticulum could also be attributed to autophagy (Axe et

al., 2008; Hayashi-Nishino et al., 2010; Hamasaki et al., 2013), which can be stimulated by changes in intracellular Ca^{2+} (Decuypere et al., 2011). A breed-specific increase in autophagy was observed in muscles with greater proportion of white fibers from 2 h to 24 h postmortem (García-Macia et al., 2014). In the present study, CSRP3 (autophagy associated protein) was more abundant in LL than PM (Table 2.1; Figure 2.4). However, the effect of muscle fiber type on postmortem autophagy need further investigation.

Taken together, our results suggest that, at early postmortem, the increased abundance of CYB5R3, CSRP3, PPIA, SARS, HSPB6, and IGFN1 could increase metabolic stability (lower ROS production), activate STAT3, alter p53 function, inhibit proapoptotic protein activity, and enhance autophagy, leading to delayed apoptosis in LL, while more abundant AK3 and HSPD1 could be related to more intensive programmed cell death in PM. These processes would result in greater oxidative phosphorylation, fatty acid oxidation, and hemoglobin oxidation in PM, which could lead to increased MOMP and MPT in PM, resulting in cytochrome c release, decreased mitochondrial function, and lower beef color stability in PM compared to LL (Ke et al., 2017; Mancini et al., 2018). Additionally, glycolytic enzymes (except ENO3) were not observed to change significantly between PM and LL, a result that contradicts previous proteomic research conducted on post-rigor meat (Joseph et al., 2012; Wu et al., 2016; Nair et al., 2018a; Yu et al., 2018). Given the greater percentage of type IIB fiber, LL could be associated with stronger glycolytic metabolism than PM (with greater proportion of type I; Hunt and Hedrick, 1977; Hwang et al., 2010). In this sense, this greater glycolytic metabolism in LL than PM could result from post-transcriptional modification of glycolytic enzymes, such as phosphorylation and oxidation. Moreover, given that PPIA and CSRP3 have critical influence on cell death and were consistently

increased in abundance in LL than PM throughout early postmortem, further research is necessary to understand the role of these proteins on postmortem change in beef muscles.

2.4 Conclusions

To summarize, the increase in abundance of antiapoptotic proteins in LL during early postmortem could cause high metabolic stability, enhanced autophagy, and delayed apoptosis, while more abundant metabolic enzymes and proapoptotic proteins in PM could accelerate the reactive oxygen species generation and programmed cell death. Moreover, the differentially abundant proteins between LL and PM during the early postmortem were primarily associated with cellular metabolism and programmed cell death. The greater oxidative and color stability in LL compared to PM could be related to the increased expression of antiapoptotic proteins and the decreased expression of metabolic enzymes and proapoptotic proteins in LL.

Note: Detailed information for the full list of identified differential proteins is presented in Table 2.1.

Table 2.1. Differentially abundant proteins between beef PM and LL muscles at 45min, 12h and 36h postmortem ($P < 0.05$).

Protein Description	Abbreviation (String Code)	Fold Change (PM vs. LL at 45min)	Fold Change (PM vs. LL at 12h)	Fold Change (PM vs. LL at 36h)
Oxidative phosphorylation				
Complex I				
NADH dehydrogenase [ubiquinone] iron-sulfur protein 8, mitochondrial	NDUFS8		1.70	
NADH dehydrogenase [ubiquinone] iron-sulfur protein 2, mitochondrial	NDUFS2		1.51	1.56
NADH dehydrogenase [ubiquinone] 1 alpha subcomplex subunit 11, mitochondrial	NDUFA11			1.52
NADH dehydrogenase [ubiquinone] flavoprotein 1, mitochondrial	NDUFV1			1.55
NADH dehydrogenase [ubiquinone] 1 alpha subcomplex subunit 9, mitochondrial	NDUFA9			1.69
NADH dehydrogenase [ubiquinone] 1 subunit C2, mitochondrial	NDUFC2			1.70
NADH dehydrogenase [ubiquinone] 1 alpha subcomplex subunit 2, mitochondrial	NDUFA2			1.70
NADH dehydrogenase [ubiquinone] 1 alpha subcomplex subunit 13, mitochondrial	NDUFA13			1.86
Acyl carrier protein, mitochondrial	NDUFAB1			1.99
Complex II				
Succinate dehydrogenase [ubiquinone] flavoprotein subunit, mitochondrial	SDHA		1.97	1.90
Succinate dehydrogenase [ubiquinone] iron-sulfur subunit, mitochondrial	SDHB		2.13	2.00
Complex III				
Cytochrome b-c1 complex subunit Rieske, mitochondrial	UQCRFS1	1.61	1.56	1.78
Cytochrome b-c1 complex subunit 2, mitochondrial	UQCRC2	1.62	1.50	1.61
Cytochrome b-c1 complex subunit 8, mitochondrial	UQCRQ	2.08		
Cytochrome c1, heme protein, mitochondrial	CYC1		1.80	
Complex IV				
Cytochrome c oxidase subunit 7A1, mitochondrial	COX7A1	1.81	1.87	
Cytochrome c oxidase subunit NDUFA4, mitochondrial	NDUFA4		1.77	
Cytochrome c oxidase subunit 6B1, mitochondrial	COX6B1		1.62	1.67
Cytochrome c oxidase subunit 2, mitochondrial	COX2			1.64
Cytochrome c oxidase subunit 7C, mitochondrial	COX7CP1			1.77
Complex V				
ATP synthase subunit g, mitochondrial	ATP5L	1.51		
ATP synthase subunit alpha, mitochondrial	ATP5A1	1.55		
ATP synthase subunit gamma, mitochondrial	ATP5C1		1.50	
ATP synthase subunit O, mitochondrial	ATP5O		1.52	
ATP synthase F(0) complex subunit B1, mitochondrial	ATP5F1		1.54	1.53

ATP synthase subunit d, mitochondrial	ATP5H		1.59	1.58
ATP synthase subunit f, mitochondrial	ATP5J2		1.62	1.57
ATP-relate transport				
ADP/ATP translocase 1, mitochondrial	SLC25A4		1.63	1.61
Phosphate carrier protein, mitochondrial	SLC25A3		1.79	1.66
TCA cycle				
Citrate synthase, mitochondrial	CS		1.61	1.59
Aconitate hydratase, mitochondrial	ACO2		1.68	
Isocitrate dehydrogenase [NADP], mitochondrial	IDH2	1.94	1.91	1.91
Succinate--CoA ligase [ADP/GDP-forming] subunit alpha, mitochondrial	SUCLG1	1.51		
Succinate--CoA ligase [GDP-forming] subunit beta, mitochondrial	SUCLG2			1.63
Fumarate hydratase, mitochondrial	FH	1.52	1.59	1.61
Malate dehydrogenase, mitochondrial	MDH2	1.58		1.51
NADPH regeneration				
NAD(P) transhydrogenase, mitochondrial	NNT	1.64	1.62	1.63
Fatty acid degradation				
Electron transfer flavoprotein subunit alpha, mitochondrial	ETFA	1.54	1.61	1.65
Fatty acid-binding protein, heart	FABP3	1.86	2.11	
Long-chain-fatty-acid--CoA ligase 1	ACSL1	1.51	1.55	1.55
Very long-chain specific acyl-CoA dehydrogenase, mitochondrial	ACADVL	1.55	1.55	1.66
Short-chain specific acyl-CoA dehydrogenase, mitochondrial	ACADS	1.84	1.97	2.00
Hydroxyacyl-CoA dehydrogenase, mitochondrial	HADH	1.99		1.73
Trifunctional enzyme subunit alpha, mitochondrial	HADHA			1.52
Trifunctional enzyme subunit beta, mitochondrial	HADHB	1.55		
Acetyl-CoA acetyltransferase, mitochondrial	ACAT1	1.79	1.80	1.75
Muscle contraction				
Myosin light chain 6B	MYL6B	0.087	0.14	0.13
Cysteine and glycine-rich protein 3	CSRP3	0.21	0.18	0.32
Immunoglobulin-like and fibronectin type III domain containing 1	IGFN1	0.34	0.32	0.34
Tropomyosin alpha-1 chain	TPM1 (ENSBTAG00000 005373)		0.61	
Myosin light chain 3	MYL3	2.59	2.88	3.19
Troponin I1, slow skeletal type	TNNI1		1.50	1.53
Troponin T, slow skeletal muscle	TNNT1			1.58
Calcium signaling				
Ryanodine receptor 3	RYR3	0.60		
Protein S100-A2	S100A2	0.31	0.34	
Sarcoplasmic reticulum calcium ATPase 2	ATP2A2	1.81	1.73	1.76
Chaperone				
Peptidyl-prolyl cis-trans isomerase A	PPIA	0.46	0.57	0.57
Heat shock protein beta-6	HSPB6	0.44		

60 kDa heat shock protein, mitochondrial	HSPD1			1.59
Oxygen transport				
Hemoglobin subunit alpha	HBA	2.27		
Hemoglobin subunit beta	HBB	2.22	2.10	1.96
Degradation of the extracellular matrix				
Basigin isoform 2	BSG			1.52
Alpha-2-macroglobulin	A2M			1.92
Other Functions				
Chromatin disassembly				
Peptidyl arginine deiminase 2	PADI2	0.29	0.22	0.29
Cytokine interaction				
Interleukin 31 receptor A	IL31RA	1.63	1.56	1.66
Amino sugar and nucleotide sugar metabolism				
NADH-cytochrome b5 reductase	CYB5R3	0.57		
Aminoacyl-tRNA biosynthesis				
Serine--tRNA ligase, cytoplasmic	SARS		0.65	
Glycolysis				
Beta-enolase	ENO3		0.65	
Purine metabolism				
GTP:AMP phosphotransferase AK3, mitochondrial	AK3			1.67
Ubiquinone biosynthesis				
Ubiquinone biosynthesis protein COQ9, mitochondrial	COQ9			1.50
Lysine degradation				
Histone-lysine N-methyltransferase 2D	KMT2D			1.77

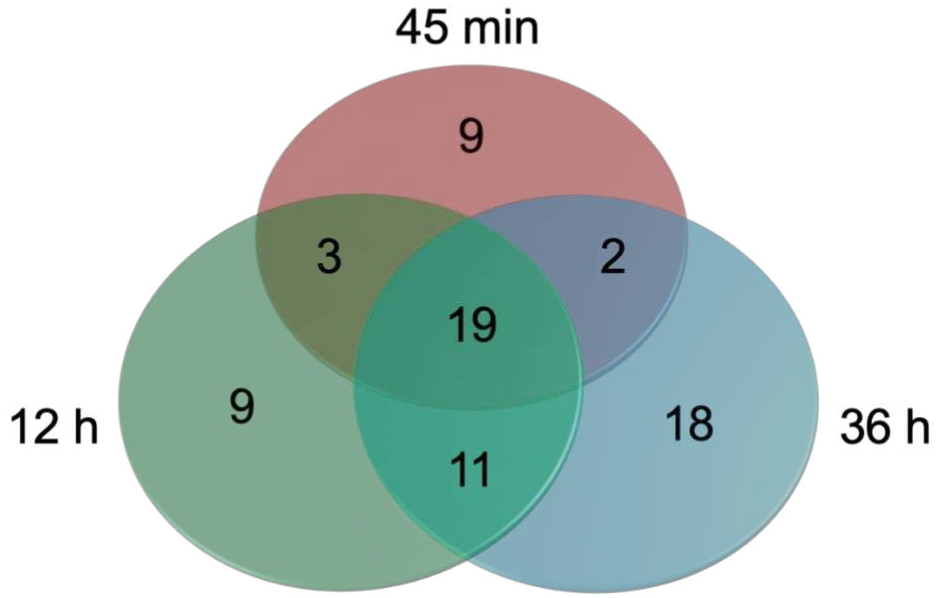

Figure 2.1. Distribution of differential proteins between *Longissimus Lumborum* (LL) and *Psoas Major* (PM) at 45min, 12h and 36h postmortem.
Note: Detailed information for the full list of identified differential proteins is presented in Table 2.1.

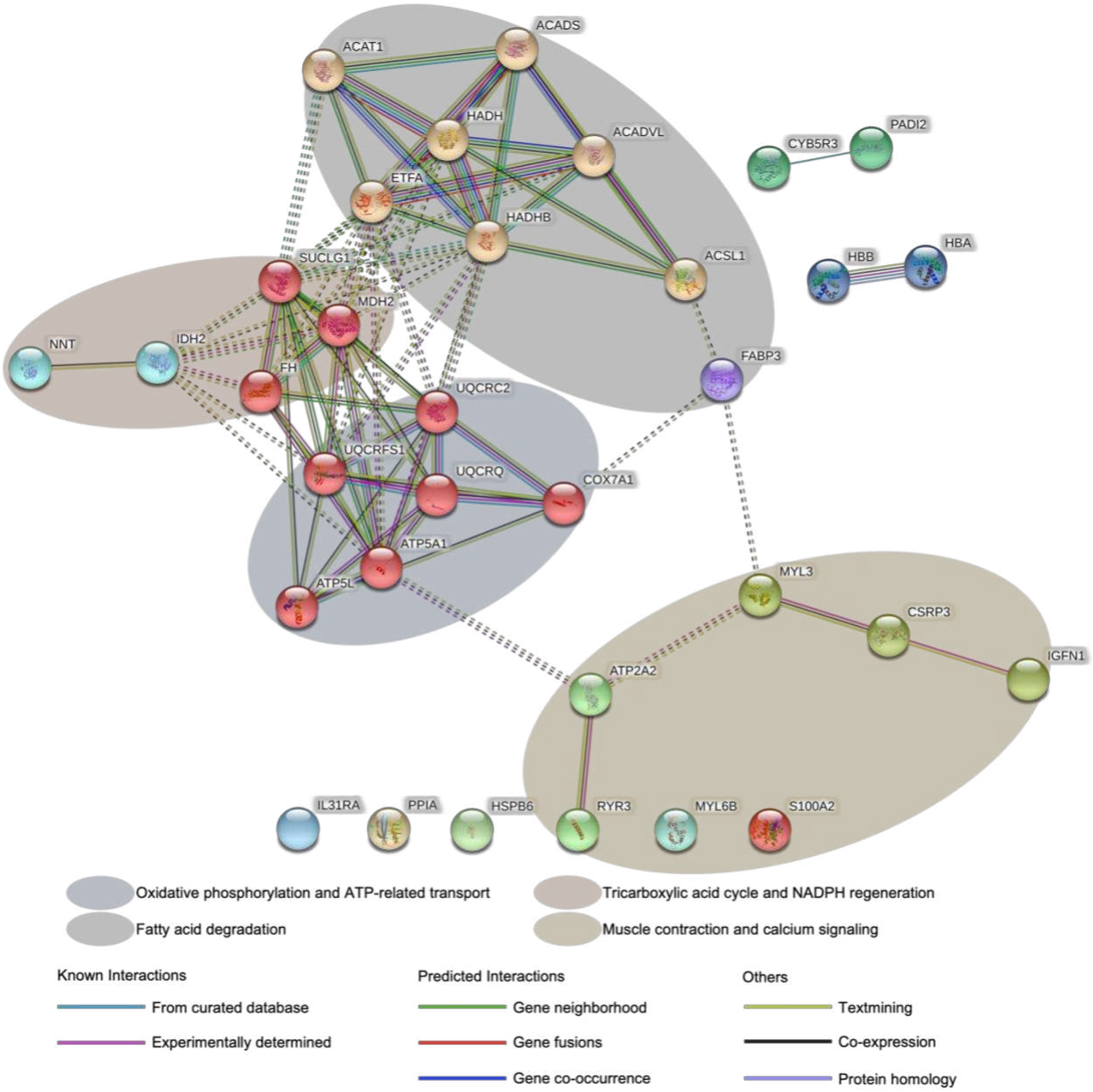

The detailed information of above differential proteins is presented in Table 1.

Figure 2.2.1, Protein-protein interaction network of differential proteins between *Longissimus Lumborum* (LL) and *Psoas Major* (PM) at 45min postmortem.

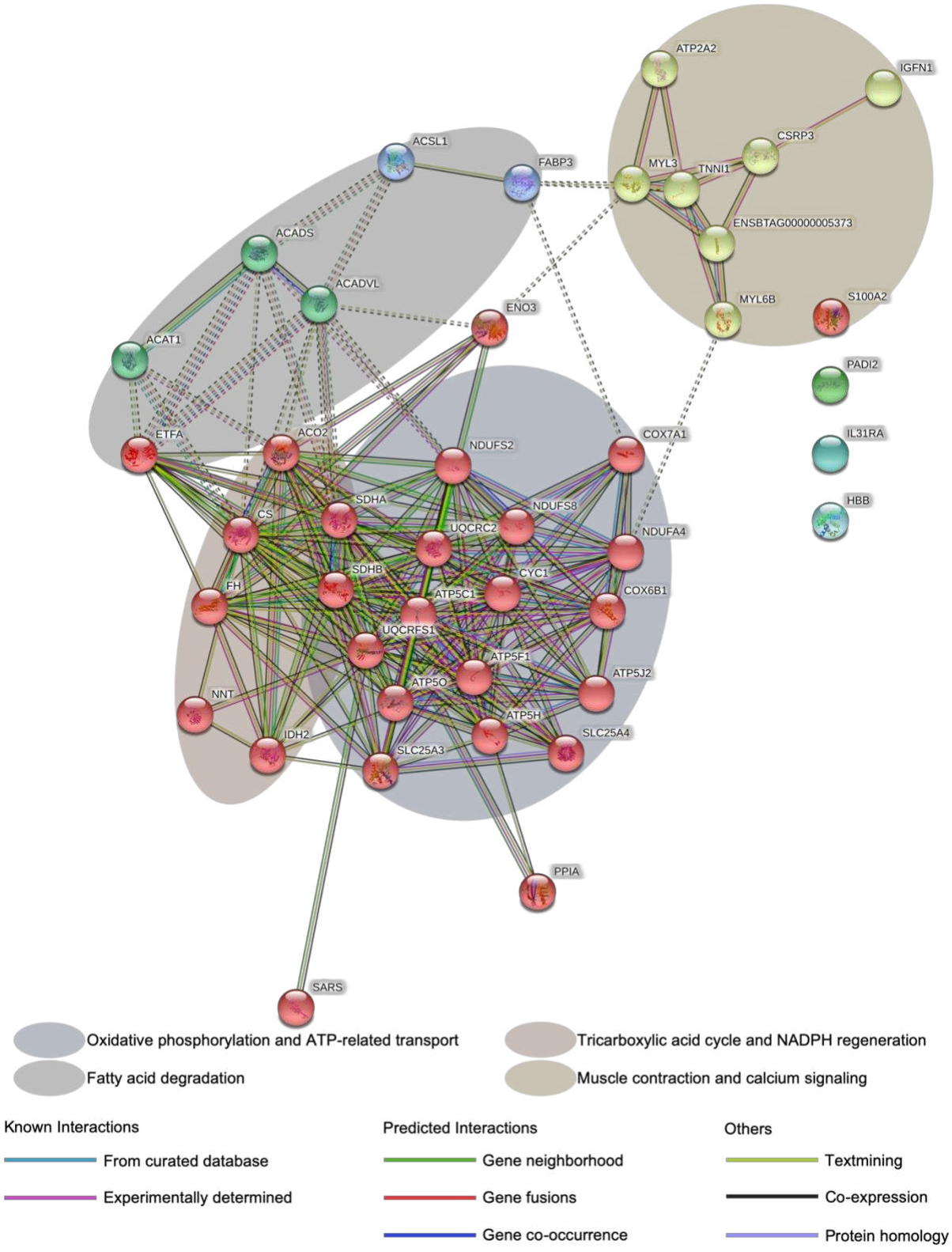

The detailed information of above differential proteins is presented in Table 1.

Figure 2.2.2. Protein-protein interaction network of differential proteins between *Longissimus Lumborum* (LL) and *Psoas Major* (PM) at 12h postmortem.

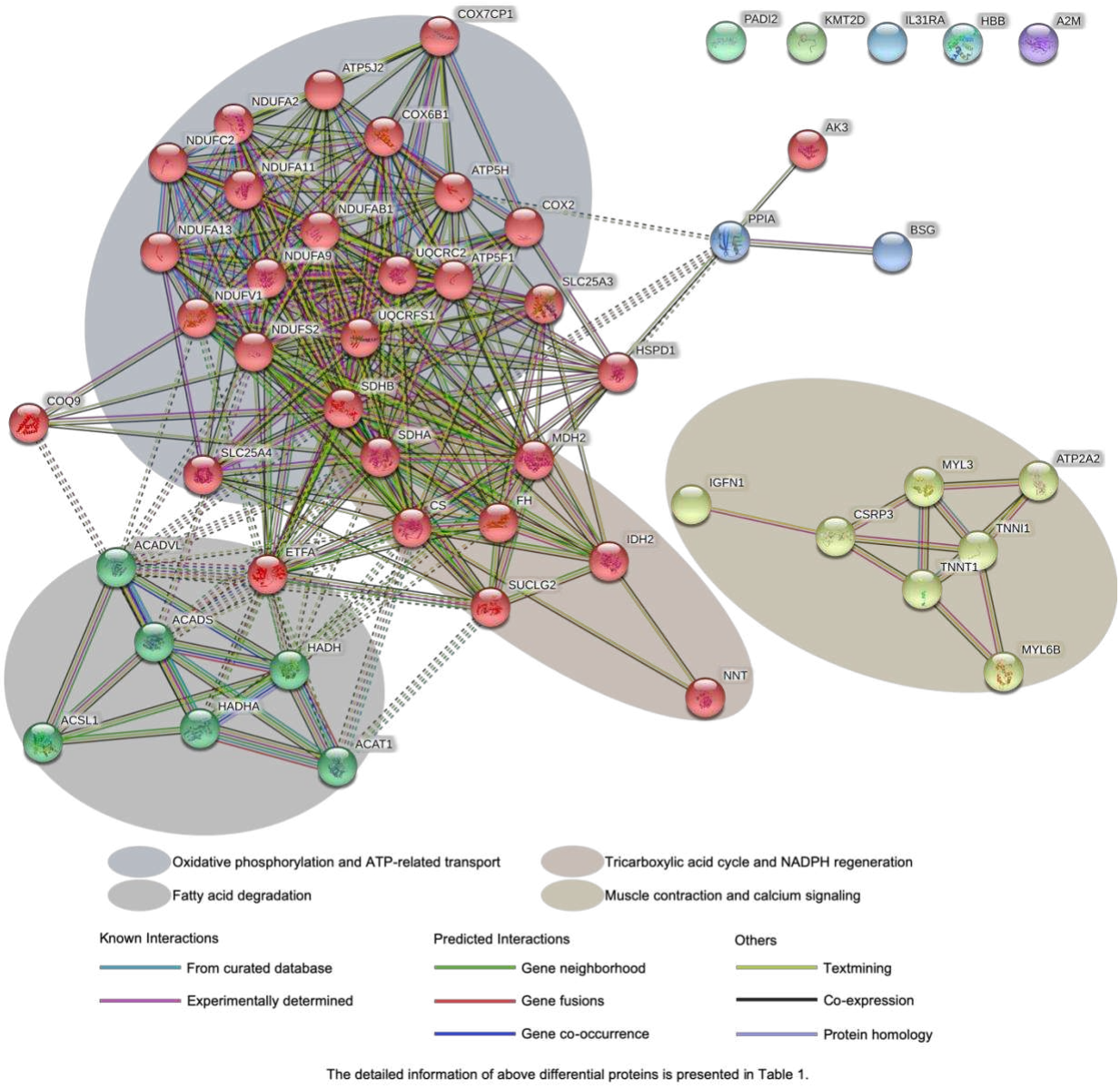

The detailed information of above differential proteins is presented in Table 1.

Figure 2.2.3. Protein-protein interaction network of differential proteins between *Longissimus Lumborum* (LL) and *Psoas Major* (PM) at 36h postmortem.

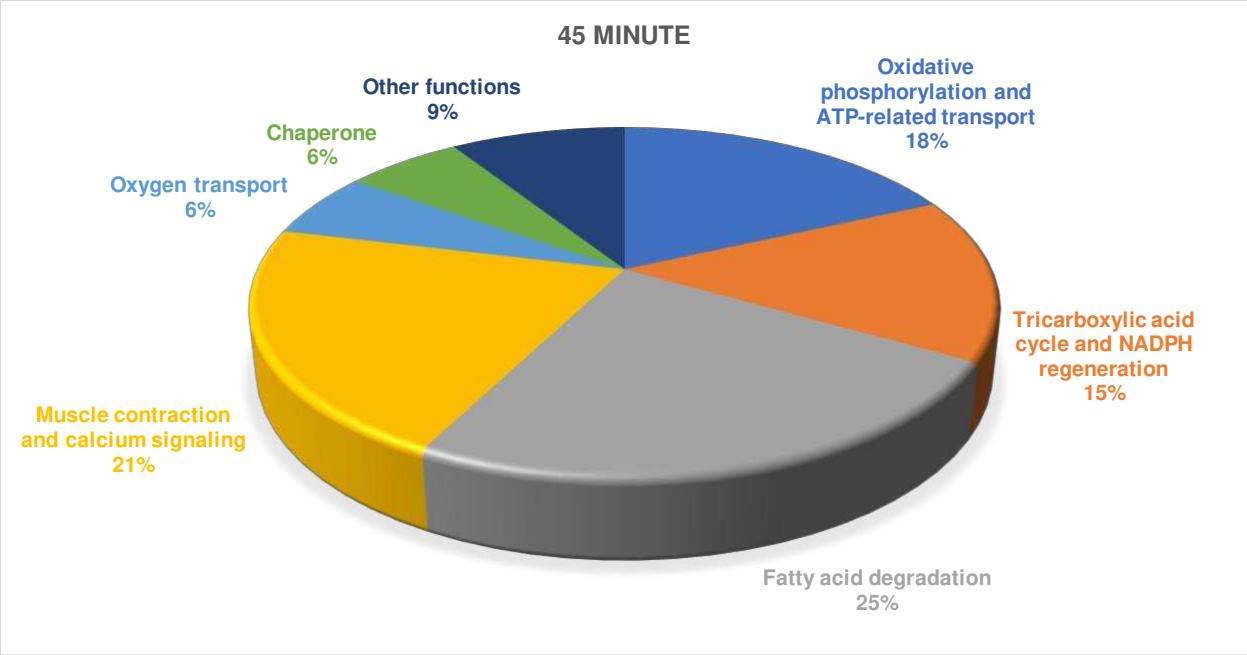

Figure 2.3.1. Distribution of the function clusters of differential proteins between *Longissimus Lumborum* (LL) and *Psoas Major* (PM) at 45min postmortem.
Note: Detailed information for the full list of identified differential proteins is presented in Table 2.1.

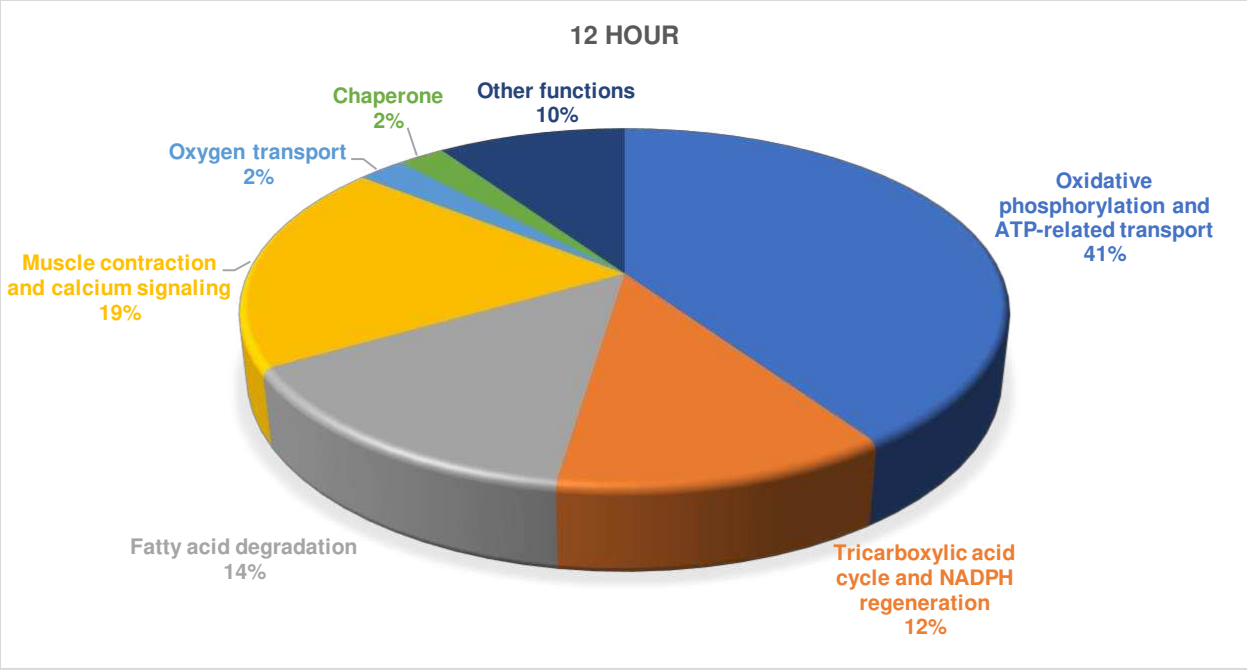

Figure 2.3.2. Distribution of the function clusters of differential proteins between *Longissimus Lumborum* (LL) and *Psoas Major* (PM) at 12h postmortem.
Note: Detailed information for the full list of identified differential proteins is presented in Table 2.1.

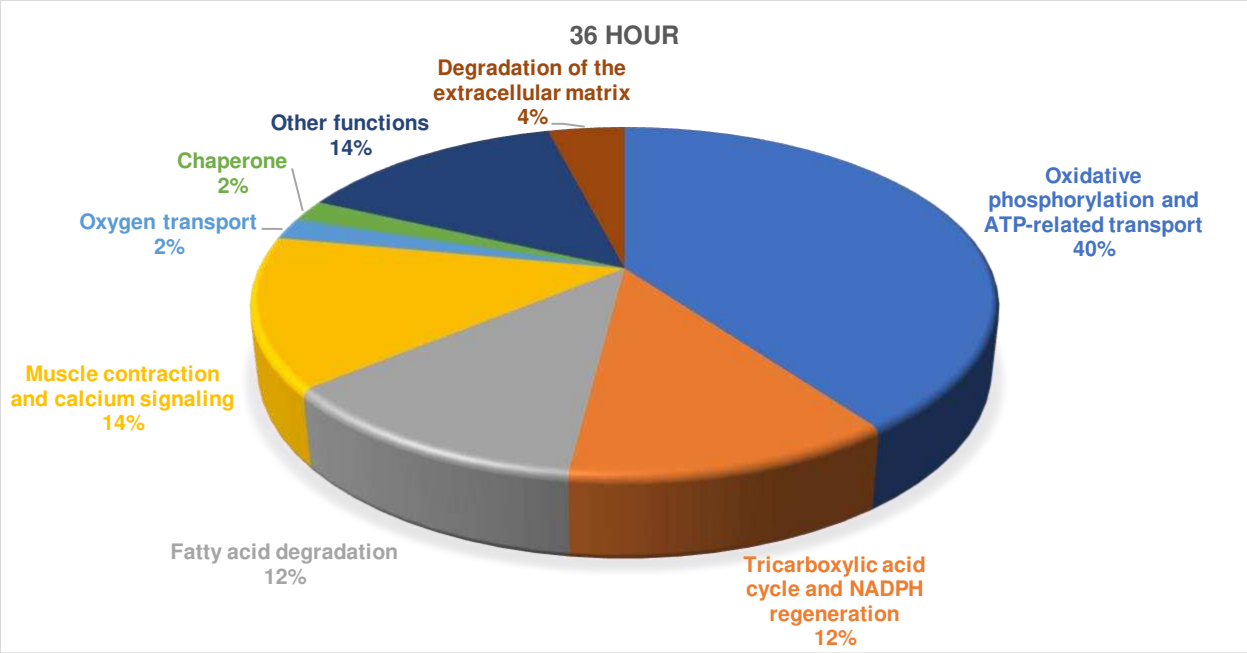

Figure 2.3.3. Distribution of the function clusters of differential proteins between *Longissimus Lumborum* (LL) and *Psoas Major* (PM) at 36h postmortem.
Note: Detailed information for the full list of identified differential proteins is presented in Table 2.1.

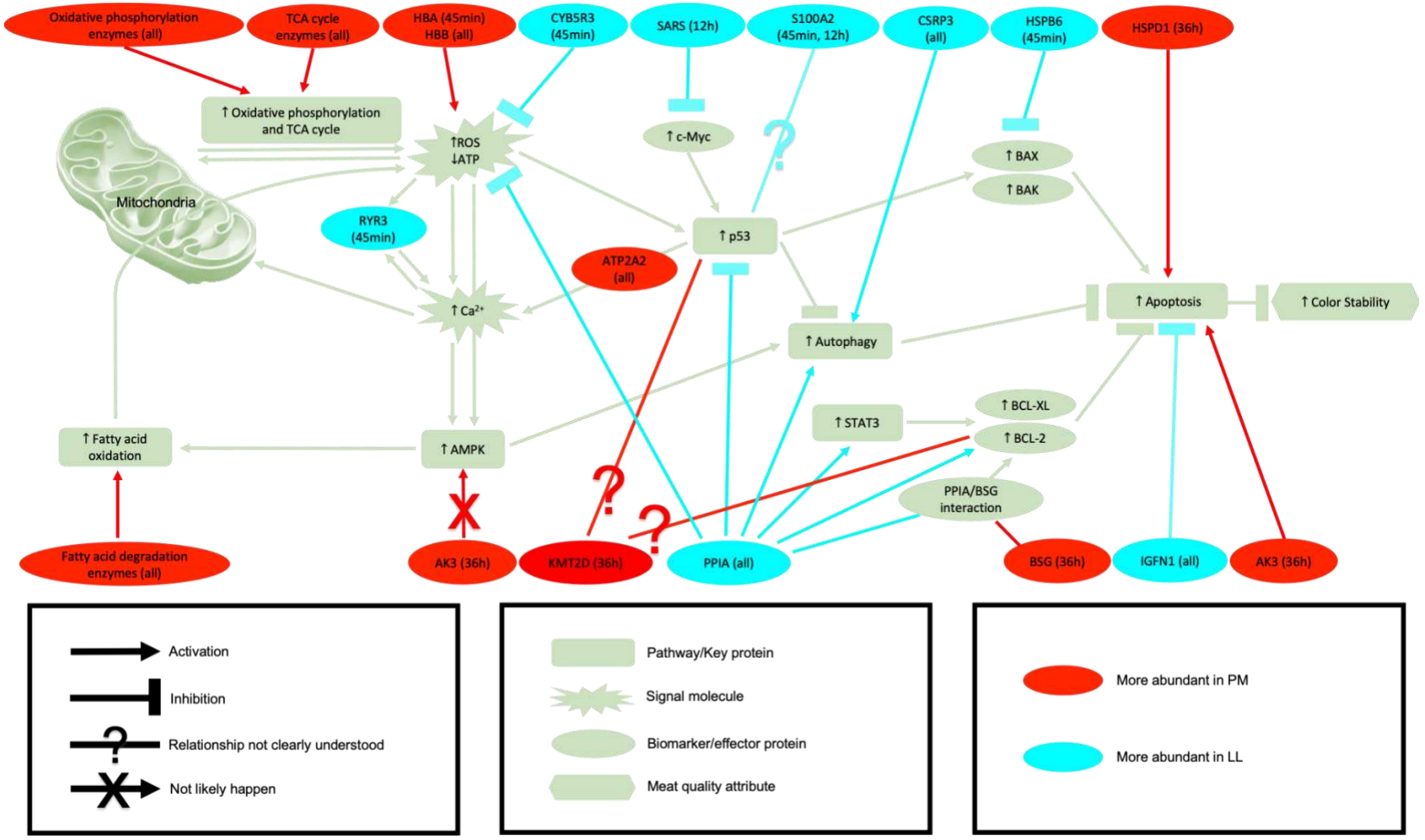

Figure 2.4. Potential key factors related with the differential proteins identified between *Longissimus Lumborum* (LL) and *Psoas Major* (PM) at early postmortem.

TCA cycle: tricarboxylic acid cycle; HBA(HBB): hemoglobin subunit alpha (beta); CYB5R3, NADH-cytochrome b5 reductase; SARS, cytoplasmic serine--tRNA ligase; S100A2, protein S100-A2; CSRP3, cysteine and glycine-rich protein 3; HSPB6, heat shock protein

beta-6; HSPD1, mitochondrial 60 kDa heat shock protein; RYR3, ryanodine receptor 3; ATP2A2, sarcoplasmic reticulum calcium ATPase 2; AK3: mitochondrial GTP:AMP phosphotransferase AK3; KMT2D, histone-lysine N-methyltransferase 2D; PPIA, peptidyl-prolyl cis-trans isomerase A; BSG, basigin isoform 2; IGFN1, immunoglobulin-like and fibronectin type III domain containing 1; ROS, reactive oxygen species; p53, tumor suppressor p53; Ca^{2+}, calcium; AMPK, AMP-activated protein kinase; STAT3, signal transducer and activator of transcription 3; c-Myc, Myc proto-oncogene protein; BAX, apoptosis regulator Bax; BAK, BCL-2 homologous antagonist/killer; BCL-XL, BCL-2-like 1 protein; BCL-2, B-cell lymphoma 2.

Note: The references for the potential functional relationships between the proteins, pathways, and signal molecules are provided in the results and discussion section under each of the differential proteins. The abbreviations of differentially abundant proteins with postmortem hours showing significant difference are presented in oval filled by blue or red

CHAPTER 3 – PULMONARY ARTERIAL PRESSURE IN FATTENED ANGUS STEERS AT MODERATE ALTITUDE INFLUENCES EARLY POSTMORTEM MITOCHONDRIA FUNCTIONALITY AND MEAT COLOR DURING RETAIL DISPLAY

3.1 Introduction

Pulmonary hypertension is a noninfectious disease of cattle at altitudes > 1524 m (5,000 ft), characterized by distension of the jugular vein, dyspnea, weakness, ascites, and edema of the jaw and brisket region. This condition results from a reduction in the partial pressure of oxygen in inspired air as elevation increases, which can lead to maladaptive changes in the cardiopulmonary system in an attempt to improve oxygen supply to body tissues. In particular, chronic alveolar hypoxia induces pulmonary arterial vasoconstriction and vascular wall remodeling that favors the development of right ventricular hypertrophy, which can progress to right-sided heart failure and death (Veit and Farrell, 1978; Holt and Callan, 2007; Stenmark et al., 2013). Approximately $60 million are lost annually due to complications associated with pulmonary hypertension in beef cattle, making it the leading cause of mortality in the Rocky Mountain region of the United States (Williams et al., 2012; Neary et al., 2013). Mean pulmonary arterial pressures (PAP) $\geqslant$50 mmHg are used as an indicator for pulmonary hypertension susceptibility in cattle (Holt and Callan, 2007). The measurement of mean PAP has allowed for genetic selection against cattle susceptible to pulmonary hypertension, resulting in the reduced incidence of high altitude disease (Shirley et al., 2008; Crawford et al., 2016; Cockrum et al., 2019).

Meat color and tenderness significantly influence consumers' purchase and repurchase decisions (Shackelford et al., 2001; Mancini and Hunt, 2005; Suman and Joseph, 2013; Neethling et al., 2017). These quality attributes have significant economic implications for the meat industry (Smith et al., 2000; Lusk et al., 2001). The conversion of muscle to meat is a complex process that

involves metabolic, chemical, and physical changes and can impact meat quality (Matarneh et al., 2017). As the main organelle responsible for energy metabolism in live animals, mitochondria have an important impact on the health of animals and their production efficiency (Bottje, 2019a, 2019b). In postmortem muscle, mitochondria can maintain structural integrity and oxygen consumption activity for up to 60 d (Tang et al., 2005), and their functionality contributes to meat color (Ramanathan and Mancini, 2018; Ramanathan et al., 2019) and tenderness (Wang et al., 2017a; Wang et al., 2018).

Recently, a study indicated that high PAP cattle entering the feedlot at moderate elevations (1,557 m) have around 20% higher feed to gain ratio due to excessive energy demands placed on their pulmonary-cardiovascular system (Thomas et al., 2019; Heffernan et al., 2020). However, the impact of pulmonary hypertension on meat quality attributes is still unknown. As noted above, muscle mitochondrial function is likely a key regulator of meat quality, but the effect of PAP on muscle mitochondria in beef cattle has not been previously investigated. Therefore, objectives of this study were to evaluate the effects of PAP on mitochondrial function during the early postmortem period and meat color during retail display.

3.2 Materials and methods

3.2.1 Animal care and use

The Institutional Animal Care and Use Committee at Colorado State University (approval number 17-7179A) approved all animal procedures.

3.2.2 Cattle information

The fattened Angus steers were placed into two groups determined by their mean PAP: high mean PAP (98 ± 13 mmHg; n = 5) and low mean PAP (41 ± 3 mmHg; n = 6). The animals (588 ± 38 kg body weight) were approximately 14-month-old and came from the same farm with

the same diet. The cattle were transported to a USDA-inspected meat laboratory in the Global Food Innovation Center of the Department of Animal Sciences at the Colorado State University. This experiment was originally designed as a balanced study, but one animal from the high PAP group died due to heart failure 8 d before slaughter. After resting time in the lairage, the animals were stunned, bled, and dehided according to commercial practice under USDA inspection. Approximately 5 g of *longissimus lumborum* (LL) was cut from the left side of each carcass at 2 and 48 h post-exsanguination. Half of the sample was immediately placed into ice-cold biopsy preservation medium (BIOPS; pH 7.1) containing 10 mM Ca-EGTA (0.1 μM free calcium), 20 mM imidazole, 20 mM taurine, 50 mM K-MES, 0.5 DTT, 6.56 mM $MgCl_2$, 5.77 mM ATP, and 15 mM phosphocreatine, whereas the other half of the sample was snap-frozen in liquid nitrogen.

3.2.3 Muscle sample preparation

Permeabilized muscle fibers from LL were prepared for high-resolution respirometry experiments as described previously (Li Puma et al., 2020). Briefly, muscle fibers were teased in ice-cold BIOPs solution containing 10 mM Ca-EGTA (0.1 μM free calcium), 20 mM imidazole, 20 mM taurine, 50 mM K-MES, 0.5 mM DTT, 6.56 mM $MgCl_2$, 5.77 mM ATP, and 15 mM phosphocreatine (pH 7.1) before incubation with 50 μg/mL saponin on ice for 20 min with gentle rocking to permeabilize cell membranes while leaving mitochondrial membranes intact (Pesta and Gnaiger, 2012). Permeabilized fiber bundles were then transferred to mitochondrial respiration medium (MiR05) containing 0.5 mM EGTA, 3 mM $MgCl_2$ hexahydrate, 60 mM lactobionic acid, 20 mM taurine, 10 mM KH_2PO_4, 20 mM HEPES, 110 mM sucrose, and 0.1% BSA (pH 7.1), and rinsed by rocking for 10 min on ice, followed by another identical 15-min rinse. Fiber bundles were then gently blotted dry for 10 to 15 s on Whatman paper and weighed immediately before adding approximately 6 mg to the 2-mL oxygraph chamber for experiments.

3.2.4 Mitochondrial respiration

Mitochondrial respiratory function was determined with permeabilized muscle fiber bundles collected at 2 and 48 h postmortem by high-resolution respirometry (HRR) using an Oxygraph-2k high-resolution respirometer (Oroboros Instruments, Innsbruck, Austria). Oxygen flux was monitored in real-time by resolving changes in the negative time derivative of the chamber oxygen concentration signal following standardized instrumental and chemical background calibrations using Datlab software (Oroboros Instruments). All respirometry data were collected at 37 °C in a hyperoxygenated environment (275–400 μmol/L) to avoid potential limitations in oxygen diffusion in the permeabilized fiber bundles (Li Puma et al., 2020). A detailed description of the respiration protocols and associated respiratory states generated by the sequential titration of each substrate is provided in Table 3.1. All the data collected were normalized by the weight of permeabilized fiber bundles.

3.2.5 Immunoblot analysis for mitochondrial oxidative phosphorylation (OXPHOS) proteins

Protein was isolated from muscle sample by mammalian lysis buffer (150 mM NaCl, 1 mM EDTA, 1 mM EGTA, 5 mM sodium pyrophosphate, 1 mM sodium orthovanadate, 20 mM sodium fluoride, 50 mL of Mammalian Protein Extraction Reagent [Thermo Scientific, 78501], 500 μL of Protease Inhibitor Cocktail [Sigma, P8340]). The concentration of the protein was detected by using BCA Protein Assay Kit (Thermo Scientific, 23225) according to manufacturer instructions and read by VERSA max microplate reader. Protein (30 μg) was loaded and separated using Invitrogen Bolt 4%–12% Bis-Tris (Invitrogen, NW04122BOX) and XCell SureLock Elecctrophorsis Cell (Invitrogen, EI0001). Then, it was transferred to PVDF membrane after activation with 100% methanol for 10 min. After three washes with TBST (100 mL of 10× TBS, 900 mL of diH2O, 1 mL of Tween [Fisher BioReagents, 125689]) (10× TBS: 24 g of Tris-base,

88 g of NaCl, 1 L of diH_2O, pH 7.6 adjusted by 6 N HCl), the membrane was blocked with 5% milk (10 mL of TBST, 0.5 g of Blotting-Grade Blocker [BIO-RAD, 170-6404]) for 1 h at room temperature. After blocking, the membrane was incubated in primary antibodies (1:1000 dilution) overnight at 4 °C. After three washes with TBST, the membrane was incubated in secondary antibodies (1:3000 dilution) for 1 h at room temperature. Then, the membrane was washed three times with TBST, incubated in SuperSignal West Dura Extended Duration Substrate (Thermo Scientific, 34075) for 30 s, imaged by UVP ChemStudio blot imager (Analytik Jena, Jena, Germany). Band density was normalized to AmidoBlack total protein (Sigma, A8181) and analyzed by ImageJ software. Mitochondrial OXPHOS protein abundance of each sample was estimated by the average of density of two protein bands, Complex II (SDHB) and Complex V (ATP5A).

3.2.6 Beef fabrication and meat sample allocation

After 12 d of aging (at 2 °C in the dark), strip loins (LL) were excised from left sides of beef carcasses (n = 5 for high PAP; n = 6 for low PAP), and six 2-cm-thick steaks were cut from each loin. The first steak from the anterior side of each loin was assigned to characterize pH and myoglobin concentration. The following five steaks from the anterior side were cut and assigned randomly to 1, 3, 5, 7, or 9 d of retail display overwrapped in polyvinyl chloride film (O_2 transmission = 23,250 mL × m^2 × d^{-1}, 72 gauge; Resinite Packaging Films, Borden, Inc., North Andover, MA).

3.2.7 Retail display

After packaging, steaks were placed in a display case maintained at 2 ± 1 °C under continuous lighting (4548 lx, 1810LX4000 LED FIXTURE; Kason, Newnan, GA; color rendering

index = 84; color temperature = 4,500 K). All steaks were rotated daily to minimize differences in light intensity or temperature caused by location.

3.2.8 Meat pH and myoglobin concentration

The pH of steaks was determined as described previously (Nair et al., 2016). Duplicate 5 g samples were homogenized in 30 mL diH_2O, and the pH was measured using an Accumet AE150 pH-meter (Fisher Scientific, Pittsburgh, PA).

Myoglobin concentration was determined according to the previous method (Faustman and Phillips, 2001) with modification. Duplicate 5 g frozen samples were homogenized in 35 mL ice cold 40 mM sodium-phosphate buffer at pH 6.8. The homogenate was filtered using Whatman No. 1 filter paper. The absorbance of the filtrate at 525 nm (A525) was recorded using a UV-1800 spectrophotometer (Shimadzu Inc., Candy, OR) with sodium phosphate buffer as blank. Myoglobin concentration was calculated using the following equation:

Myoglobin (mg/g)=[A525/(7.6 mM^{-1} cm^{-1}×1 cm)] x [17,000/1000]×8

where, 7.6 mM^{-1} cm^{-1} = millimolar extinction coefficient of myoglobin at 525 nm; 1 cm = path length of cuvette; 17,000 Da = average molecular mass of myoglobin; 8 = dilution factor.

3.2.9 Instrumental color

CIE lightness (L∗), redness (a∗), hue, and chroma values were measured at three random locations on the light-exposed steak surfaces with a HunterLab MiniScan LabScan EZ4500 colorimeter (Hunter Associates Laboratory, Reston, VA) using 2.54-cm diameter aperture, illuminant A, and 10° standard observer (AMSA, 2012). The instrument was calibrated with standard black and white plates. In addition, the ratio of reflectance at 630 and 580 nm (R630/580) was calculated as an indirect estimate of surface color stability.

3.2.10 Samples for metmyoglobin reducing activity and lipid oxidation

After color measurement, steaks displayed for 1, 3, 5, 7, or 9 d were halved, with one half being used for measuring MRA, and the other half being used to measure lipid oxidation. The interior of the steak half assigned to MRA was dissected parallel to the oxygenated surface to expose the interior (resulting in two interior pieces) and used for measuring MRA. Representative samples from the other half containing both oxygenated surface and interior were collected for measuring lipid oxidation.

3.2.11 Metmyoglobin reducing activity

Metmyoglobin reducing activity (MRA) was evaluated according to the method described previously (Zhai et al., 2019). Samples from the interior of steak halves (5 × 5 × 1.5 cm) were removed from the light-exposed surfaces and submerged in a solution of 0.3% sodium nitrite for 20 min at room temperature to induce metmyoglobin formation. Samples were blotted dry, vacuum packaged, and the reflectance spectra from 700 to 400 nm were recorded immediately on the light-exposed surface using a HunterLab LabSca XE colorimeter. The vacuum-packaged samples were then incubated at 30 °C for 2 h to induce reduction of metmyoglobin, and the reflectance data were taken again. The percentage of surface metmyoglobin (pre-incubation as well as post-incubation) was calculated based on K/S ratios and according to established formulas (AMSA, 2012). MRA was calculated using the following equation: Metmyoglobin reducing activity = 100 × [(% pre-incubation surface metmyoglobin − % post-incubation surface metmyoglobin)/% pre-incubation surface metmyoglobin].

3.2.12 Lipid oxidation

Lipid oxidation was analyzed employing thiobarbituric acid assay described previously (Yin et al., 1993; Nair et al., 2016). Briefly, 5-g representative samples, taken from multiple

locations, were mixed with 22.5 mL of 11% trichloroacetic acid, homogenized (PRO250, PRO Scientific Inc, Oxford, CT), and filtered using Whatman No. 1 filter paper. One milliliter of filtrate was mixed with 1 mL of aqueous thiobarbituric acid (20 mM) and incubated at 25 °C for 20 h. The absorbance of samples at 532 nm measured spectrophotometrically (UV-1800 spectrophotometer, Shimadzu Inc., Candy, OR) was reported as thiobarbituric acid reactive substances (TBARS).

3.2.13 Statistical analysis

A split-plot design was used to evaluate 1) the effects of PAP and postmortem hour on mitochondrial functions and 2) the effects of PAP and retail display day on instrumental color, MRA, and lipid oxidation. Samples were assigned to PAP x postmortem hour combinations for mitochondrial function evaluation and PAP x display day combinations for color, MRA, and lipid oxidation measurement. Data analysis was performed by R (version 3.6.1) using the lme4 package as a mixed model, where PAP (high or low), postmortem hour (or display day), and their interactions were fixed effects, and the random effect in the model was an individual animal. The differences between least-square means ($P < 0.05$) were determined by Tukey's multiple comparison.

A completely randomized design was used to evaluate the effects of PAP on ultimate pH and myoglobin concentration. A one-way ANOVA was conducted, followed by least-square means test (emmeans function in R) in order to better understand the difference between two PAP groups ($P < 0.05$).

3.3 Results and discussion

3.3.1 Muscle mitochondrial respiration and OXPHOS protein abundance

Mitochondrial respiratory capacity was determined in permeabilized LL muscle fiber bundles from high and low PAP cattle under a variety of substrate oxidation states using high-

resolution respirometry (Figure 3.1). Overall, high PAP muscle tended to have greater substrate oxidation (respiratory) capacity than low PAP muscles at 2 h postmortem (Figure 3.1B) but rapidly declined to be similar to low PAP muscle by 48 h postmortem (P = 0.008 and 0.023 for PAP × postmortem-time interaction in NL and NP states, respectively; Figure 3.1B). These differences were most robust under conditions of abundant substrate availability in the absence of ADP (NL or "leak" respiration) at 2 h postmortem, indicating a greater capacity of high PAP muscle for endogenous fuel oxidation premortem when ATP demand is absent. In addition, the "leak" respiration, which reflects the extent of proton leak across the inner mitochondrial membrane (Pesta and Gnaiger, 2012; Chicco et al., 2014), may also reflect lower muscle OXPHOS efficiency in high PAP animals premortem.

There was a decline in maximal OXPHOS-linked respiration supported by maximal delivery of NADH (N; P = 0.0007) and NADH + succinate (NS; P = 0.0003), as well as the maximal oxygen reductase capacity of complex IV (CIV; P =0.005) in LL muscle from 2 to 48 h postmortem. This was seen in both high and low PAP groups, suggesting that maximal LL respiratory capacity declined after animal slaughter independent of PAP. In addition, nearly identical maximal CIV enzymatic capacities were seen between high and low PAP groups at 2 and 48 h postmortem, suggesting that the "leak" respiration (NL; oxidative capacity under conditions of low ATP demand) accounted for the observed difference in OXPHOS-linked respiration (NP) between groups, not maximal respiratory capacity. Despite these variations in LL respiratory capacity between groups and postmortem timepoints, tissue OXPHOS protein expression was greater in low PAP than high PAP animals (P = 0.046) and remained stable from 2 to 48 h postmortem (Figure 3.2).

3.3.2 pH value, myoglobin concentration, and instrumental color of LL steak

No difference ($P = 0.2622$) in pH and myoglobin concentration of LL steak was observed between the high PAP group and low PAP group (Table 3.2). Therefore, these results suggested that PAP did not influence the ultimate pH and myoglobin concentration.

The PAP did not affect ($P > 0.05$) the L∗ value (lightness) during retail display (Table 3.3). However, a PAP × display-day interaction ($P = 0.017$) was observed for redness (a∗ value) during retail display. There were no difference ($P > 0.05$) observed in redness between the two PAP groups from days 1 to 7, but the low PAP group had higher ($P = 0.001$) redness than the high PAP group on day 9. Within treatment, redness decreased ($P = 0.032$) from days 1 to 7 in the high PAP group, whereas the low PAP group did not exhibit a decrease in redness until day 9 ($P = 0.007$). Display-day had a main effect on b∗ value regardless of PAP ($P = 0.000001$). The yellowness decreased ($P = 0.0001$) from days 1 to 9 for both PAP groups.

A PAP × display-day interaction was observed for chroma ($P = 0.039$), hue ($P = 0.007$), and the ratio of reflectance at 630 and 580 nm (R630/580; $P = 0.011$). There were no differences in chroma, hue, and R630/580 between high PAP and low PAP groups from days 1 to 7, but the low PAP group had higher chroma ($P = 0.004$), hue ($P = 0.0004$), and R630/580 value ($P = 0.0002$) than the high PAP group on day 9. Within treatment, chroma ($P = 0.0152$) and R630/580 ($P = 0.015$) significantly decrease from days 1 to 7 in the high PAP group, whereas the low PAP group did not show decreased chroma ($P = 0.004$) and R630/580 ($P = 0.0003$) value until day 9. Similarly, the hue value significantly decreased from days 1 to 9 in the high PAP group ($P = 0.0001$), whereas the low PAP group did not show any decrease during retail display ($P = 0.669$). Overall, our results suggested that although LL is a beef muscle with relevantly high color stability and long color

shelf-life (McKenna et al., 2005; Seyfert et al., 2006), the LL steaks from the high PAP group discolored faster than those from the low PAP group during simulated retail display.

3.3.3 MRA and lipid oxidation

A PAP × display-day interaction was observed for MRA ($P = 0.017$; Table 3.3). On day 5, the low PAP group had greater ($P = 0.035$) MRA than the high PAP group, but there was no difference ($P > 0.05$) between treatments on the other display days. Within treatment, MRA decreased ($P = 0.001$) from days 1 to 5 in the high PAP group, whereas the low PAP group did not show decreased MRA until day 7 ($P = 0.0002$). Display-day had a main effect on TBARS values regardless of PAP ($P = 0.00003$; Table 3.2); however, within the treatment, TBARS increased from days 1 to 7 in the high PAP group ($P = 0.005$), whereas no change ($P > 0.05$) was observed in low PAP group during display. Along with our observation of color attributes, these results suggested that the LL steaks from the high PAP group had lower color stability than those from the low PAP group during simulated retail display.

3.3.4 Discussion

Recently, it was reported that high PAP cattle entering the feedlot at moderate elevations have around 20% higher feed to gain ratio compared to low PAP cattle (Thomas et al., 2019; Heffernan et al., 2020). In the present study, muscle from high PAP cattle exhibited greater proton leak-associated respiration (NL; Figure 3.1B) than low PAP muscle at 2 h postmortem in the present study, which suggested lower OXPHOS efficiency and greater fuel oxidation rates under conditions of low ATP demand in vivo. Consistent with this interpretation, greater mitochondrial proton leak in broilers' skeletal muscle has been previously found in low feed efficiency than the high feed efficiency group (Bottje et al., 2009). Therefore, the observed lower feed efficiency in

high PAP cattle as compared to low PAP cattle could also be attributed to the higher proton leak-associated respiration in skeletal muscle and warrants additional study.

It is also worth noting that the difference in proton leak-associated respiration (NL; Figure 3.1B) and between two PAP groups disappeared as postmortem time extended, and a much greater postmortem decline happened in the high PAP's muscle OXPHOS-linked respiration (NP; Figure 3.1B) than low PAP cattle. These reflect a loss of mitochondrial integral function (membrane integrity or/and protein function) over time, which could be due to the accumulated damage from reactive oxygen species (ROS) known to be produced at high rates during leak respiration states (Li Puma et al., 2020). Previous research has shown that the broilers with pulmonary hypertension had greater ROS production from respiratory complexes I and III compared to the control group (Tang et al., 2002), which are the primary sites of ROS production during leak respiration (Jastroch et al., 2010). Moreover, increased oxidative stress level is often observed during pulmonary hypertension development (Mikhael et al., 2019).

Meat color is determined by biomolecular interaction between myoglobin, mitochondria, metabolites, and lipid oxidation (Ramanathan et al., 2020b). Metmyoglobin reducing activity is one of the essential biochemical processes that facilitates the sustained bright-red color of beef during retail display (Ledward, 1985). A greater and stable mitochondrial functionality can maintain meat color by improved MRA (Ramanathan and Mancini, 2018; Ramanathan et al., 2019). Conversely, mitochondria are the major ROS production sites in mammalian cells (Murphy, 2009; Mazat et al., 2020). In postmortem muscle, ROS can increase oxidative stress, damage mitochondrial membrane, and promote mitochondrial degradation, resulting in faster meat tenderization (Wang et al., 2018; Zhang et al., 2019a; Chen et al., 2020), increased lipid oxidation, and reduced color stability (Ke et al., 2017; Mancini et al., 2018; Mitacek et al., 2019). The faster

decline of MRA observed in the high PAP group steaks is consistent with these interpretations and further supports a link between muscle mitochondrial function and meat quality.

Additionally, there were differences in the mitochondrial OXPHOS protein abundance between the two PAP groups in this study. A previous human clinical study indicated that pulmonary arterial hypertension caused a decreased type I/type II muscle fiber ratio in skeletal muscle (Batt et al., 2013), which could explain the lower OXPHOS protein abundances in the high PAP group. The muscle fiber type was not measured in the current study. However, we hypothesize a similar change of muscle fiber ratio in skeletal muscle from the high PAP cattle.

The same clinical study also reported that increased phosphorylation of ryanodine receptor 1 receptors in skeletal muscle was caused by pulmonary arterial hypertension (Batt et al., 2013), which could result in destabilization and leakiness of the sarcoplasmic reticulum Ca^{2+} channel, disturbing the control of cytosolic free Ca^{2+} and impairing skeletal muscle contractility (Bellinger et al., 2008a, 2008b; Andersson and Marks, 2010). A diminished exercise capacity and atrophy of the quadriceps femoris muscle were observed in human with pulmonary arterial hypertension (Batt et al., 2013).

3.4 Conclusions

High PAP muscle had greater proton leak-associated respiration than low PAP muscles at 2 h postmortem, suggesting high PAP caused a lower OXPHOS efficiency and greater fuel oxidation rates under conditions of low ATP demand in premortem beef LL muscle. This difference could explain the lower feed efficiency in high PAP feedlot cattle compared to low PAP counterparts. Although maximal LL respiratory capacity declined after animal slaughter regardless of PAP, OXPHOS-linked respiration declined faster in high PAP muscle from 2 to 48 h postmortem, reflecting a faster loss of mitochondrial integral function (membrane integrity or/and

protein function). OXPHOS protein expression was also lower in high PAP compared to low PAP muscle, highlighting the need for further investigation into the potentially decreased type I/type II muscle fiber ratio in high PAP muscle. The muscle pH and myoglobin concentration were similar between the two PAP groups. However, the high PAP group steaks had lower a∗, chroma, hue, and R630/580 values than low PAP steers on day 9 and a lower MRA on day 5. High PAP group steaks also showed a significant increase in lipid oxidation on day 7, whereas no change was observed in the low PAP group during display. These results suggested that high PAP group LL had lower color stability than the low PAP group during simulated retail display, which could be partially attributed to the loss of muscle mitochondrial function at early postmortem by ROS damage in high PAP muscle.

Table 3.1. High-resolution respirometry protocols and associated respiratory flux states assessed in mitochondrial respiration experiment

Protocol titrations (final concentration in chamber)	High-resolution respirometry flux state	Explanation
Pyruvate (5 mM) + malate (1 mM)	NL	Proton leak-associated respiration supported by high NADH, but no ADP
ADP (2.5 mM)	NP	OXPHOS-linked respiration supported by pyruvate + malate oxidation
Glutamate (10 mM)	N	Maximal OXPHOS-linked respiration supported by NADH
Succinate (20 mM)	NS	Maximal OXPHOS-linked respiration supported by NADH and succinate
Ascorbate (2 mM) + TMPD (0.5 mM)	CIV	Maximal oxygen reductase capacity of Complex IV using an artificial electron donor

Table 3.2. pH and myoglobin concentration of beef longissimus steaks from cattle with different pulmonary arterial pressure (PAP; n = 6 for low PAP; n = 5 for high PAP).

Parameter	PAP	Value	SE[#]
pH	High	5.53	0.02
	Low	5.49	0.02
Myoglobin Concentration	High	7.67	0.33
	Low	7.66	0.30

[#]SE = standard error.

Table 3.3. Lightness (L* value), redness (a* value), chroma, hue, R630/580, MRA, and TBARS of beef longissimus steaks from cattle with different pulmonary arterial pressure (PAP) during display (n = 6 for low PAP; n = 5 for high PAP).

Parameter	PAP	Display d					SE
		1	3	5	7	9	
L* value	High	41.5 a[#]	38.9 b	40.1 ab	39.9 ab	40.4 ab	1.09
	Low	41.4	41.6	41.5	41.8	42.4	0.99
a* value	High	18.6 a,x	17.3 ab,x	17.3 ab,x	16.6 b,x	13.5 c,x	0.60
	Low	18.7 a,x	18.0 ab,x	18.1 ab,x	17.6 ab,x	16.6 b,y	0.55
b* value	High	13.9 a	12.7 bc	13.3 ab	12.7 bc	11.7 c	0.45
	Low	14.1 a	13.7 ab	13.8 ab	13.4 ab	13.0 b	0.41
Chroma	High	23.2 a,x	21.5 ab,x	21.9 ab,x	20.9 b,x	17.9 c,x	0.72
	Low	23.4 a,x	22.6 ab,x	22.8 ab,x	22.1 ab,x	21.1 b,y	0.66
Hue	High	53.2 a,x	53.8 a,x	52.5 a,x	52.7 a,x	48.8 b,x	0.60
	Low	52.9 a,x	52.6 a,x	52.6 a,x	52.6 a,x	51.9 a,y	0.55
R630/580	High	3.37 a,x	3.24 ab,x	3.09 ab,x	2.97 b,x	2.25 c,x	0.10
	Low	3.38 a,x	3.20 a,x	3.18 a,x	3.06 ab,x	2.81 b,y	0.09
% MRA	High	53.30 a,x	46.54 a,x	26.10 b,x	15.51 bc,x	3.43 c,x	7.43
	Low	55.49 a,x	43.39 ab,x	49.24 a,y	27.67 bc,x	21.52 c,x	6.79
TBARS	High	0.163 a	0.223 ab	0.305 ab	0.353 b	0.358 b	0.06
	Low	0.164	0.164	0.246	0.284	0.286	0.06

[#]Least square means for the same trait in a column without a common letter (x-y) differ ($P < 0.05$). Least square means in a row without a common letter (a-c) differ ($P < 0.05$).

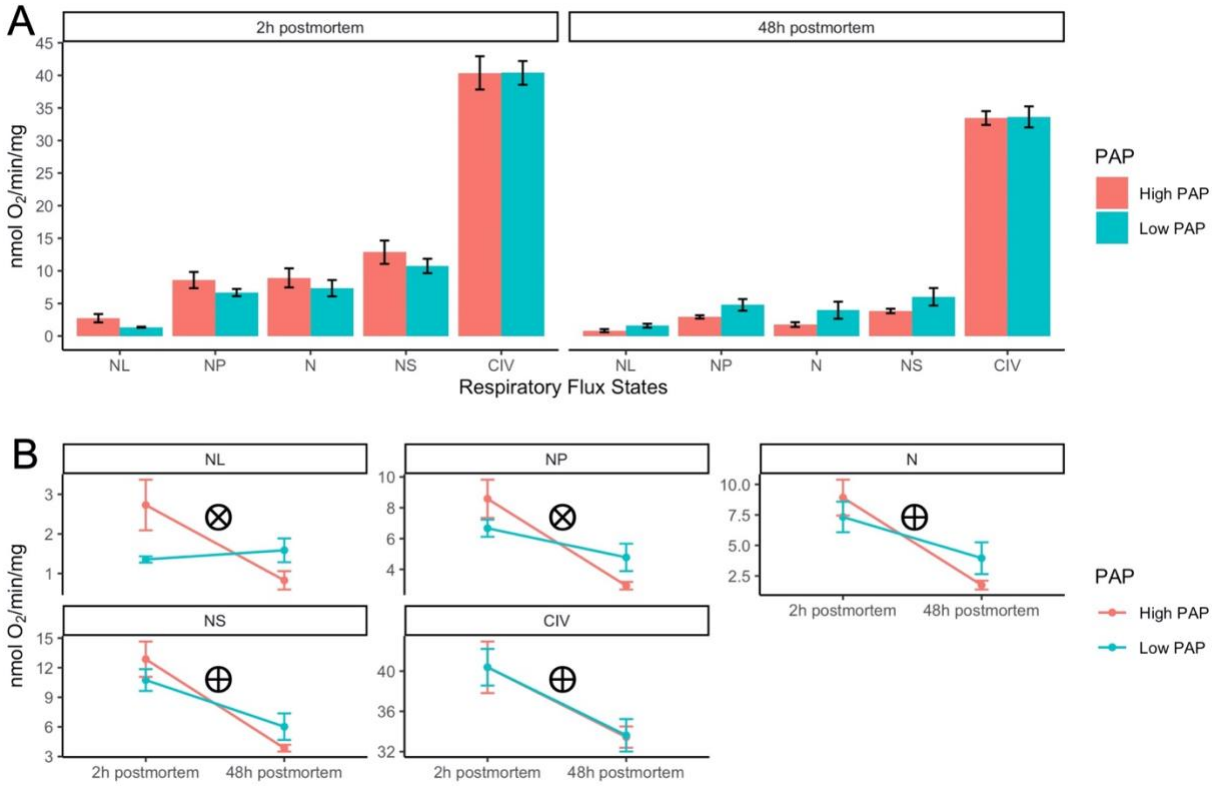

Figure 3.1. Muscle respiration under each respiratory flux state at 2 h and 48 h postmortem (n = 6 for low pulmonary arterial pressure (PAP); n = 5 for high PAP).
NL: proton leak-associated respiration supported by high NADH, but no ADP; NP: OXPHOS-linked-respiration supported by pyruvate + malate oxidation; N: OXPHOS-linked respiration supported by malate + pyruvate + glutamate oxidation; NS: maximal OXPHOS-linked respiration supported by NADH and succinate; CIV: maximal oxygen reductase capacity of Complex IV using an artificial electron donor; ⊗: a significant PAP × postmortem-hour interaction (NL: $P = 0.008$; NP: $P = 0.028$); ⊕: a significant postmortem-hour effect (N: $P = 0.0007$; NS: $P = 0.0003$; CIV: $P = 0.005$).
Note: Detailed information for each respiratory flux state is presented in Table 3.1.

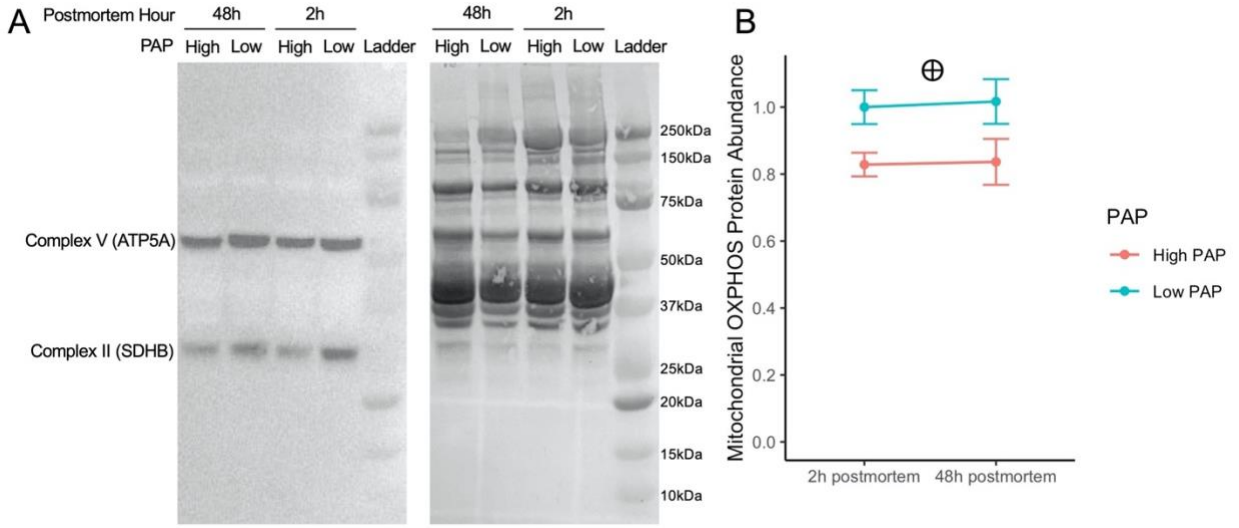

Figure 3.2A. Representative western blots of the abundance of complex II (SDHB) and complex V (ATP5A) and Amido Black stained total protein in beef longissimus steaks from cattle with different pulmonary arterial pressure (PAP) at early postmortem.

Figure 3.2B. Mitochondrial OXPHOS protein abundance in beef longissimus steaks from cattle with different PAP at early postmortem (n = 6 for low PAP; n = 5 for high PAP).

⊕: a significant PAP effect ($P < 0.05$).

CHAPTER 4 – VALIDATING THE ABILITY OF RAPID EVAPORATIVE IONIZATION MASS SPECTROMETRY TO DIFFERENTIATE LAMB FLAVOR PERFORMANCE BASED ON CONSUMER PERFERENCE

4.1 Introduction

Tenderness, juiciness, and flavor are the main factors influencing consumer choice and acceptance of cooked meat (Resurreccion, 2004). US consumers rank lamb last among the seven meats (beef, chicken, fish, lamb, pork, turkey, and veal) for taste and overall preference (Ward et al., 1995). Previous studies indicated that tenderness was the primary determinant for eating satisfaction, however the response for lamb has shifted toward flavor (Hoffman, 2015). Pre-slaughter and postmortem factors like animal breed, sex, age, feed, aging and cooking conditions all contribute to the flavor development of cooked meat (Calkins and Hodgen, 2007; Khan et al., 2015).

Rapid Evaporative Ionization Mass Spectrometry (REIMS) is a type of ambient ionization mass spectrometry which can be performed on intact samples (no sample processing required) and yields a chemical fingerprint that, when coupled with chemometrics, enables real-time evaluation of several complex traits from a single measurement. REIMS has been successfully used in meat science (Ross et al., 2021), as well as for characterization of production metrics such as aging method, aging time, and geographical origin of beef (Zhang et al., 2021a) and lamb (Zhang et al., 2021b). REIMS has also been used for prediction of beef quality attributes such as carcass type, production background, breed type, and muscle tenderness (Gredell et al., 2019). The results of these studies demonstrated the possibility of applying real-time metabolomic analysis in meat production and inspection systems. However, there are limited studies using REIMS analysis of raw meat to predict cooked meat flavor.

The I-Knife (monopolar) and Meat Probe (bipolar) are two types of ambient ionization sources (electrodes) available for generation of aerosols for REIMS analysis. The bipolar design of the Meat Probe provides the important advantage that it does not require removing samples from tissue origin for analysis. However, as this is still a new device the ability of data generated by Meat Probe to predict carcass background and meat flavor has not yet been investigated. Therefore, the objectives of this study were (1) to investigate the capability of REIMS (with I-Knife) to accurately predict cooked sheep meat flavor and carcass characteristics based on consumer response utilizing chemical fingerprints acquired from different types of raw samples, and (2) to compare the REIMS data generated by the two electrodes (Meat Probe vs. I-Knife) in their ability to differentiate carcass background and sheep meat flavor.

4.2 Materials and methods

4.2.1 Product selection

Samples were collected from 200 sheep carcasses representing two age classifications (n = 99 lamb, n =101 yearling), two diet classifications (n = 101 grass, n = 99 grain), and two gender classifications (n = 96 female, n = 104 male) from three different USDA inspected commercial harvest facilities located in both California and Colorado. Collections were completed between the months of September 2019 and January 2020. One external fat tissue sample and one fat free lean tissue sample was collected from one side of each carcass 45 min post-mortem. At 24 h post-mortem, one leg from each carcass was collected and transported back to Texas Tech University in Lubbock, TX for fabrication. The legs were boned and trimmed of all fat (external and seam), finely ground, and shaped into slider sized patties (2 inches in diameter). The patties were then vacuum packaged and stored at -80 °C. Patties were shipped overnight to Colorado State University for further analysis. For each carcass, one fat sample, one lean sample and one patty

were allocated to I-Knife REIMS analysis. An additional patty was allocated to Meat Probe REIMS analysis. Further, six patties were allocated for sensory analysis and were frozen (-20 °C) in vacuum bags until sensory analysis.

4.2.2 Consumer panel evaluation

The Colorado State University Institutional Review Board approved the procedures used in this study (IRB exemption # 2039, January 27, 2020). Consumers (n = 200) for the sensory evaluation were recruited from Fort Collins, CO, and the surrounding areas. The consumer demographics for the 200 participants of the sensory portion are presented in Table 4.1. Sensory panels were conducted in a lecture style classroom at Colorado State University in groups of 20 panelists per session. Patties were thawed at 2 to 4 °C for 24 h prior to consumer evaluation and cooked to an internal temperature of 71 °C using a combi-oven (Model SCC WE 61 E; Rational, Landsberg am Lech, Germany) with the temperature set to 204.5 °C and the humidity set to 0%. Patties were cooked for approximately 6 minutes to achieve a minimum internal temperature of 71 °C and immediately served to consumers. Panelists were each provided with a napkin, plastic fork, plastic knife, a toothpick, expectorant cup, and apple juice (10% apple juice dilution), water, and unsalted crackers to use as palate cleansers.

Each consumer evaluated 1 familiarization sample followed by 6 test samples (n = 7 samples/ panelist) in a predetermined and balanced order, representing variation in animal age class and production background, on an electronic tablet (iPad Pro; Model A1670; Apple Inc, Cupertino, CA) using a digital survey (Qualtrics core XM; Qualtrics Software, Provo, UT). Consumers rated each sample for flavor intensity, flavor liking, and overall liking on 100 mm continuous line scales anchored at both ends and the midpoint with 0 = extremely low, and extremely dislike and 100 = extremely high and extremely like. Consumers were also asked to

evaluate flavor intensity acceptance, flavor acceptance, off flavors presence, and overall acceptance with a binary ("yes" or "no") answer and perceived acceptance levels were left to the consumers interpretation.

4.2.3 Sensory data binary classification

In addition to the three carcass background classifications (age, diet, and gender), five sensory attributes were further classified according to consumer's evaluation (Table 4.2). The flavor intensity model was also classified into three groups which included 1) mild, 2) medium, and 3) intense. Flavor intensity groupings were developed based on a normal standard curve using plus or minus one standard deviation from the mean as separation. Within each of the rest of four sensory attributes, average liking score and binary responses ("yes" or "no") for each sample were summarized. The attributes were further classified into two groups (acceptable or unacceptable) using the average liking scores of each attribute (analyzed using an analysis of variance). To be classified as "acceptable," one of the following requirements had to be met: 1) average of liking score of a class (number of "yes" in response) had to be greater than the overall mean of all classes, or 2) the upper 95% confidence interval of the mean of liking score of a class had to encompass the overall mean of all classes. Four model sets (Table 4.2) were defined by the following sensory attributes: flavor intensity acceptance, flavor acceptance, off flavors presence, and overall acceptance. Finally, for intensity acceptance, flavor acceptance, and overall acceptance, classes (number of "yes" in response) 5 and 6 were classified as "acceptable," and classes 0, 1, 2, 3, and 4 were categorized as "unacceptable." For off flavors presence, classes (number of "yes" in response) 0 and 1 were classified as "acceptable," and classes 2, 3, 4, 5, and 6 were categorized as "unacceptable."

4.2.4 Rapid evaporative ionization mass spectrometry (REIMS)

Chemical fingerprints of fat tissues, lean tissues, and ground sensory patties were acquired using REIMS. Prior to analysis, samples were thawed at 0–4 °C for 16–24 h. Samples were analyzed using a Synapt G2 Si Q-ToF mass spectrometer (Waters Corporation, Milford, MA), fitted with a REIMS ionization source coupled with a monopolar electrosurgical hand piece ("I-Knife," Waters Corporation) or a bipolar electrosurgical hand piece ("Meat Probe," Waters Corporation) powered by an Erbotom ICC 300 electrosurgical generator (Erbe Elektromedizin GmbH, Tubingen, Germany) using "dry cut" mode at a power of 30 V for lean and patty samples or 50 V for fat sample.

A continual flow (200 μL/min) of 200 ng/mL leucine-enkephalin was introduced directly to the REIMS source during sampling. The heater bias was set to 80 V. At least five "burns" were collected for each sample within a 2.54 × 2.54 cm square from the center of the sample, with each burn lasting approximately 3 sec. Spectra were collected in negative mode ionization from 50–1,500 m/z. Preprocessing was performed using the AMX recognition software version 1.0.2184.0 (Waters Corporation), including lock mass correction (leucine-enkephalin), background subtraction using standard Masslynx preprocessing algorithms, and normalization to total ion current. Peak binning was performed at intervals of 0.5 m/z resulting in a total of 2,900 bins. The bins from the five burns were summed to create a single value for each sample. Mass bins in the range of 550–600 were excluded from the data matrix to remove the internal standard signal (leucine-enkephalin, m/z 554.632).

To evaluate the capability of REIMS to accurately identify and predict cooked sheep meat flavor and carcass characteristics based on consumer response utilizing chemical fingerprints acquired from raw samples by I-Knife, mass bins in the range of 100 to 550 and of 660 to 1000

were selected for further analysis resulting in a final data matrix containing 1,700 variables (m/z bins) and 200 observations (samples) for each sample.

For comparison of the data generated by the two electrodes (Meat Probe vs. I-Knife) mass bins in the range of 50 to 550 and 660 to 1500 were used for further analysis resulting a in a final data matrix containing 2,800 variables (m/z bins) and 200 observations (samples) for each sample. The time required for REIMS analysis per sample using Meat Probe and I-Knife was also recorded. All data matrixes can be found in supplemental files.

4.2.5 REIMS data analysis

Data reduction, machine learning, and evaluation of predictive models was performed within the R statistical environment (R Core Team, 2021). Data were grouped together to create the desired classifications for each model set (Table 4.2) defined as: age, diet, gender, flavor intensity level, flavor intensity acceptance, flavor acceptance, off flavors presence, and overall acceptance.

4.2.6 Data pre-processing with dimension reduction

Dimension reduction was performed using (i) feature selection (FS) or (ii) principal component analysis followed by feature selection (PCA-FS) as described by Gredell et al. (2019). The PCA dimension reduction was performed using the PCA function in the package FactoMineR with unit variance scaling (Husson et al. 2018). The FS was performed separately for each model set in the study (i.e., overall acceptance) using the caret R package (Kuhn, 2008; Kuhn and Johnson, 2013). All 2,800 m/z bins were first pre-processed by removing highly correlated m/z bins (Pearson's $|r| > 0.90$) followed by the rfe function and finally assessed with 5-fold cross validation. The PCA-FS consisted of performing a similar feature selection process on the principal components rather than the 2,800 mass bins with 10-fold cross validation. For all model

assessments performed in this study, leave-one-out cross validation refers to the removal of one sample as a validation set where the remaining samples are used as the training set. This procedure was repeated for every sample, and average prediction accuracy was recorded.

4.2.7 Machine learning algorithms to predict carcass background and meat sensory evaluation

In total, the accuracy of fourteen machine learning algorithms were compared for each model set. These included: (1) support vector machine with a radial kernel (SVM-Radial), (2) support vector machine with a linear kernel (SVM-Linear), (3) support vector machine with a polynomial kernel (SVM-Poly), (4) K-nearest neighbor (Knn), (5) random forest (RF), (6) linear discriminant analysis (LDA), (7) penalized discriminant analysis (PDA), (8) logistic boosting (LogitBoost), (9) extreme gradient boosting (XGBoost), (10) stochastic gradient boosting (GBM), (11) elastic-net regularized generalized linear model (GLMNET), (12) multivariate adaptive regression spline (Earth), (13) classification and regression trees with rpart (Rpart), and (14) bagged classification and regression trees (Treebag). An initial screening of all the machine learning algorithms was performed using the train function from the caret package.

For I-Knife tissue comparison (fat vs. lean vs. patty), partial least squares discriminant analysis (PLSDA) is included at fifteenth machine learning algorithm. PLSDA is not supported in the train function, and thus PLSDA models were constructed using the plsDA function (Pérez-Enciso and Tenenhaus, 2003) built into the DiscriMiner package. For electrode comparison, generalized linear model (GLM) is included at fifteenth machine learning algorithm and performed using the train function from the caret package. For each of the eight model sets (age, diet, gender, flavor intensity level, flavor intensity acceptance, flavor acceptance, off flavors presence, and overall acceptance), the fifteen machine learning algorithms were applied to data following the two pre-processing options, FS and PCA-FS reduction.

Leave-one-out cross validation was used to evaluate the prediction accuracy (correct predictions/total predictions) of all fifteen machine learning algorithms in order to reduce the bias and increase repeatability (James et al., 2021). The best performing model (in terms of prediction accuracy based on leave-one-out cross validation) for each model set were recorded (Table 4.3).

4.3 Results and discussion

4.3.1 Tissue comparison of I-Knife REIMS prediction

In the current study, three types of tissue were analyzed by I-Knife REIMS to differentiate carcass background and sheep meat flavor based on consumer preference. Combinations of two methods of dimension reduction and fifteen machine learning algorithms were used to explore the prediction accuracy of REIMS data on eight model sets (Table 4.2; age, diet, gender, flavor intensity level, flavor intensity acceptance, flavor acceptance, off flavors presence, and overall acceptance). The performance of each machine learning algorithm and data reduction combination was assessed in the initial screening step (Appendix A 1-8). Performance was evaluated in terms of prediction accuracy using a leave-one-out cross validation.

The maximum prediction accuracy of data generated by I-Knife REIMS based on leave-one-out cross validation varied in each model set and across sample types (Table 4.3). The maximal prediction accuracies from models based on data collected from fat tissue REIMS analysis for each classification model set were: age (76.5%), diet (94.5%), gender (73%), intensity level (73.5%), intensity acceptances (82%), flavor acceptance (81%), off flavors presence (93%), and overall acceptance (81%). The maximal prediction accuracies from models based on data collected from lean tissue REIMS analysis for each classification model set were: age (82%), diet (85%), gender (71.5%), intensity level (73%), intensity acceptances (84%), flavor acceptance (80.5%), off flavors presence (75%), and overall acceptance (84%). The maximal prediction

accuracies from models based on data collected from patty REIMS analysis for each classification model set were: age (78.5%), diet (92.5%), gender (76%), intensity level (69.5%), intensity acceptances (94%), flavor acceptance (79.5%), off flavors presence (755%), and overall acceptance (83%).

Regardless of tissue type, from high to low, the maximum prediction accuracies of the eight classification model sets were: diet (94.5%), flavor intensity acceptance (94%), off flavors presence (93%), overall acceptance (85.1%), age (82%), flavor acceptance (81%), gender (76%), and flavor intensity level (73.5%). For each classification model set, the maximum prediction accuracy achieved by I-Knife REIMS varied among different tissue types (Figure 4.3). Fat tissue had higher maximum prediction accuracies for diet (94.5%), off flavors presence (93%), flavor acceptance (81%), and flavor intensity level (73.5%), while lean tissue has higher maximum prediction accuracies for overall acceptance (85.1%) and age (82%). Patty had higher maximum prediction accuracies for flavor intensity acceptance (94%) and gender (76%).

According to previous studies, REIMS can be used for prediction of beef quality attributes such as carcass type, production background, breed type, and muscle tenderness (Gredell et al., 2019) as well as aging method, aging time, and geographical origin of beef (Zhang et al., 2021a) and lamb (Zhang et al., 2021b). In the current study, regardless of tissue type, the maximum prediction accuracies of diet, flavor intensity acceptance, off flavors presence, overall acceptance, age, and flavor acceptance classification were greater than 80%, which for the first time indicated that REIMS analysis of raw meat coupled with machine learning algorithm can accurately predict cooked sheep meat flavor and carcass characteristics.

Except for flavor intensity acceptance and gender, I-Knife REIMS data from fat and lean tissue collected at 45 min postmortem achieved higher maximal prediction accuracies for diet

(94.5%), off flavors presence (93%), overall acceptance (84%), age (82%), flavor acceptance (81%), and flavor intensity level (73.5%). These results demonstrated that REIMS data collected from both lean and fat tissue at 45 min postmortem is reflective of meat sensory data collected at 24 h postmortem as well as carcass background information.

For carcass background prediction, the highest prediction accuracy was achieved for diet classification by fat tissue (94.5%) using the support vector machine with a polynomial kernel (SVM-Poly; 80 mass-bins) model. The second highest prediction accuracy was achieved for age classification by lean tissue (82%) using the support vector machine with a polynomial kernel (SVM-Poly; 75 mass-bins) model. The next highest prediction accuracy was achieved for gender classification by patty (76%) using the support vector machine with a radial kernel (SVM-Radial; 29 principal components) model.

For cooked sheep meat flavor prediction, the highest prediction accuracy was achieved for flavor intensity acceptance by patty (94%) using the generalized linear model (GLM; 1474 mass-bins). The second highest prediction accuracy for sheep meat flavor was achieved for off flavors presence by fat tissue (93%) using the generalized linear model (GLM; 1295 mass-bins). The next highest prediction accuracy was achieved for overall acceptance by lean tissue (84%) using the SVM-Poly (35 principal components) model. Characterizations of flavor acceptance were also evaluated, and the highest prediction accuracy (81%) was achieved by fat tissue using stochastic gradient boosting model (GBM; 49 principal components). The highest prediction accuracies for flavor intensity level was achieved using Svm Poly model to 73.5% by fat tissue with 23 principal components.

4.3.2 Electrodes comparison

In the current study, two types of REIMS electrodes were used to differentiate carcass background and sheep meat flavor based on consumer preference. Combinations of two methods of dimension reduction and fifteen machine learning algorithms were used to explore the prediction accuracy of REIMS data on eight classification model sets (Table 4.2; age, diet, gender, flavor intensity level, flavor intensity acceptance, flavor acceptance, off flavors presence, and overall acceptance). The performance of each machine learning algorithm and data reduction combination was assessed in the initial screening step (Appendix B 1-8). Performance was evaluated in terms of prediction accuracy using a leave-one-out cross validation.

The maximal prediction accuracies from models based on data generated by I-Knife REIMS analysis (Table 4.4) for each classification were: age (75%), diet (92%), gender (73%), intensity level (73%), intensity acceptances (84.5%), flavor acceptance (81.5%), off flavors presence (78%), overall acceptance (84%). The maximal prediction accuracies from models based on data generated by Meat Probe REIMS analysis (Table 4.4) for each classification were: age (81.5%), diet (90%), gender (72.5%), intensity level (71%), intensity acceptances (86%), flavor acceptance (80%), off flavors presence (77.5%), overall acceptance (85%).

Data generated using the Meat Probe resulted in models with better or similar prediction accuracies of carcass background (age, diet, and gender) and consumer preference (intensity acceptance, flavor acceptance, off flavors presence, and overall acceptance) as compared to models based on data generated using the I-Knife.

For carcass background prediction, the highest prediction accuracy was achieved for diet classification by I-Knife (92%) and Meat Probe (90%) using the support vector machine with a polynomial kernel (SVM-Poly; 34 mass-bins) model and support vector machine with a linear

kernel (SVM Linear; 29 principal components) model, respectively. The second highest prediction accuracy was achieved for age classification by I-Knife (75%) and Meat Probe (81.5%) using the K-nearest neighbor (Knn; 1949 mass-bins) model and SVM-Poly (86 principal components) model, respectively. The following highest prediction accuracy was achieved for gender classification by I-Knife (73%) and Meat Probe (72.5%) using the random forest (RF; 79 principal components) model and XGBoost (17 principal components) model, respectively.

For cooked sheep meat flavor prediction, the highest prediction accuracy was achieved for flavor intensity acceptance by I-Knife (84.5%) and Meat Probe (86%) using the extreme gradient boosting (XGBoost; 33 principal components) model and Svm-Linear (29 principal components) model, respectively. The second highest prediction accuracy was achieved for overall acceptance by I-Knife (84%) and Meat Probe (85%) using the XGBoost (71 mass-bins/33 principal components) model and partial least squares discriminant analysis (PLSDA; 114 mass-bins) model, respectively. The following highest prediction accuracy was achieved for flavor acceptance by I-Knife (81.5%) and Meat Probe (80%) both using the XGBoost model with 63 mass-bins and 49 principal components, respectively. Characterizations of flavor intensity level were also evaluated, and the highest prediction accuracies (73% for I-Knife and 71% for Meat Probe) were achieved using stochastic gradient boosting model (GBM; 76 mass-bins) and XGBoost model (995 mass-bins). The highest prediction accuracy for off flavor presence was achieved both using Svm Poly model to 78% for I-Knife with 40 principal components and to 77.5% for Meat Probe with 33 principal components.

Analysis using the Meat Probe required 45 seconds per sample (5 readings), whereas analysis using the I-Knife required 90 seconds per sample (5 readings). Also, REIMS analysis using I-Knife required the cleaning procedure around every 80 samples (400 reading), while

REIMS analysis using Meat Probe required cleaning procedure around every 160 samples (800 readings), which indicated that Meat Probe generates cleaner signal than I-Knife.

4.4 Conclusions

In summary, these data demonstrate that REIMS analysis of raw meat samples can be used to accurately predict and classify cooked sheep meat flavor and carcass characteristics (based on consumer response). Specifically, the lean and fat tissue collected at 45 min postmortem can be used to predict carcass characteristics and post rigor meat flavor. Models for diet, flavor intensity acceptance, off flavors presence, overall acceptance, age, and flavor acceptance achieved prediction accuracies higher than 80%. In addition, data generated using the Meat Probe resulted in models with better or similar prediction accuracies of carcass background (age, diet, and gender) and consumer preference (intensity acceptance, flavor acceptance, off flavors presence, and overall acceptance) as compared to models based on data generated using the I-Knife. The Meat Probe was more user-friendly, faster, and cleaner than I-Knife for REIMS analysis. Further investigations are necessary to evaluate the use of the Meat Probe for REIMS analysis in other applications.

Table 4.1. Demographic characteristics of consumers (N = 200) who participated in consumer sensory panels.

Characteristic	Response	Number of Consumer
Gender	Female	112
	Male	97
	No response	1
Marital Status	Married	79
	Single	120
	No response	1
Age	20-29 years	109
	30-39 years	35
	40-49 years	19
	50-59 years	22
	60 years or older	14
	No response	1
Ethnicity	African-American	2
	Asian	22
	Caucasian/white	134
	Hispanic	24
	Native American	6
	Mixed race	8
	No response	4
Household income	Under $25,000	66
	$25,001-$34,999	15
	$35,000-$49,999	22
	$50,000-$74,999	27
	$75,000-$99,999	22
	$100,000-$199,999	30
	Over $199,999	16
	No response	2
Education level	Non-high school/graduate	2
	High school graduate	5
	Some college/technical school	38
	College graduate	74
	Post-college graduate	81
	No response	2

Table 4.2. Summary of classification groupings and number of observations used for each of the six model sets

	Prediction Model Sets							
	Age	**Diet**	**Gender**	**Flavor Intensity Level**	**Flavor Intensity Acceptance**	**Flavor Acceptance**	**Off Flavor Presence**	**Overall Acceptance**
Classifications (number of observations)	Lamb (99)	Grass (101)	Male (104)	Intense (34)	Acceptable (159)	Acceptable (151)	Absence (116)	Acceptable (157)
	Yearling (101)	Grain (99)	Female (96)	Medium (135)	Unacceptable (41)	Unacceptable (49)	Presence (84)	Unacceptable (43)

Table 4.3. Summary of final prediction accuracies in each tissue type based on leave-one-out cross validation for the top machine learning algorithm and data reduction approach combination for each model set

Model Set	Tissue Type	Dimension Reduction Approach	Number of Predictors	Machine Learning Algorithm	Final Accuracy
Age	Fat	PCA-FS	126 PCs	Svm Poly/PDA/LDA	0.765
	Lean	FS	75 mass-bins	Svm Poly	0.820
	Patty	FS	113 mass-bins	RF	0.785
Diet	Fat	FS	80 mass-bins	Svm Poly	0.945
	Lean	PCA-FS	40 PCs	XGBoost	0.850
	Patty	FS	18 mass-bins	Svm Poly	0.925
Gender	Fat	FS	4 mass-bins	LogitBoost	0.730
	Lean	PCA-FS	24 PCs	Svm Poly	0.715
	Patty	PCA-FS	29 PCs	Svm Radial	0.760
Flavor Intensity Level	Fat	PCA-FS	23 PCs	Svm Poly	0.735
	Lean	PCA-FS	29 PCs	Svm Poly	0.730
	Patty	FS/PCA-FS	318 mass-bins/ 22 PCs	XGBoost	0.695
Flavor Intensity Acceptance	Fat	PCA-FS	42 PCs	XGBoost	0.820
	Lean	PCA-FS	24 PCs	XGBoost/Svm Poly	0.840
	Patty	FS	1474 mass-bins	GLM	0.940
Flavor Acceptance	Fat	PCA-FS	49 PCs	GBM	0.810
	Lean	PCA-FS	31 PCs	GBM	0.805
	Patty	PCA-FS	47 PCs	Svm Poly	0.795
Off Flavors Presence	Fat	FS	1295 mass-bins	GLM	0.930
	Lean	PCA-FS	130 PCs	Svm Poly	0.750
	Patty	PCA-FS	59 PCs	Svm Poly	0.755
Overall Acceptance	Fat	PCA-FS	47 PCs	XGBoost	0.810
	Lean	PCA-FS	35 PCs	Svm Poly	0.840
	Patty	FS/PCA-FS	46 mass-bins/32 PCs	RF/Svm Linear	0.830

PCA-FS: principal component analysis followed by feature selection; FS: feature selection; PCs: principal components.

Table 4.4. Summary of final prediction accuracies in each electrode based on leave-one-out cross validation for the top machine learning algorithm and data reduction approach combination for each model set

Model Set	Electrode	Dimension Reduction Approach	Number of Predictors	Machine Learning Algorithm	Final Accuracy
Age	I-Knife	FS	1949 mass-bins	Knn	0.750
	Meat Probe	PCA-FS	86 PCs	Svm Poly	0.815
Diet	I-Knife	FS	34 mass-bins	Svm Poly	0.920
	Meat Probe	PCA-FS	29 PCs	Svm Linear	0.900
Gender	I-Knife	PCA-FS	79 PCs	RF	0.730
	Meat Probe	PCA-FS	17 PCs	XGBoost	0.725
Flavor Intensity Level	I-Knife	FS	76 mass-bins	GBM	0.730
	Meat Probe	FS	995 mass-bins	XGBoost	0.710
Flavor Intensity Acceptance	I-Knife	PCA-FS	33 PCs	XGBoost	0.845
	Meat Probe	PCA-FS	29 PCs	Svm Linear	0.86
Flavor Acceptance	I-Knife	FS	63 mass-bins	XGBoost	0.815
	Meat Probe	PCA-FS	49 PCs	XGBoost	0.800
Off Flavors Presence	I-Knife	PCA-FS	40 PCs	Svm Poly	0.780
	Meat Probe	PCA-FS	33 PCs	Svm Poly	0.775
Overall Acceptance	I-Knife	FS/PCA-FS	71 mass-bins/33 PCs	XGBoost	0.84
	Meat Probe	FS	114 mass-bins	PLSDA	0.85

PCA-FS: principal component analysis followed by feature selection; FS: feature selection; PCs: principal components.

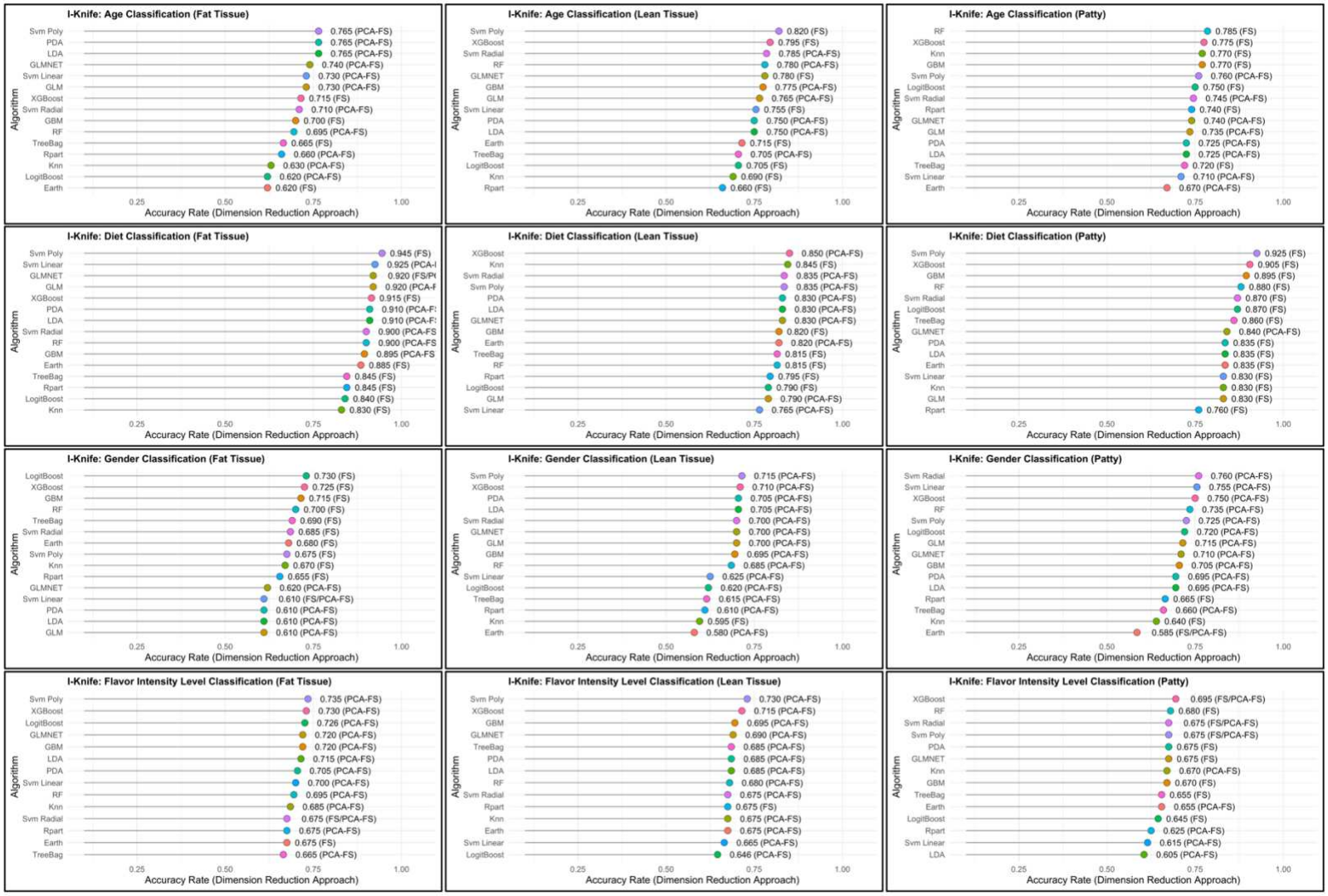

Figure 4.1A Prediction accuracies in each tissue type (based on leave-one-out cross validation) for the top performing machine learning algorithm and data reduction approach combinations for age, diet, gender, and flavor intensity level classification. PCA-FS: principal component analysis followed by feature selection; FS: feature selection; PCs: principal components.

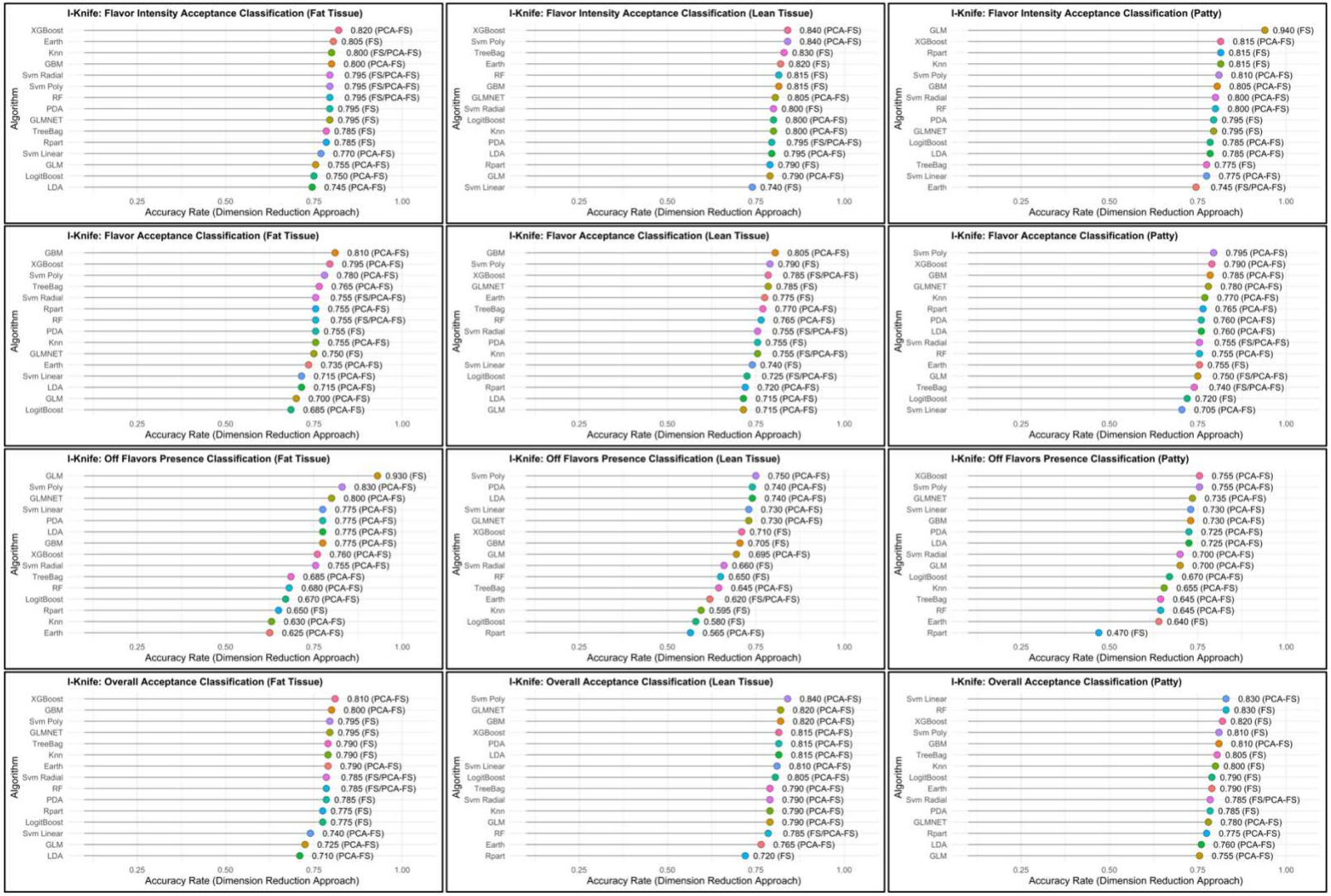

Figure 4.1B Prediction accuracies in each tissue type (based on leave-one-out cross validation) for the top performing machine learning algorithm and data reduction approach combinations for age, diet, gender, and flavor intensity level classification. PCA-FS: principal component analysis followed by feature selection; FS: feature selection; PCs: principal components.

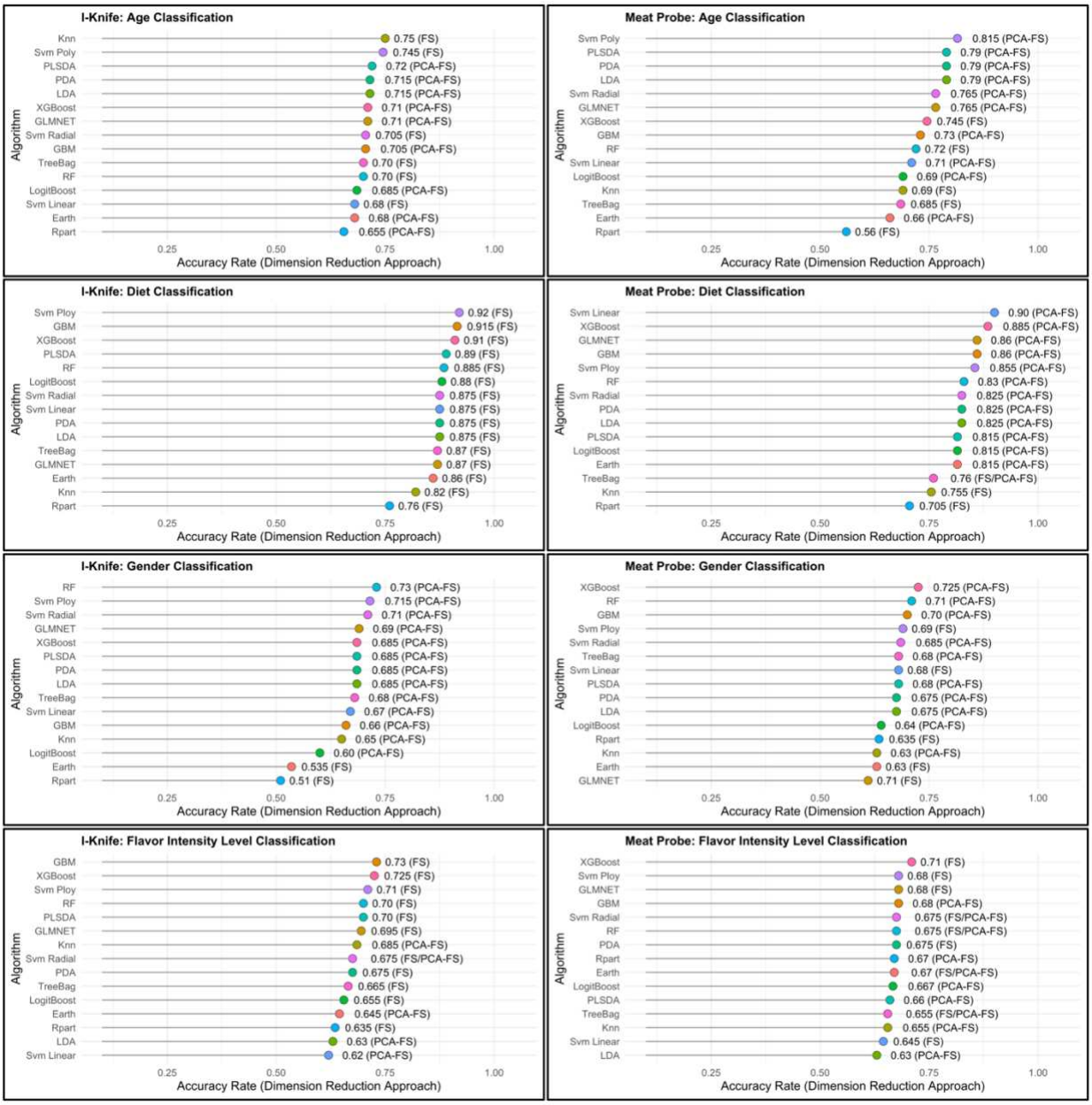

Figure 4.2A Prediction accuracies in each electrode (based on leave-one-out cross validation) for the top performing machine learning algorithm and data reduction approach combinations for age, diet, gender, and flavor intensity level classification. PCA-FS: principal component analysis followed by feature selection; FS: feature selection; PCs: principal components.

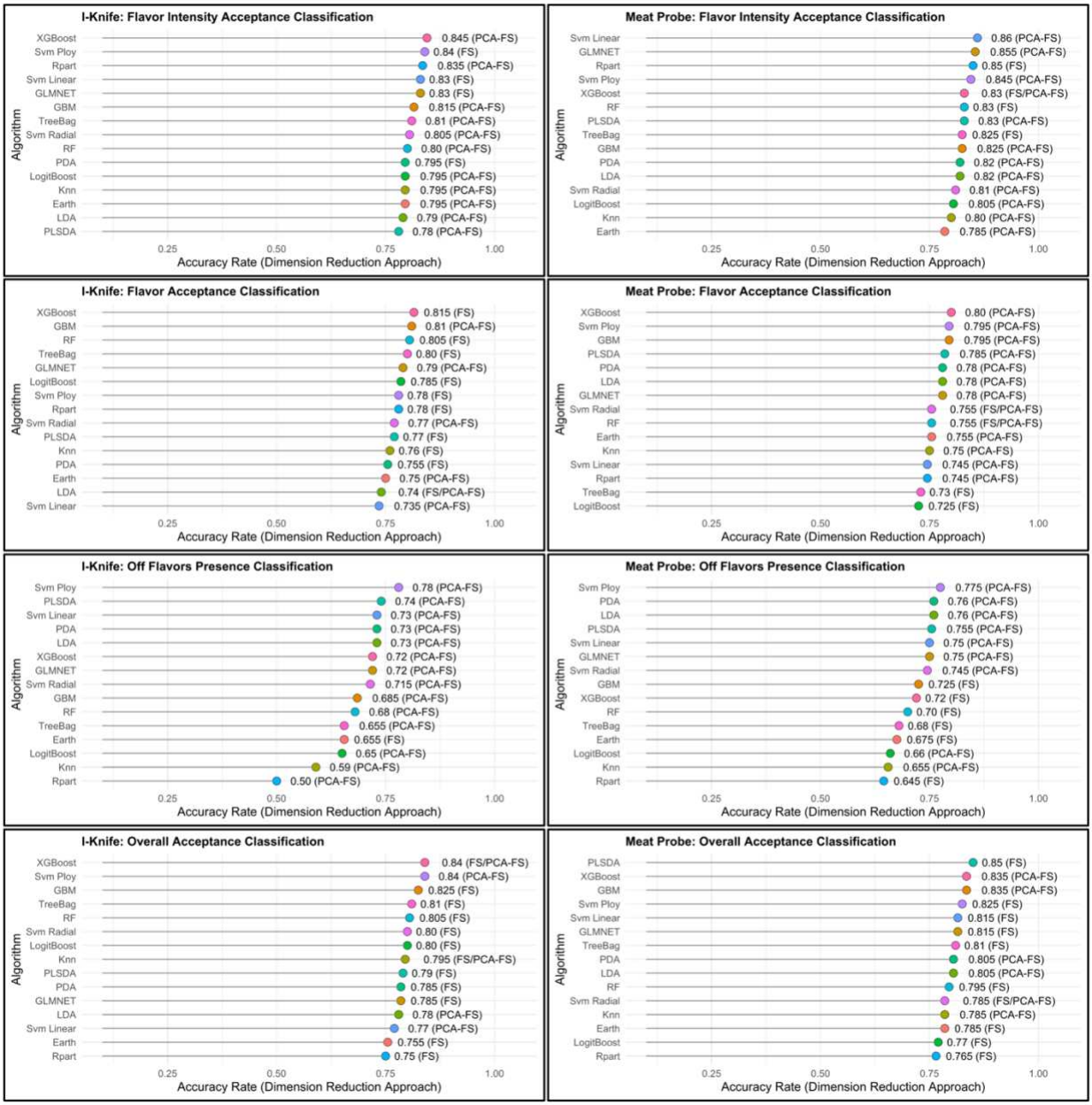

Figure 4.2B Prediction accuracies in each electrode (based on leave-one-out cross validation) for the top performing machine learning algorithm and data reduction approach combinations for flavor intensity acceptance, flavor acceptance, off flavors presence, and overall acceptance classification. PCA-FS: principal component analysis followed by feature selection; FS: feature selection; PCs: principal components.

REFERENCES

Abasht, B., M. F. Mutryn, R. D. Michalek, and W. R. Lee. 2016. Oxidative stress and metabolic perturbations in Wooden Breast disorder in chickens. PLOS ONE. 11:e0153750. doi:10.1371/journal.pone.0153750.

Aggarwal, K., L. H. Choe, and K. H. Lee. 2006. Shotgun proteomics using the iTRAQ isobaric tags. Brief Funct. Genomics. 5:112–120. doi:10.1093/bfgp/ell018.

Aghdasi, B., M. B. Reid, and S. L. Hamilton. 1997. Nitric oxide protects the skeletal muscle Ca^{2+} release channel from oxidation induced activation. J. Biol. Chem. 272:25462–25467. doi:10.1074/jbc.272.41.25462.

Alban, A., S. O. David, L. Bjorkesten, C. Andersson, E. Sloge, S. Lewis, and I. Currie. 2003. A novel experimental design for comparative two-dimensional gel analysis: Two-dimensional difference gel electrophoresis incorporating a pooled internal standard. Proteomics. 3:36–44. doi:10.1002/pmic.200390006.

Alderton, A. L., C. Faustman, D. C. Liebler, and D. W. Hill. 2003. Induction of Redox Instability of Bovine Myoglobin by Adduction with 4-Hydroxy-2-nonenal. Biochemistry. 42:4398–4405. doi:10.1021/bi0271695.

AMSA. 2012. Meat Color Measurement Guidelines (December 2012 ed.). Champaign, IL: The American Meat Science Association (AMSA).

Anderson, M. J., S. M. Lonergan, C. A. Fedler, K. J. Prusa, J. M. Binning, and E. Huff-Lonergan. 2012. Profile of biochemical traits influencing tenderness of muscles from the beef round. Meat Sci. 91:247–254. doi:10.1016/j.meatsci.2012.01.022.

Andersson, D. C., and A. R. Marks. 2010. Fixing ryanodine receptor Ca^{2+} leak – a novel therapeutic strategy for contractile failure in heart and skeletal muscle. Drug Discov. Today: Disease Mechanisms. 7:e151–e157. doi:10.1016/j.ddmec.2010.09.009.

Ankarcrona, M., B. Zhivotovsky, T. Holmström, A. Diana, J. E. Eriksson, S. Orrenius, and P. Nicotera. 1996. Lamin and β-tubulin fragmentation precede chromatin degradation in glutamate-induced neuronal apoptosis. NeuroReport. 7:2659–2664.

Antharavally, B. S., B. Carter, P. A. Bell, and A. Krishna Mallia. 2004. A high-affinity reversible protein stain for Western blots. Anal. Biochem. 329:276–280. doi:10.1016/j.ab.2004.02.049.

Arihara, K., R. G. Cassens, M. L. Greaser, J. B. Luchansky, and P. E. Mozdziak. 1995. Localization of metmyoglobin-reducing enzyme (NADH-cytochrome b5 reductase) system components in bovine skeletal muscle. Meat Sci. 39:205–213. doi:10.1016/0309-1740(94)P1821-C.

Aslam, B., M. Basit, M. A. Nisar, M. Khurshid, and M. H. Rasool. 2017. Proteomics: Technologies and Their Applications. J. Chromatogr. Sci. 55:182–196. doi:10.1093/chromsci/bmw167.

Axe, E. L., S. A. Walker, M. Manifava, P. Chandra, H. L. Roderick, A. Habermann, G. Griffiths, and N. T. Ktistakis. 2008. Autophagosome formation from membrane compartments enriched in phosphatidylinositol 3-phosphate and dynamically connected to the endoplasmic reticulum. J. Cell Biol. 182:685–701. doi:10.1083/jcb.200803137.

Baggerman, G., E. Vierstraete, A. De Loof, and L. Schoofs. 2005. Gel-based versus gel-free proteomics: A review. Comb. Chem. High T. Scr. 8:669–677. doi:10.2174/138620705774962490.

Baker, J., G. Riley, M. R. Romero, A. R. Haynes, H. Hilton, M. Simon, J. Hancock, H. Tateossian, V. M. Ripoll, and G. Blanco. 2010. Identification of a Z-band associated protein complex involving KY, FLNC and IGFN1. Exp. Cell Res. 316:1856–1870. doi:10.1016/j.yexcr.2010.02.027.

Bantscheff, M., M. Schirle, G. Sweetman, J. Rick, and B. Kuster. 2007. Quantitative mass spectrometry in proteomics: a critical review. Anal. Bioanal. Chem. 389:1017–1031. doi:10.1007/s00216-007-1486-6.

Batt, J., S. S. Ahmed, J. Correa, A. Bain, and J. Granton. 2013. Skeletal muscle dysfunction in idiopathic pulmonary arterial hypertension. Am. J. Resp. Cell Mol. 50:74–86. doi:10.1165/rcmb.2012-0506OC.

Bauer, K., A. K. Kretzschmar, H. Cvijic, C. Blumert, D. Löffler, K. Brocke-Heidrich, C. Schiene-Fischer, G. Fischer, A. Sinz, C. V. Clevenger, and F. Horn. 2009. Cyclophilins contribute to Stat3 signaling and survival of multiple myeloma cells. Oncogene. 28:2784–2795. doi:10.1038/onc.2009.142.

Baum, N., C. Schiene-Fischer, M. Frost, M. Schumann, K. Sabapathy, O. Ohlenschläger, F. Grosse, and B. Schlott. 2009. The prolyl cis/trans isomerase cyclophilin 18 interacts with the tumor suppressor p53 and modifies its functions in cell cycle regulation and apoptosis. Oncogene. 28:3915–3925. doi:10.1038/onc.2009.248.

Becila, S., C. H. Herrera-Mendez, G. Coulis, R. Labas, T. Astruc, B. Picard, A. Boudjellal, P. Pelissier, L. Bremaud, and A. Ouali. 2010. Postmortem muscle cells die through apoptosis. Eur. Food Res. Technol. 231:485–493. doi:10.1007/s00217-010-1296-5.

Belew, J. B., J. C. Brooks, D. R. McKenna, and J. W. Savell. 2003. Warner–Bratzler shear evaluations of 40 bovine muscles. Meat Sci. 64:507–512. doi:10.1016/S0309-1740(02)00242-5.

Bellinger, A. M., M. Mongillo, and A. R. Marks. 2008a. Stressed out: the skeletal muscle ryanodine receptor as a target of stress. J. Clin. Invest. 118:445–453. doi:10.1172/JCI34006.

Bellinger, A. M., S. Reiken, M. Dura, P. W. Murphy, S.-X. Deng, D. W. Landry, D. Nieman, S. E. Lehnart, M. Samaru, A. LaCampagne, and A. R. Marks. 2008b. Remodeling of ryanodine receptor complex causes "leaky" channels: A molecular mechanism for decreased exercise capacity. P. Natl. Acad. Sci. USA. 105:2198–2202. doi:10.1073/pnas.0711074105.

Bendixen, E. 2005. The use of proteomics in meat science. Meat Sci. 71:138–149. doi:10.1016/j.meatsci.2005.03.013.

Benjamini, Y., and Y. Hochberg. 1995. Controlling the False Discovery Rate: A practical and powerful approach to multiple testing. J. Roy. Stat. Soc. B. Met. 57:289–300.

Bhattacharya, S., C. G. Bunick, and W. J. Chazin. 2004. Target selectivity in EF-hand calcium binding proteins. BBA-Mol Cell Res. 1742:69–79. doi:10.1016/j.bbamcr.2004.09.002.

Bhattacharya, S., R. M. Ray, and L. R. Johnson. 2005. STAT3-mediated transcription of Bcl-2, Mcl-1 and c-IAP2 prevents apoptosis in polyamine-depleted cells. Biochem. J. 392:335–344. doi:10.1042/BJ20050465.

Bjarnadóttir, S. G., K. Hollung, M. Høy, E. Bendixen, M. C. Codrea, and E. Veiseth-Kent. 2012. Changes in protein abundance between tender and tough meat from bovine Longissimus thoracis muscle assessed by isobaric Tag for Relative and Absolute Quantitation (iTRAQ) and 2-dimensional gel electrophoresis analysis. J. Anim. Sci. 90:2035–2043. doi:10.2527/jas.2011-4721.

Boerboom, G., T. van Kempen, A. Navarro-Villa, and A. Pérez-Bonilla. 2018. Unraveling the cause of white striping in broilers using metabolomics. Poultry Sci. 97:3977–3986. doi:10.3382/ps/pey266.

Bonora, M., S. Patergnani, A. Rimessi, E. De Marchi, J. M. Suski, A. Bononi, C. Giorgi, S. Marchi, S. Missiroli, F. Poletti, M. R. Wieckowski, and P. Pinton. 2012. ATP synthesis and storage. Purinerg. Signal. 8:343–357. doi:10.1007/s11302-012-9305-8.

Bonora, M., M. R. Wieckowski, C. Chinopoulos, O. Kepp, G. Kroemer, L. Galluzzi, and P. Pinton. 2015. Molecular mechanisms of cell death: central implication of ATP synthase in mitochondrial permeability transition. Oncogene. 34:1475–1486. doi:10.1038/onc.2014.96.

van den Bosch, B. J. C., C. M. M. van den Burg, K. Schoonderwoerd, P. J. Lindsey, H. R. Scholte, R. F. M. de Coo, E. van Rooij, H. A. Rockman, P. A. Doevendans, and H. J. M. Smeets. 2005. Regional absence of mitochondria causing energy depletion in the myocardium of muscle LIM protein knockout mice. Cardiovasc. Res. 65:411–418. doi:10.1016/j.cardiores.2004.10.025.

Bottje, W., M. D. Brand, C. Ojano-Dirain, K. Lassiter, M. Toyomizu, and T. Wing. 2009. Mitochondrial proton leak kinetics and relationship with feed efficiency within a single genetic line of male broilers. Poultry Sci. 88:1683–1693. doi:10.3382/ps.2009-00100.

Bottje, W. G. 2019. Oxidative metabolism and efficiency: the delicate balancing act of mitochondria. Poultry Sci. 98:4223–4230. doi:10.3382/ps/pey405.

Bottje, Walter G. 2019. BOARD INVITED REVIEW: Oxidative stress and efficiency: the tightrope act of mitochondria in health and disease. J. Anim. Sci. 97:3169–3179. doi:10.1093/jas/skz219.

Boulos, S., B. P. Meloni, P. G. Arthur, B. Majda, C. Bojarski, and N. W. Knuckey. 2007. Evidence that intracellular cyclophilin A and cyclophilin A/CD147 receptor-mediated ERK1/2 signalling can protect neurons against in vitro oxidative and ischemic injury. Neurobiol. Dis. 25:54–64. doi:10.1016/j.nbd.2006.08.012.

Brohée, S., and J. van Helden. 2006. Evaluation of clustering algorithms for protein-protein interaction networks. BMC Bioinformatics. 7:488. doi:10.1186/1471-2105-7-488.

Brown, G. C. 1999. Nitric oxide and mitochondrial respiration. BBA-Bioenergetics. 1411:351–369. doi:10.1016/S0005-2728(99)00025-0.

Budanov, A. V., and M. Karin. 2008. p53 target genes sestrin1 and sestrin2 connect genotoxic stress and mTOR signaling. Cell. 134:451–460. doi:10.1016/j.cell.2008.06.028.

Cai, K., W. Shao, X. Chen, Y. L. Campbell, M. N. Nair, S. P. Suman, C. M. Beach, M. C. Guyton, and M. W. Schilling. 2018. Meat quality traits and proteome profile of woody broiler breast (pectoralis major) meat. Poultry Sci. 97:337–346. doi:10.3382/ps/pex284.

Calkins, C. R., and J. M. Hodgen. 2007. A fresh look at meat flavor. Meat Sci. 77:63–80. doi:10.1016/j.meatsci.2007.04.016.

Cameron, R. T., S. D. Quinn, L. S. Cairns, R. MacLeod, I. D. W. Samuel, B. O. Smith, J. Carlos Penedo, and G. S. Baillie. 2014. The phosphorylation of Hsp20 enhances its association with amyloid-β to increase protection against neuronal cell death. Mol. Cell. Neurosci. 61:46–55. doi:10.1016/j.mcn.2014.05.002.

Canto, A. C. V. C. S., B. R. C. Costa-Lima, S. P. Suman, M. L. G. Monteiro, F. M. Viana, A. P. A. A. Salim, M. N. Nair, T. J. P. Silva, and C. A. Conte-Junior. 2016. Color attributes and oxidative stability of longissimus lumborum and psoas major muscles from Nellore bulls. Meat Sci. 121:19–26. doi:10.1016/j.meatsci.2016.05.015.

Carmack, C. F., C. L. Kastner, M. E. Dikeman, J. R. Schwenke, and C. M. García Zepeda. 1995. Sensory evaluation of beef-flavor-intensity, tenderness, and juiciness among major muscles. Meat Sci. 39:143–147. doi:10.1016/0309-1740(95)80016-6.

Catlett-Falcone, R., T. H. Landowski, M. M. Oshiro, J. Turkson, A. Levitzki, R. Savino, G. Ciliberto, L. Moscinski, J. L. Fernández-Luna, G. Nuñez, W. S. Dalton, and R. Jove. 1999. Constitutive activation of stat3 signaling confers resistance to apoptosis in human U266 myeloma cells. Immunity. 10:105–115. doi:10.1016/S1074-7613(00)80011-4.

Chandra, D., G. Choy, and D. G. Tang. 2007. Cytosolic accumulation of HSP60 during apoptosis with or without apparent mitochondrial release evidence that its pro-apoptotic or pro-survival functions involve differential interactions with caspase-3. J. Biol. Chem. 282:31289–31301. doi:10.1074/jbc.M702777200.

Chemaly, E. R., L. Troncone, and D. Lebeche. 2018. SERCA control of cell death and survival. Cell Calcium. 69:46–61. doi:10.1016/j.ceca.2017.07.001.

Chen, C., J. Zhang, Z. Guo, X. Shi, Y. Zhang, L. Zhang, Q. Yu, and L. Han. 2020. Effect of oxidative stress on AIF-mediated apoptosis and bovine muscle tenderness during postmortem aging. J. Food Sci. 85:77–85. doi:10.1111/1750-3841.14969.

Chen, X., L. Zhang, J. Li, F. Gao, and G. Zhou. 2017. Hydrogen peroxide-induced change in meat quality of the breast muscle of broilers is mediated by ROS generation, apoptosis, and autophagy in the NF-κB signal pathway. J. Agric. Food Chem. 65:3986–3994. doi:10.1021/acs.jafc.7b01267.

Cheng, S., M. Luo, C. Ding, C. Peng, Z. Lv, R. Tong, H. Xiao, H. Xie, L. Zhou, J. Wu, and S. Zheng. 2016. Downregulation of peptidylprolyl isomerase A promotes cell death and enhances doxorubicin-induced apoptosis in hepatocellular carcinoma. Gene. 591:236–244. doi:10.1016/j.gene.2016.07.020.

Chicco, A. J., C. H. Le, A. Schlater, A. Nguyen, S. Kaye, J. W. Beals, R. L. Scalzo, C. Bell, E. Gnaiger, D. P. Costa, D. E. Crocker, and S. B. Kanatous. 2014. High fatty acid oxidation capacity and phosphorylation control despite elevated leak and reduced respiratory capacity in northern elephant seal muscle mitochondria. J. Exp. Biol. 217:2947–2955. doi:10.1242/jeb.105916.

Chipuk, J. E., L. Bouchier-Hayes, T. Kuwana, D. D. Newmeyer, and D. R. Green. 2005. PUMA couples the nuclear and cytoplasmic proapoptotic function of p53. Science. 309:1732–1735. doi:10.1126/science.1114297.

Chipuk, J. E., T. Kuwana, L. Bouchier-Hayes, N. M. Droin, D. D. Newmeyer, M. Schuler, and D. R. Green. 2004. Direct activation of Bax by p53 mediates mitochondrial membrane permeabilization and apoptosis. Science. 303:1010–1014. doi:10.1126/science.1092734.

Choi, K. J., Y. J. Piao, M. J. Lim, J. H. Kim, J. Ha, W. Choe, and S. S. Kim. 2007. Overexpressed cyclophilin A in cancer cells renders resistance to hypoxia- and cisplatin-induced cell death. Cancer Res. 67:3654–3662. doi:10.1158/0008-5472.CAN-06-1759.

Christensen, S., and P. P. Purslow. 2016. The role of matrix metalloproteinases in muscle and adipose tissue development and meat quality: A review. Meat Sci. 119:138–146. doi:10.1016/j.meatsci.2016.04.025.

Churchman, M. L., J. Low, C. Qu, E. M. Paietta, L. H. Kasper, Y. Chang, D. Payne-Turner, M. J. Althoff, G. Song, S.-C. Chen, J. Ma, M. Rusch, D. McGoldrick, M. Edmonson, P. Gupta, Y.-D. Wang, W. Caufield, B. Freeman, L. Li, J. C. Panetta, S. Baker, Y.-L. Yang, K. G. Roberts, K. McCastlain, I. Iacobucci, J. L. Peters, V. E. Centonze, F. Notta, S. M. Dobson,

S. Zandi, J. E. Dick, L. Janke, J. Peng, K. Kodali, V. Pagala, J. Min, A. Mayasundari, R. T. Williams, C. L. Willman, J. Rowe, S. Luger, R. A. Dickins, R. K. Guy, T. Chen, and C. G. Mullighan. 2015. Efficacy of retinoids in IKZF1-mutated BCR-ABL1 acute lymphoblastic leukemia. Cancer Cell. 28:343–356. doi:10.1016/j.ccell.2015.07.016.

Clerens, S., A. Thomas, J. Gathercole, J. E. Plowman, T.-Y. Yu, A. J. Grosvenor, S. R. Haines, P. Dobbie, K. Taukiri, K. Rosenvold, J. M. Dyer, and S. Deb-Choudhury. 2016. Proteomic and peptidomic differences and similarities between four muscle types from New Zealand raised Angus steers. Meat Sci. 121:53–63. doi:10.1016/j.meatsci.2016.05.014.

Cockrum, R. R., S. E. Speidel, N. F. Crawford, X. Zeng, H. D. Blackburn, T. Holt, R. M. Enns, and M. G. Thomas. 2019. Genotypes identified by genome-wide association analyses influence yearling pulmonary arterial pressure and growth traits in Angus heifers from a high-altitude beef production system. Livestock Sci. 224:75–86. doi:10.1016/j.livsci.2019.04.004.

Consonni, R., and L. R. Cagliani. 2019. The potentiality of NMR-based metabolomics in food science and food authentication assessment. Magn. Reson. Chem. 57:558–578. doi:10.1002/mrc.4807.

Cramer, T., M. L. Penick, J. N. Waddell, C. A. Bidwell, and Y. H. B. Kim. 2018. A new insight into meat toughness of callipyge lamb loins - The relevance of anti-apoptotic systems to decreased proteolysis. Meat Sci. 140:66–71. doi:10.1016/j.meatsci.2018.03.002.

Crawford, N. F., M. G. Thomas, T. N. Holt, S. E. Speidel, and R. M. Enns. 2016. Heritabilities and genetic correlations of pulmonary arterial pressure and performance traits in Angus cattle at high altitude. J. Anim. Sci. 94:4483–4490. doi:10.2527/jas.2016-0703.

D´Alessandro, A., C. Marrocco, V. Zolla, M. D´Andrea, and L. Zolla. 2011. Meat quality of the longissimus lumborum muscle of Casertana and Large White pigs: Metabolomics and proteomics intertwined. J. Proteomics. 75:610–627. doi:10.1016/j.jprot.2011.08.024.

D'Alessandro, A., C. Marrocco, S. Rinalducci, C. Mirasole, S. Failla, and L. Zolla. 2012a. Chianina beef tenderness investigated through integrated Omics. J. Proteomics. 75:4381–4398. doi:10.1016/j.jprot.2012.03.052.

D'Alessandro, A., S. Rinalducci, C. Marrocco, V. Zolla, F. Napolitano, and L. Zolla. 2012b. Love me tender: An Omics window on the bovine meat tenderness network. J. Proteomics. 75:4360–4380. doi:10.1016/j.jprot.2012.02.013.

D'Alessandro, A., and L. Zolla. 2013. Meat science: From proteomics to integrated omics towards system biology. J. Proteomics. 78:558–577. doi:10.1016/j.jprot.2012.10.023.

Decuypere, J.-P., G. Bultynck, and J. B. Parys. 2011. A dual role for Ca^{2+} in autophagy regulation. Cell Calcium. 50:242–250. doi:10.1016/j.ceca.2011.04.001.

Denton, R. M. 2009. Regulation of mitochondrial dehydrogenases by calcium ions. BBA-Bioenergetics. 1787:1309–1316. doi:10.1016/j.bbabio.2009.01.005.

Denton, R. M., P. J. Randle, and B. R. Martin. 1972. Stimulation by calcium ions of pyruvate dehydrogenase phosphate phosphatase. Biochem. J. 128:161–163. doi:10.1042/bj1280161.

Desai, M. A., V. Jackson, W. Zhai, S. P. Suman, M. N. Nair, C. M. Beach, and M. W. Schilling. 2016. Proteome basis of pale, soft, and exudative-like (PSE-like) broiler breast (Pectoralis major) meat. Poultry Sci. 95:2696–2706. doi:10.3382/ps/pew213.

Di Luca, A., R. M. Hamill, A. M. Mullen, N. Slavov, and G. Elia. 2016. Comparative proteomic profiling of divergent phenotypes for water holding capacity across the post mortem ageing period in porcine muscle exudate. PLOS ONE. 11:e0150605. doi:10.1371/journal.pone.0150605.

Di Luca, A., A. M. Mullen, G. Elia, G. Davey, and R. M. Hamill. 2011. Centrifugal drip is an accessible source for protein indicators of pork ageing and water-holding capacity. Meat Sci. 88:261–270. doi:10.1016/j.meatsci.2010.12.033.

van Dieck, J., D. P. Teufel, A. M. Jaulent, M. R. Fernandez-Fernandez, T. J. Rutherford, A. Wyslouch-Cieszynska, and A. R. Fersht. 2009. Posttranslational modifications affect the interaction of S100 proteins with tumor suppressor p53. J. Mol. Biol. 394:922–930. doi:10.1016/j.jmb.2009.10.002.

Doherty, M. K., L. McLean, J. R. Hayter, J. M. Pratt, D. H. L. Robertson, A. El-Shafei, S. J. Gaskell, and R. J. Beynon. 2004. The proteome of chicken skeletal muscle: Changes in soluble protein expression during growth in a layer strain. Proteomics. 4:2082–2093. doi:10.1002/pmic.200300716.

Doyle, V., S. Virji, and M. Crompton. 1999. Evidence that cyclophilin-A protects cells against oxidative stress. Biochem. J. 341:127–132. doi:10.1042/bj3410127.

Dröse, S., and U. Brandt. 2008. The mechanism of mitochondrial superoxide production by the cytochrome bc1 complex. J. Biol. Chem. 283:21649–21654. doi:10.1074/jbc.M803236200.

Dzeja, P. P., S. Chung, R. S. Faustino, A. Behfar, and A. Terzic. 2011. Developmental enhancement of adenylate kinase-AMPK metabolic signaling axis supports stem cell cardiac differentiation. PLOS ONE. 6:e19300. doi:10.1371/journal.pone.0019300.

Dzeja, P., and A. Terzic. 2009. Adenylate kinase and AMP signaling networks: Metabolic monitoring, signal communication and body energy sensing. Int. J. Mol. Sci. 10:1729–1772. doi:10.3390/ijms10041729.

Egan, D. F., D. B. Shackelford, M. M. Mihaylova, S. Gelino, R. A. Kohnz, W. Mair, D. S. Vasquez, A. Joshi, D. M. Gwinn, R. Taylor, J. M. Asara, J. Fitzpatrick, A. Dillin, B. Viollet, M. Kundu, M. Hansen, and R. J. Shaw. 2011. Phosphorylation of ULK1 (hATG1) by AMP-activated protein kinase connects energy sensing to mitophagy. Science. 331:456–461. doi:10.1126/science.1196371.

England, E. M., T. L. Scheffler, S. C. Kasten, S. K. Matarneh, and D. E. Gerrard. 2013. Exploring the unknowns involved in the transformation of muscle to meat. Meat Sci. 95:837–843. doi:10.1016/j.meatsci.2013.04.031.

Esposito, G., L. F. Santana, K. Dilly, J. D. S. Cruz, L. Mao, W. J. Lederer, and H. A. Rockman. 2000. Cellular and functional defects in a mouse model of heart failure. Am. J. Physiol-Heart C. 279:H3101–H3112. doi:10.1152/ajpheart.2000.279.6.H3101.

Faustman, C., D. C. Liebler, T. D. McClure, and Q. Sun. 1999. α,β-unsaturated aldehydes accelerate oxymyoglobin oxidation. J. Agric. Food Chem. 47:3140–3144. doi:10.1021/jf990016c.

Faustman, C., and A. Phillips. 2001. Measurement of discoloration in fresh meat. Current protocols in food analytical chemistry. 00:F3.3.1-F3.3.13. doi:10.1002/0471142913.faf0303s00.

Faustman, C., Q. Sun, R. Mancini, and S. P. Suman. 2010. Myoglobin and lipid oxidation interactions: Mechanistic bases and control. Meat Sci. 86:86–94. doi:10.1016/j.meatsci.2010.04.025.

Favero, T. G., A. C. Zable, and J. J. Abramson. 1995. Hydrogen peroxide stimulates the Ca^{2+} release channel from skeletal muscle sarcoplasmic reticulum. J. Biol. Chem. 270:25557–25563. doi:10.1074/jbc.270.43.25557.

Fiehn, O. 2002. Metabolomics — the link between genotypes and phenotypes. In: C. Town, editor. Functional Genomics. Springer Netherlands, Dordrecht. p. 155–171.

Fortes, M. A. S., G. N. Marzuca-Nassr, K. F. Vitzel, C. H. da Justa Pinheiro, P. Newsholme, and R. Curi. 2016. Housekeeping proteins: How useful are they in skeletal muscle diabetes studies and muscle hypertrophy models? Anal. Biochem. 504:38–40. doi:10.1016/j.ab.2016.03.023.

Gagaoua, M., M. Bonnet, L. De Koning, and B. Picard. 2018. Reverse Phase Protein array for the quantification and validation of protein biomarkers of beef qualities: The case of meat color from Charolais breed. Meat Sci. 145:308–319. doi:10.1016/j.meatsci.2018.06.039.

Gagaoua, M., E. M. Claudia Terlouw, A. Boudjellal, and B. Picard. 2015a. Coherent correlation networks among protein biomarkers of beef tenderness: What they reveal. J. Proteomics. 128:365–374. doi:10.1016/j.jprot.2015.08.022.

Gagaoua, M., E. M. C. Terlouw, D. Micol, A. Boudjellal, J.-F. Hocquette, and B. Picard. 2015b. Understanding Early Post-Mortem Biochemical Processes Underlying Meat Color and pH Decline in the Longissimus thoracis Muscle of Young Blond d'Aquitaine Bulls Using Protein Biomarkers. J. Agric. Food Chem. 63:6799–6809. doi:10.1021/acs.jafc.5b02615.

Gagaoua, M., E. M. C. Terlouw, and B. Picard. 2017. The study of protein biomarkers to understand the biochemical processes underlying beef color development in young bulls. Meat Sci. 134:18–27. doi:10.1016/j.meatsci.2017.07.014.

García-Macia, M., V. Sierra, A. Palanca, I. Vega-Naredo, D. de Gonzalo-Calvo, S. Rodríguez-González, M. Oliván, and A. Coto-Montes. 2014. Autophagy during beef aging. Autophagy. 10:137–143. doi:10.4161/auto.26659.

Genova, M. L., B. Ventura, G. Giuliano, C. Bovina, G. Formiggini, G. P. Castelli, and G. Lenaz. 2001. The site of production of superoxide radical in mitochondrial Complex I is not a bound ubisemiquinone but presumably iron–sulfur cluster N2. FEBS Lett. 505:364–368. doi:10.1016/S0014-5793(01)02850-2.

Ghilardi, N., J. Li, J.-A. Hongo, S. Yi, A. Gurney, and F. J. de Sauvage. 2002. A novel type I cytokine receptor is expressed on monocytes, signals proliferation, and activates STAT-3 and STAT-5. J. Biol. Chem. 277:16831–16836. doi:10.1074/jbc.M201140200.

Giallongo, A., S. Venturella, D. Oliva, G. Barbieri, P. Rubino, and S. Feo. 1993. Structural features of the human gene for muscle-specific enolase. Eur. J. Biochem. 214:367–374. doi:10.1111/j.1432-1033.1993.tb17932.x.

Gimona, M., Z. Lando, Y. Dolginov, J. Vandekerckhove, R. Kobayashi, A. Sobieszek, and D. M. Helfman. 1997. Ca^{2+}-dependent interaction of S100A2 with muscle and nonmuscle tropomyosins. J. Cell Sci. 110:611–621.

Giorgi, C., M. Bonora, G. Sorrentino, S. Missiroli, F. Poletti, J. M. Suski, F. G. Ramirez, R. Rizzuto, F. D. Virgilio, E. Zito, P. P. Pandolfi, M. R. Wieckowski, F. Mammano, G. D. Sal, and P. Pinton. 2015. p53 at the endoplasmic reticulum regulates apoptosis in a Ca2+-dependent manner. P. Natl. Acad. Sci. USA. 112:1779–1784. doi:10.1073/pnas.1410723112.

Gogvadze, V., J. D. Robertson, B. Zhivotovsky, and S. Orrenius. 2001. Cytochrome c release occurs via Ca^{2+}-dependent and Ca^{2+}-independent mechanisms that are regulated by Bax. J. Biol. Chem. 276:19066–19071. doi:10.1074/jbc.M100614200.

Gredell, D. A., A. R. Schroeder, K. E. Belk, C. D. Broeckling, A. L. Heuberger, S.-Y. Kim, D. A. King, S. D. Shackelford, J. L. Sharp, T. L. Wheeler, D. R. Woerner, and J. E. Prenni. 2019. Comparison of machine learning algorithms for predictive modeling of beef attributes using rapid evaporative ionization mass spectrometry (REIMS) data. Sci. Rep-UK. 9:5721. doi:10.1038/s41598-019-40927-6.

Green, D. R., L. Galluzzi, and G. Kroemer. 2014. Metabolic control of cell death. Science. 345:1250256–1250256. doi:10.1126/science.1250256.

Green, D. R., and B. Levine. 2014. To be or not to be? How selective autophagy and cell Death govern cell fate. Cell. 157:65–75. doi:10.1016/j.cell.2014.02.049.

Green, D. R., and F. Llambi. 2015. Cell Death Signaling. Cold Spring Harb Perspect Biol. 7:a006080. doi:10.1101/cshperspect.a006080.

Gruber, S. L., J. D. Tatum, J. A. Scanga, P. L. Chapman, G. C. Smith, and K. E. Belk. 2006. Effects of postmortem aging and USDA quality grade on Warner-Bratzler shear force values of seventeen individual beef muscles. J. Anim. Sci. 84:3387–3396. doi:10.2527/jas.2006-194.

Guillemin, N., M. Bonnet, C. Jurie, and B. Picard. 2011a. Functional analysis of beef tenderness. J. Proteomics. 75:352–365. doi:10.1016/j.jprot.2011.07.026.

Guillemin, N., C. Jurie, I. Cassar-Malek, J.-F. Hocquette, G. Renand, and B. Picard. 2011b. Variations in the abundance of 24 protein biomarkers of beef tenderness according to muscle and animal type. Animal. 5:885–894. doi:10.1017/S1751731110002612.

Gupta, M. P., S. A. Samant, S. H. Smith, and S. G. Shroff. 2008. HDAC4 and PCAF bind to cardiac sarcomeres and play a role in regulating myofilament contractile activity. J. Biol. Chem. 283:10135–10146. doi:10.1074/jbc.M710277200.

Hagler, L., R. I. Coppes, and R. H. Herman. 1979. Metmyoglobin reductase. Identification and purification of a reduced nicotinamide adenine dinucleotide-dependent enzyme from bovine heart which reduces metmyoglobin. J. Biol. Chem. 254:6505–6514.

Hamasaki, M., S. T. Shibutani, and T. Yoshimori. 2013. Up-to-date membrane biogenesis in the autophagosome formation. Curr. Opin. Cell Biol. 25:455–460. doi:10.1016/j.ceb.2013.03.004.

Han, E.-S., F. L. Muller, V. I. Pérez, W. Qi, H. Liang, L. Xi, C. Fu, E. Doyle, M. Hickey, J. Cornell, C. J. Epstein, L. J. Roberts, H. Van Remmen, and A. Richardson. 2008. The in vivo gene expression signature of oxidative stress. Physiol. Genomics. 34:112–126. doi:10.1152/physiolgenomics.00239.2007.

Hayashi-Nishino, M., N. Fujita, T. Noda, A. Yamaguchi, T. Yoshimori, and A. Yamamoto. 2010. Electron tomography reveals the endoplasmic reticulum as a membrane source for autophagosome formation. Autophagy. 6:301–303. doi:10.4161/auto.6.2.11134.

Heffernan, K. R., M. G. Thomas, R. M. Enns, T. Holt, and S. E. Speidel. 2020. Phenotypic relationships between heart score and feed efficiency, carcass, and pulmonary arterial pressure traits. Transl. Anim. Sci. 4:S103–S107. doi:10.1093/tas/txaa114.

Hermeking, H., and D. Eick. 1994. Mediation of c-Myc-induced apoptosis by p53. Science. 265:2091–2093. doi:10.1126/science.8091232.

Herrera-Mendez, C. H., S. Becila, A. Boudjellal, and A. Ouali. 2006. Meat ageing: Reconsideration of the current concept. Trends Food Sci. Tech. 17:394–405. doi:10.1016/j.tifs.2006.01.011.

Herzig, S., and R. J. Shaw. 2018. AMPK: guardian of metabolism and mitochondrial homeostasis. Nat Rev Mol Cell Biol. 19:121–135. doi:10.1038/nrm.2017.95.

Higdon, R., and E. Kolker. 2015. Can "normal" protein expression ranges be estimated with high-throughput proteomics? J. Proteome Res. 14:2398–2407. doi:10.1021/acs.jproteome.5b00176.

Hoffman, T. W. 2015. BENCHMARK OF LAMB QUALITY IN U.S. RETAIL AND FOODSERVICE MARKETS. 122.

Hollung, K., E. Veiseth, X. Jia, E. M. Færgestad, and K. I. Hildrum. 2007. Application of proteomics to understand the molecular mechanisms behind meat quality. Meat Sci. 77:97–104. doi:10.1016/j.meatsci.2007.03.018.

Holt, T. N., and R. J. Callan. 2007. Pulmonary arterial pressure testing for high mountain disease in cattle. Vet. Clin. N. Am. Food A. 23:575–596. doi:10.1016/j.cvfa.2007.08.001.

Huang, F., M. Huang, H. Zhang, C. Zhang, D. Zhang, and G. Zhou. 2016. Changes in apoptotic factors and caspase activation pathways during the postmortem aging of beef muscle. Food Chem. 190:110–114. doi:10.1016/j.foodchem.2015.05.056.

Huang, H., and R. Lametsch. 2013. Challenges and Applications of Proteomics for Analysis of Changes in Early Postmortem Meat. In: F. Toldrá and L. M. L. Nollet, editors. Proteomics in Foods: Principles and Applications. Springer US, Boston, MA. p. 103–109.

Huang, H., M. R. Larsen, A. H. Karlsson, L. Pomponio, L. N. Costa, and R. Lametsch. 2011. Gel-based phosphoproteomics analysis of sarcoplasmic proteins in postmortem porcine muscle with pH decline rate and time differences. Proteomics. 11:4063–4076. doi:10.1002/pmic.201100173.

Huff Lonergan, E., W. Zhang, and S. M. Lonergan. 2010. Biochemistry of postmortem muscle — Lessons on mechanisms of meat tenderization. Meat Sci. 86:184–195. doi:10.1016/j.meatsci.2010.05.004.

Hughes, J. M., S. K. Oiseth, P. P. Purslow, and R. D. Warner. 2014. A structural approach to understanding the interactions between colour, water-holding capacity and tenderness. Meat Sci. 98:520–532. doi:10.1016/j.meatsci.2014.05.022.

Hunt, M. C., and H. B. Hedrick. 1977. Profile of fiber types and related properties of five bovine muscles. J Food Sci. 42:513–517. doi:10.1111/j.1365-2621.1977.tb01535.x.

Husson, F., S. Le, and J. Pagès. Exploratory Multivariate Analysis by Example Using R. 77.

Hwang, I. H., B. Y. Park, S. H. Cho, J. H. Kim, Y. S. Choi, and J. M. Lee. 2004. Identification of muscle proteins related to objective meat quality in korean native black pig. Asian-Austral. J. Anim. Sci. 17:1599–1607. doi:10.5713/ajas.2004.1599.

Hwang, Y.-H., G.-D. Kim, J.-Y. Jeong, S.-J. Hur, and S.-T. Joo. 2010. The relationship between muscle fiber characteristics and meat quality traits of highly marbled Hanwoo (Korean native cattle) steers. Meat Sci. 86:456–461. doi:10.1016/j.meatsci.2010.05.034.

Hyun, D.-H., and G.-H. Lee. 2015. Cytochrome b5 reductase, a plasma membrane redox enzyme, protects neuronal cells against metabolic and oxidative stress through maintaining redox state and bioenergetics. Age. 37:122. doi:10.1007/s11357-015-9859-9.

James, G., D. Witten, T. Hastie, and R. Tibshirani. 2021. Resampling Methods. In: G. James, D. Witten, T. Hastie, and R. Tibshirani, editors. An Introduction to Statistical Learning: with Applications in R. Springer US, New York, NY. p. 197–223.

Jastroch, M., A. S. Divakaruni, S. Mookerjee, J. R. Treberg, and M. D. Brand. 2010. Mitochondrial proton and electron leaks. Essays Biochem. 47:53–67. doi:10.1042/bse0470053.

Ji, J.-R., and K. Takahashi. 2006. Changes in concentration of sarcoplasmic free calcium during post-mortem ageing of meat. Meat Sci. 73:395–403. doi:10.1016/j.meatsci.2005.09.010.

Jia, X., E. Veiseth-Kent, H. Grove, P. Kuziora, L. Aass, K. I. Hildrum, and K. Hollung. 2009. Peroxiredoxin-6—A potential protein marker for meat tenderness in bovine longissimus thoracis muscle. J. Anim. Sci. 87:2391–2399. doi:10.2527/jas.2009-1792.

Jiang, T., and C. L. Bratcher. 2016. Differentiation of commercial ground beef products and correlation between metabolites and sensory attributes: A metabolomic approach. Food Res. Int. 90:298–306. doi:10.1016/j.foodres.2016.11.002.

Jones, R. G., D. R. Plas, S. Kubek, M. Buzzai, J. Mu, Y. Xu, M. J. Birnbaum, and C. B. Thompson. 2005. AMP-activated protein kinase induces a p53-dependent metabolic checkpoint. Mol. Cell. 18:283–293. doi:10.1016/j.molcel.2005.03.027.

Joseph, P., S. P. Suman, G. Rentfrow, S. Li, and C. M. Beach. 2012. Proteomics of muscle-specific beef color stability. J. Agric. Food Chem. 60:3196–3203. doi:10.1021/jf204188v.

Jouaville, L. S., P. Pinton, C. Bastianutto, G. A. Rutter, and R. Rizzuto. 1999. Regulation of mitochondrial ATP synthesis by calcium: Evidence for a long-term metabolic priming. P. Natl. Acad. Sci. USA. 96:13807–13812. doi:10.1073/pnas.96.24.13807.

Junot, C., F. Fenaille, B. Colsch, and F. Bécher. 2014. High resolution mass spectrometry based techniques at the crossroads of metabolic pathways. Mass Spectrom. Rev. 33:471–500. doi:10.1002/mas.21401.

Käll, L., J. D. Storey, M. J. MacCoss, and W. S. Noble. 2008. Assigning significance to peptides identified by tandem mass spectrometry using decoy databases. J. Proteome Res. 7:29–34. doi:10.1021/pr700600n.

Kanias, T., and J. P. Acker. 2010. Biopreservation of red blood cells – the struggle with hemoglobin oxidation. FEBS J. 277:343–356. doi:10.1111/j.1742-4658.2009.07472.x.

Ke, Y., R. M. Mitacek, A. Abraham, G. G. Mafi, D. L. VanOverbeke, U. DeSilva, and R. Ramanathan. 2017. Effects of Muscle-Specific Oxidative Stress on Cytochrome c Release and Oxidation–Reduction Potential Properties. J. Agric. Food Chem. 65:7749–7755. doi:10.1021/acs.jafc.7b01735.

Keller, A., A. I. Nesvizhskii, E. Kolker, and R. Aebersold. 2002. Empirical Statistical Model To Estimate the Accuracy of Peptide Identifications Made by MS/MS and Database Search. Anal. Chem. 74:5383–5392. doi:10.1021/ac025747h.

Kemecsei, P., Z. Miklós, T. Bíró, R. Marincsák, B. I. Tóth, E. Komlódi-Pásztor, E. Barnucz, É. Mirk, G. J. Van der Vusse, L. Ligeti, and T. Ivanics. 2010. Hearts of surviving MLP-KO mice show transient changes of intracellular calcium handling. Mol Cell Biochem. 342:251–260. doi:10.1007/s11010-010-0492-8.

Kemp, C. M., and T. Parr. 2012. Advances in apoptotic mediated proteolysis in meat tenderisation. Meat Sci. 92:252–259. doi:10.1016/j.meatsci.2012.03.013.

Khan, M. I., C. Jo, and M. R. Tariq. 2015. Meat flavor precursors and factors influencing flavor precursors—A systematic review. Meat Sci. 110:278–284. doi:10.1016/j.meatsci.2015.08.002.

Kim, G.-D., H.-S. Yang, and J.-Y. Jeong. 2018. Intramuscular variations of proteome and muscle fiber type distribution in semimembranosus and semitendinosus muscles associated with pork quality. Food Chem. 244:143–152. doi:10.1016/j.foodchem.2017.10.046.

Kim, J., M. Kundu, B. Viollet, and K.-L. Guan. 2011. AMPK and mTOR regulate autophagy through direct phosphorylation of Ulk1. Nat. Cell Biol. 13:132–141. doi:10.1038/ncb2152.

Kim Se-Chan, Stice James P., Chen Le, Jung James S., Gupta Sanjiv, Wang Yin, Baumgarten Georg, Trial Joann, and Knowlton Anne A. 2009. Extracellular heat shock protein 60, cardiac myocytes, and apoptosis. circulation research. 105:1186–1195. doi:10.1161/CIRCRESAHA.109.209643.

Kirchofer, K. S., C. R. Calkins, and B. L. Gwartney. 2002. Fiber-type composition of muscles of the beef chuck and round. J. Anim. Sci. 80:2872–2878. doi:10.2527/2002.80112872x.

Kuhn, M. 2008. Building predictive models in R using the caret package. J. Stat. Softw. 28:1–26. doi:10.18637/jss.v028.i05.

Kuhn, M., and K. Johnson. 2013. Applied Predictive Modeling. Springer New York, New York, NY.

Kushnareva, Y., A. N. Murphy, and A. Andreyev. 2002. Complex I-mediated reactive oxygen species generation: modulation by cytochrome c and NAD(P)$^+$ oxidation–reduction state. Biochem. J. 368:545–553. doi:10.1042/bj20021121.

Kwasiborski, A., T. Sayd, C. Chambon, V. Santé-Lhoutellier, D. Rocha, and C. Terlouw. 2008. Pig Longissimus lumborum proteome: Part II: Relationships between protein content and meat quality. Meat Sci. 80:982–996. doi:10.1016/j.meatsci.2008.04.032.

Lai, F. A., and G. Meissner. 1989. The muscle ryanodine receptor and its intrinsic Ca^{2+} channel activity. J. Bioenerg. Biomembr. 21:227–246. doi:10.1007/BF00812070.

Lametsch, R., A. Karlsson, K. Rosenvold, H. J. Andersen, P. Roepstorff, and E. Bendixen. 2003. Postmortem proteome changes of porcine muscle related to tenderness. J. Agric. Food Chem. 51:6992–6997. doi:10.1021/jf034083p.

Lametsch, R., P. Roepstorff, H. S. Møller, and E. Bendixen. 2004. Identification of myofibrillar substrates for μ-calpain. Meat Sci. 68:515–521. doi:10.1016/j.meatsci.2004.03.018.

Lana, A., and L. Zolla. 2015. Apoptosis or autophagy, that is the question: Two ways for muscle sacrifice towards meat. Trends Food Sci. Tech. 46:231–241. doi:10.1016/j.tifs.2015.10.001.

Lana, A., and L. Zolla. 2016. Proteolysis in meat tenderization from the point of view of each single protein: A proteomic perspective. J. Proteomics. 147:85–97. doi:10.1016/j.jprot.2016.02.011.

Laville, E., T. Sayd, M. Morzel, S. Blinet, C. Chambon, J. Lepetit, G. Renand, and J. F. Hocquette. 2009. Proteome changes during meat aging in tough and tender beef suggest the importance of apoptosis and protein solubility for beef aging and tenderization. J. Agric. Food Chem. 57:10755–10764. doi:10.1021/jf901949r.

Ledward, D. A. 1985. Post-slaughter influences on the formation of metyyoglobin in beef muscles. Meat Sci. 15:149–171. doi:10.1016/0309-1740(85)90034-8.

Lee, J., D.-H. Kim, S. Lee, Q.-H. Yang, D. K. Lee, S.-K. Lee, R. G. Roeder, and J. W. Lee. 2009. A tumor suppressive coactivator complex of p53 containing ASC-2 and histone H3-lysine-4 methyltransferase MLL3 or its paralogue MLL4. P. Natl. Acad. Sci. USA. 106:8513–8518. doi:10.1073/pnas.0902873106.

Lee, S. M., G. Y. Kwon, K.-O. Kim, and Y.-S. Kim. 2011. Metabolomic approach for determination of key volatile compounds related to beef flavor in glutathione-Maillard reaction products. Anal. Chim. Acta. 703:204–211. doi:10.1016/j.aca.2011.07.028.

Lee, S. P., Y. S. Hwang, Y. J. Kim, K.-S. Kwon, H. J. Kim, K. Kim, and H. Z. Chae. 2001. Cyclophilin a binds to peroxiredoxins and activates its peroxidase activity. J. Biol. Chem. 276:29826–29832. doi:10.1074/jbc.M101822200.

Lee, S., A. L. Phillips, D. C. Liebler, and C. Faustman. 2003. Porcine oxymyoglobin and lipid oxidation in vitro. Meat Sci. 63:241–247. doi:10.1016/S0309-1740(02)00076-1.

Lefaucheur, L. 2010. A second look into fibre typing – Relation to meat quality. Meat Sci. 84:257–270. doi:10.1016/j.meatsci.2009.05.004.

Lemasters, J. J., T. P. Theruvath, Z. Zhong, and A.-L. Nieminen. 2009. Mitochondrial calcium and the permeability transition in cell death. BBA-Bioenergetics. 1787:1395–1401. doi:10.1016/j.bbabio.2009.06.009.

Lescuyer, P., D. F. Hochstrasser, and J.-C. Sanchez. 2004. Comprehensive proteome analysis by chromatographic protein prefractionation. Electrophoresis. 25:1125–1135. doi:10.1002/elps.200305792.

Leu, J. I.-J., P. Dumont, M. Hafey, M. E. Murphy, and D. L. George. 2004. Mitochondrial p53 activates Bak and causes disruption of a Bak–Mcl1 complex. Nat. Cell Biol. 6:443–450. doi:10.1038/ncb1123.

Lewis, C., P. Doran, and K. Ohlendieck. 2012. Proteomic analysis of dystrophic muscle. In: J. X. DiMario, editor. Myogenesis: Methods and Protocols. Humana Press, Totowa, NJ. p. 357–369.

Li Puma, L. C., M. Hedges, J. M. Heckman, A. B. Mathias, M. R. Engstrom, A. B. Brown, and A. J. Chicco. 2020. Experimental oxygen concentration influences rates of mitochondrial hydrogen peroxide release from cardiac and skeletal muscle preparations. Am. J. Physiol-Reg. I. 318:R972–R980. doi:10.1152/ajpregu.00227.2019.

Li, X., J. Baker, T. Cracknell, A. R. Haynes, and G. Blanco. 2017. IGFN1_v1 is required for myoblast fusion and differentiation. PLOS ONE. 12:e0180217. doi:10.1371/journal.pone.0180217.

Li, Z., M. Li, X. Li, J. Xin, Y. Wang, Q. W. Shen, and D. Zhang. 2018. Quantitative phosphoproteomic analysis among muscles of different color stability using tandem mass tag labeling. Food Chem. 249:8–15. doi:10.1016/j.foodchem.2017.12.047.

Liebler, D. C. 2002. Proteomics and the New Biology. In: D. C. Liebler, editor. Introduction to Proteomics: Tools for the New Biology. Humana Press, Totowa, NJ. p. 3–13.

Lin, S.-C., and D. G. Hardie. 2018. AMPK: Sensing glucose as well as cellular energy status. Cell Metab. 27:299–313. doi:10.1016/j.cmet.2017.10.009.

Liu, R., Q. Fu, S. Lonergan, E. Huff-Lonergan, L. Xing, L. Zhang, Y. Bai, G. Zhou, and W. Zhang. 2018. Identification of S-nitrosylated proteins in postmortem pork muscle using modified biotin switch method coupled with isobaric tags. Meat Sci. 145:431–439. doi:10.1016/j.meatsci.2018.07.027.

Lomiwes, D., M. M. Farouk, E. Wiklund, and O. A. Young. 2014. Small heat shock proteins and their role in meat tenderness: A review. Meat Sci. 96:26–40. doi:10.1016/j.meatsci.2013.06.008.

Longo, V., A. Lana, M. T. Bottero, and L. Zolla. 2015. Apoptosis in muscle-to-meat aging process: The omic witness. J. Proteomics. 125:29–40. doi:10.1016/j.jprot.2015.04.023.

Lopert, P., and M. Patel. 2014. Nicotinamide nucleotide transhydrogenase (Nnt) links the substrate requirement in brain mitochondria for hydrogen peroxide removal to the thioredoxin/peroxiredoxin (Trx/Prx) system. J. Biol. Chem. 289:15611–15620. doi:10.1074/jbc.M113.533653.

Lum, J. J., D. E. Bauer, M. Kong, M. H. Harris, C. Li, T. Lindsten, and C. B. Thompson. 2005. Growth factor regulation of autophagy and cell survival in the absence of apoptosis. Cell. 120:237–248. doi:10.1016/j.cell.2004.11.046.

Lund, T. C., L. B. Anderson, V. McCullar, L. Higgins, G. H. Yun, B. Grzywacz, M. R. Verneris, and J. S. Miller. 2007. iTRAQ Is a useful method to screen for membrane-bound proteins differentially expressed in human natural killer cell types. J. Proteome Res. 6:644–653. doi:10.1021/pr0603912.

Lusk, J. L., J. A. Fox, T. C. Schroeder, J. Mintert, and M. Koohmaraie. 2001. In-store valuation of steak tenderness. Am. J. Agric. Econ. 83:539–550. doi:10.1111/0002-9092.00176.

Lv, S., L. Ji, B. Chen, S. Liu, C. Lei, X. Liu, X. Qi, Y. Wang, E. L.-H. Leung, H. Wang, L. Zhang, X. Yu, Z. Liu, Q. Wei, and L. Lu. 2018. Histone methyltransferase KMT2D sustains prostate carcinogenesis and metastasis via epigenetically activating LIFR and KLF4. Oncogene. 37:1354. doi:10.1038/s41388-017-0026-x.

Ma, D., Y. H. B. Kim, B. Cooper, J.-H. Oh, H. Chun, J.-H. Choe, J. P. Schoonmaker, K. Ajuwon, and B. Min. 2017. Metabolomics profiling to determine the effect of postmortem aging on color and lipid oxidative stabilities of different bovine muscles. J. Agric. Food Chem. 65:6708–6716. doi:10.1021/acs.jafc.7b02175.

Malheiros, J. M., C. P. Braga, R. A. Grove, F. A. Ribeiro, C. R. Calkins, J. Adamec, and L. A. L. Chardulo. 2019. Influence of oxidative damage to proteins on meat tenderness using a proteomics approach. Meat Sci. 148:64–71. doi:10.1016/j.meatsci.2018.08.016.

Mancini, R. A., K. Belskie, S. P. Suman, and R. Ramanathan. 2018. Muscle-specific mitochondrial functionality and its influence on fresh beef color stability. J. Food Sci. 83:2077–2082. doi:10.1111/1750-3841.14219.

Mancini, R. A., and M. C. Hunt. 2005. Current research in meat color. Meat Sci. 71:100–121. doi:10.1016/j.meatsci.2005.03.003.

Mansilla, F., C. A. G. Dominguez, J. E. Yeadon, T. J. Corydon, S. J. Burden, and C. R. Knudsen. 2008. Translation elongation factor eEF1A binds to a novel myosin binding protein-C-like protein. J. Cell. Biochem. 105:847–858. doi:10.1002/jcb.21880.

Mao, M., X. Yu, X. Ge, R. Gu, Q. Li, S. Song, X. Zheng, T. Shen, X. Li, Y. Fu, J. Li, and D. Zhu. 2017. Acetylated cyclophilin A is a major mediator in hypoxia-induced autophagy and pulmonary vascular angiogenesis. J. Hypertens. 35:798. doi:10.1097/HJH.0000000000001224.

Mao, Y., D. L. Hopkins, Y. Zhang, P. Li, L. Zhu, P. Dong, R. Liang, J. Dai, X. Wang, and X. Luo. 2016. Beef quality with different intramuscular fat content and proteomic analysis using isobaric tag for relative and absolute quantitation of differentially expressed proteins. Meat Sci. 118:96–102. doi:10.1016/j.meatsci.2016.03.028.

Marcos, B., and A. M. Mullen. 2014. High pressure induced changes in beef muscle proteome: Correlation with quality parameters. Meat Sci. 97:11–20. doi:10.1016/j.meatsci.2013.12.008.

Marino, R., A. della Malva, and M. Albenzio. 2015. Proteolytic changes of myofibrillar proteins in Podolian meat during aging: focusing on tenderness. J. Anim. Sci. 93:1376–1387. doi:10.2527/jas.2014-8351.

Martin-Montalvo, A., Y. Sun, A. Diaz-Ruiz, A. Ali, V. Gutierrez, H. H. Palacios, J. Curtis, E. Siendones, J. Ariza, G. A. Abulwerdi, X. Sun, A. X. Wang, K. J. Pearson, K. W. Fishbein, R. G. Spencer, M. Wang, X. Han, M. Scheibye-Knudsen, J. A. Baur, H. G. Shertzer, P. Navas, J. M. Villalba, S. Zou, M. Bernier, and R. de Cabo. 2016. Cytochrome b5 reductase and the control of lipid metabolism and healthspan. npj Aging and Mechanisms of Disease. 2:16006. doi:10.1038/npjamd.2016.6.

Marzano, V., B. Tilocca, A. G. Fiocchi, P. Vernocchi, S. Levi Mortera, A. Urbani, P. Roncada, and L. Putignani. 2020. Perusal of food allergens analysis by mass spectrometry-based proteomics. J. Proteomics. 215:103636. doi:10.1016/j.jprot.2020.103636.

Matarneh, S. K., E. M. England, T. L. Scheffler, and D. E. Gerrard. 2017. Chapter 5 - The Conversion of Muscle to Meat. In: F. Toldra´, editor. Lawrie´s Meat Science (Eighth Edition). Woodhead Publishing. p. 159–185.

Mazat, J.-P., A. Devin, and S. Ransac. 2020. Modelling mitochondrial ROS production by the respiratory chain. Cell Mol. Life Sci. 77:455–465. doi:10.1007/s00018-019-03381-1.

McCormack, J. G., A. P. Halestrap, and R. M. Denton. 1990. Role of calcium ions in regulation of mammalian intramitochondrial metabolism. Physiol. Rev. 70:391–425. doi:10.1152/physrev.1990.70.2.391.

McKenna, D. R., P. D. Mies, B. E. Baird, K. D. Pfeiffer, J. W. Ellebracht, and J. W. Savell. 2005. Biochemical and physical factors affecting discoloration characteristics of 19 bovine muscles. Meat Sci. 70:665–682. doi:10.1016/j.meatsci.2005.02.016.

Melody, J. L., S. M. Lonergan, L. J. Rowe, T. W. Huiatt, M. S. Mayes, and E. Huff-Lonergan. 2004. Early postmortem biochemical factors influence tenderness and water-holding capacity of three porcine muscles. J. Anim. Sci. 82:1195–1205.

Mertz, J., H. Tan, V. Pagala, B. Bai, P.-C. Chen, Y. Li, J.-H. Cho, T. Shaw, X. Wang, and J. Peng. 2015. Sequential elution interactome analysis of the mind bomb 1 ubiquitin ligase reveals a novel role in dendritic spine outgrowth. Mol. Cell. Proteomics. 14:1898–1910. doi:10.1074/mcp.M114.045898.

Mikhael, M., C. Makar, A. Wissa, T. Le, M. Eghbali, and S. Umar. 2019. Oxidative stress and its Implications in the right ventricular remodeling secondary to pulmonary hypertension. Front Physiol. 10:1233. doi:10.3389/fphys.2019.01233.

Minetti, M., C. Mallozzi, G. Scorza, M. D. Scott, F. A. Kuypers, and B. H. Lubin. 1993. Role of oxygen and carbon radicals in hemoglobin oxidation. Arch. Biochem. Biophys. 302:233–244. doi:10.1006/abbi.1993.1205.

Misra, H. P., and I. Fridovich. 1972. The generation of superoxide radical during the autoxidation of hemoglobin. J. Biol. Chem. 247:6960–6962.

Mitacek, R. M., Y. Ke, J. E. Prenni, R. Jadeja, D. L. VanOverbeke, G. G. Mafi, and R. Ramanathan. 2019. Mitochondrial degeneration, depletion of NADH, and oxidative stress decrease color stability of wet-aged beef longissimus steaks. J. Food Sci. 84:38–50. doi:10.1111/1750-3841.14396.

Morzel, M., C. Terlouw, C. Chambon, D. Micol, and B. Picard. 2008. Muscle proteome and meat eating qualities of Longissimus thoracis of "Blonde d'Aquitaine" young bulls: A central role of HSP27 isoforms. Meat Sci. 78:297–304. doi:10.1016/j.meatsci.2007.06.016.

Moxness, M. S., L. S. Brunauer, and W. H. Huestis. 1996. Hemoglobin oxidation products extract phospholipids from the membrane of human erythrocytes. Biochemistry. 35:7181–7187. doi:10.1021/bi952167o.

Mueller, A., B. W. Schäfer, S. Ferrari, M. Weibel, M. Makek, M. Höchli, and C. W. Heizmann. 2005. The calcium-binding protein S100A2 interacts with p53 and modulates its transcriptional activity. J. Biol. Chem. 280:29186–29193. doi:10.1074/jbc.M505000200.

Mullen, A. M., P. C. Stapleton, D. Corcoran, R. M. Hamill, and A. White. 2006. Understanding meat quality through the application of genomic and proteomic approaches. Meat Sci. 74:3–16. doi:10.1016/j.meatsci.2006.04.015.

Mungai, P. T., G. B. Waypa, A. Jairaman, M. Prakriya, D. Dokic, M. K. Ball, and P. T. Schumacker. 2011. Hypoxia triggers AMPK activation through reactive oxygen species-mediated activation of calcium release-activated calcium channels. Mol. Cell. Biol. 31:3531–3545. doi:10.1128/MCB.05124-11.

Muroya, S., M. Ohnishi-Kameyama, M. Oe, I. Nakajima, and K. Chikuni. 2007a. Postmortem changes in bovine troponin T isoforms on two-dimensional electrophoretic gel analyzed using mass spectrometry and western blotting: The limited fragmentation into basic polypeptides. Meat Sci. 75:506–514. doi:10.1016/j.meatsci.2006.08.012.

Muroya, S., M. Ohnishi-Kameyama, M. Oe, I. Nakajima, M. Shibata, and K. Chikuni. 2007b. Double phosphorylation of the myosin regulatory light chain during rigor mortis of bovine longissimus muscle. J. Agric. Food Chem. 55:3998–4004. doi:10.1021/jf063200o.

Muroya, S., S. Ueda, T. Komatsu, T. Miyakawa, and P. Ertbjerg. 2020. MEATabolomics: Muscle and meat metabolomics in domestic animals. Metabolites. 10:188. doi:10.3390/metabo10050188.

Murphy, M. P. 2009. How mitochondria produce reactive oxygen species. Biochem. J. 417:1–13. doi:10.1042/BJ20081386.

Nagasawa, T., R. Matsushima-Nishiwaki, H. Toyoda, J. Matsuura, T. Kumada, and O. Kozawa. 2014. Heat shock protein 20 (HSPB6) regulates apoptosis in human hepatocellular carcinoma cells: Direct association with Bax. Oncology Rep. 32:1291–1295. doi:10.3892/or.2014.3278.

Nair, M. N., B. R. C. Costa-Lima, M. Wes Schilling, and S. P. Suman. 2017. Chapter 10 - Proteomics of Color in Fresh Muscle Foods. In: M. L. Colgrave, editor. rosa. Academic Press. p. 163–175.

Nair, M. N., S. Li, C. M. Beach, G. Rentfrow, and S. P. Suman. 2018a. Changes in the sarcoplasmic proteome of beef muscles with differential color stability during postmortem aging. Meat Muscle Biol. 2:1–17. doi:10.22175/mmb2017.07.0037.

Nair, M. N., S. Li, C. Beach, G. Rentfrow, and S. P. Suman. 2018b. Intramuscular variations in color and sarcoplasmic proteome of beef semimembranosus during postmortem aging. Meat Muscle Biol. 2:92–101. doi:10.22175/mmb2017.11.0055.

Nair, M. N., S. P. Suman, M. K. Chatli, S. Li, P. Joseph, C. M. Beach, and G. Rentfrow. 2016. Proteome basis for intramuscular variation in color stability of beef semimembranosus. Meat Sci. 113:9–16. doi:10.1016/j.meatsci.2015.11.003.

Nair, M. N., S. P. Suman, S. Li, P. Joseph, and C. M. Beach. 2014. Lipid oxidation–induced oxidation in emu and ostrich myoglobins. Meat Sci. 96:984–993. doi:10.1016/j.meatsci.2013.08.029.

Neary, J. M., D. H. Gould, F. B. Garry, A. P. Knight, D. A. Dargatz, and T. N. Holt. 2013. An investigation into beef calf mortality on five high-altitude ranches that selected sires with low pulmonary arterial pressures for over 20 years. J. Vet. Diagn. Invest. 25:210–218. doi:10.1177/1040638713478608.

Neethling, N. E., S. P. Suman, G. O. Sigge, L. C. Hoffman, and M. C. Hunt. 2017. Exogenous and endogenous factors influencing color of fresh meat from ungulates. Meat Muscle Biol. 1:253–275. doi:10.22175/mmb2017.06.0032.

Nesvizhskii, A. I., A. Keller, E. Kolker, and R. Aebersold. 2003. A statistical model for identifying proteins by tandem mass spectrometry. Anal. Chem. 75:4646–4658. doi:10.1021/ac0341261.

Nieminen, A. I., V. M. Eskelinen, H. M. Haikala, T. A. Tervonen, Y. Yan, J. I. Partanen, and J. Klefström. 2013. Myc-induced AMPK-phospho p53 pathway activates Bak to sensitize mitochondrial apoptosis. P. Natl. Acad. Sci. USA. E1839–E1848. doi:10.1073/pnas.1208530110.

Nishimura, T. 2015. Role of extracellular matrix in development of skeletal muscle and postmortem aging of meat. Meat Sci. 109:48–55. doi:10.1016/j.meatsci.2015.05.015.

Obchoei, S., S. Wongkhan, C. Wongkham, M. Li, Q. Yao, and C. Chen. 2009. Cyclophilin A: potential functions and therapeutic target for human cancer. Med. Sci. Monit. 15:RA221–RA232.

Oberg, A. L., D. W. Mahoney, J. E. Eckel-Passow, C. J. Malone, R. D. Wolfinger, E. G. Hill, L. T. Cooper, O. K. Onuma, C. Spiro, T. M. Therneau, and I. Bergen H. Robert. 2008. Statistical Analysis of Relative Labeled Mass Spectrometry Data from Complex Samples Using ANOVA. J. Proteome Res. 7:225–233. doi:10.1021/pr700734f.

Oe, M., I. Nakajima, S. Muroya, M. Shibata, and K. Chikuni. 2009. Relationships between tropomyosin and myosin heavy chain isoforms in bovine skeletal muscle. Anim. Sci. J. 80:193–197. doi:10.1111/j.1740-0929.2008.00613.x.

Oe, M., M. Ohnishi-Kameyama, I. Nakajima, S. Muroya, and K. Chikuni. 2007. Muscle type specific expression of tropomyosin isoforms in bovine skeletal muscles. Meat Sci. 75:558–563. doi:10.1016/j.meatsci.2006.09.003.

O'Keeffe, M., and D. E. Hood. 1982. Biochemical factors influencing metmyoglobin formation on beef from muscles of differing colour stability. Meat Sci. 7:209–228. doi:10.1016/0309-1740(82)90087-0.

Okumura, N., A. Hashida-Okumura, K. Kita, M. Matsubae, T. Matsubara, T. Takao, and K. Nagai. 2005. Proteomic analysis of slow- and fast-twitch skeletal muscles. Proteomics. 5:2896–2906. doi:10.1002/pmic.200401181.

Olsson, M. G., M. Centlow, S. Rutardóttir, I. Stenfors, J. Larsson, B. Hosseini-Maaf, M. L. Olsson, S. R. Hansson, and B. Åkerström. 2010. Increased levels of cell-free hemoglobin, oxidation markers, and the antioxidative heme scavenger α1-microglobulin in preeclampsia. Free Radical Biol. Med. 48:284–291. doi:10.1016/j.freeradbiomed.2009.10.052.

O'Neill, L. A. J., and D. G. Hardie. 2013. Metabolism of inflammation limited by AMPK and pseudo-starvation. Nature. 493:346–355. doi:10.1038/nature11862.

Otey, C. A., R. Dixon, C. Stack, and S. M. Goicoechea. 2009. Cytoplasmic Ig-domain proteins: Cytoskeletal regulators with a role in human disease. Cell Motility. 66:618–634. doi:10.1002/cm.20385.

Ouali, A., C. H. Herrera-Mendez, G. Coulis, S. Becila, A. Boudjellal, L. Aubry, and M. A. Sentandreu. 2006. Revisiting the conversion of muscle into meat and the underlying mechanisms. Meat Sci. 74:44–58. doi:10.1016/j.meatsci.2006.05.010.

Ozawa, S., T. Mitsuhashi, M. Mitsumoto, S. Matsumoto, N. Itoh, K. Itagaki, Y. Kohno, and T. Dohgo. 2000. The characteristics of muscle fiber types of longissimus thoracis muscle and their influences on the quantity and quality of meat from Japanese Black steers. Meat Sci. 54:65–70. doi:10.1016/S0309-1740(99)00072-8.

Pérez-Enciso, M., and M. Tenenhaus. 2003. Prediction of clinical outcome with microarray data: a partial least squares discriminant analysis (PLS-DA) approach. Hum. Genet. 112:581–592. doi:10.1007/s00439-003-0921-9.

Pesta, D., and E. Gnaiger. 2012. High-resolution respirometry: OXPHOS protocols for human cells and permeabilized fibers from small biopsies of human muscle. In: C. M. Palmeira and A. J. Moreno, editors. Mitochondrial Bioenergetics: Methods and Protocols. Humana Press, Totowa, NJ. p. 25–58.

Phongpa-Ngan, P., A. Grider, J. H. Mulligan, S. E. Aggrey, and L. Wicker. 2011. Proteomic analysis and differential expression in protein extracted from chicken with a varying growth rate and water-holding capacity. J. Agric. Food Chem. 59:13181–13187. doi:10.1021/jf202622n.

Picard, B., and M. Gagaoua. 2017. Chapter 11 - Proteomic Investigations of Beef Tenderness. In: M. L. Colgrave, editor. Proteomics in Food Science. Academic Press. p. 177–197.

Picard, B., M. Gagaoua, M. Al-Jammas, L. D. Koning, A. Valais, and M. Bonnet. 2018. Beef tenderness and intramuscular fat proteomic biomarkers: muscle type effect. PeerJ. 6:e4891. doi:10.7717/peerj.4891.

Picard, B., M. Gagaoua, D. Micol, I. Cassar-Malek, J.-F. Hocquette, and C. E. M. Terlouw. 2014. Inverse relationships between biomarkers and beef tenderness according to contractile and metabolic properties of the muscle. J. Agric. Food Chem. 62:9808–9818. doi:10.1021/jf501528s.

Piras, C., V. M. Morittu, A. A. Spina, A. Soggiu, V. Greco, C. Ramé, E. Briant, N. Mellouk, B. Tilocca, L. Bonizzi, P. Roncada, and J. Dupont. 2019. Unraveling the adipose tissue proteome of transition cows through severe negative energy balance. Animals. 9:1013. doi:10.3390/ani9121013.

Poleti, Mirele D., C. T. Moncau, B. Silva-Vignato, A. F. Rosa, A. R. Lobo, T. R. Cataldi, J. A. Negrão, S. L. Silva, J. P. Eler, and J. C. de Carvalho Balieiro. 2018. Label-free quantitative proteomic analysis reveals muscle contraction and metabolism proteins linked to ultimate pH in bovine skeletal muscle. Meat Sci. 145:209–219. doi:10.1016/j.meatsci.2018.06.041.

Poleti, Mirele D., L. C. A. Regitano, G. H. M. F. Souza, A. S. M. Cesar, R. C. Simas, B. Silva-Vignato, G. B. Oliveira, S. C. S. Andrade, L. C. Cameron, and L. L. Coutinho. 2018. Longissimus dorsi muscle label-free quantitative proteomic reveals biological mechanisms associated with intramuscular fat deposition. J. Proteomics. 179:30–41. doi:10.1016/j.jprot.2018.02.028.

Przybylski, W., P. Sałek, L. Kozłowska, D. Jaworska, and J. Stańczuk. 2022. Metabolomic analysis indicates that higher drip loss may be related to the production of methylglyoxal as a by-product of glycolysis. Poultry Sci. 101:101608. doi:10.1016/j.psj.2021.101608.

Quinlan, C. L., A. L. Orr, I. V. Perevoshchikova, J. R. Treberg, B. A. Ackrell, and M. D. Brand. 2012. Mitochondrial complex II can generate reactive oxygen species at high rates in both

the forward and reverse reactions. J. Biol. Chem. 287:27255–27264. doi:10.1074/jbc.M112.374629.

Rabilloud, T. 2002. Two-dimensional gel electrophoresis in proteomics: Old, old fashioned, but it still climbs up the mountains. Proteomics. 2:3–10.

R Core Team. 2021. R: A language and environment for statistical computing. R Foundation for Statistical Computing, Vienna, Austria. URL https://www.R-project.org/

Ramanathan, R., F. Kiyimba, J. Gonzalez, G. Mafi, and U. DeSilva. 2020a. Impact of up- and downregulation of metabolites and mitochondrial content on pH and color of the Longissimus muscle from normal-pH and dark-cutting beef. J. Agric. Food Chem. 68:7194–7203. doi:10.1021/acs.jafc.0c01884.

Ramanathan, R., and R. A. Mancini. 2018. Role of mitochondria in beef color: A review. Meat Muscle Biol. 2:309–320. doi:10.22175/mmb2018.05.0013.

Ramanathan, R., M. N. Nair, M. C. Hunt, and S. P. Suman. 2019. Mitochondrial functionality and beef colour: A review of recent research. S. Afr. J. Anim. Sci. 49:12.

Ramanathan, R., S. P. Suman, and C. Faustman. 2020b. Biomolecular interactions governing fresh meat color in post-mortem skeletal muscle: A review. J. Agric. Food Chem. 68:12779–12787. doi:10.1021/acs.jafc.9b08098.

Rashid, M. M., A. Runci, M. A. Russo, and M. Tafani. 2015. Muscle LIM protein (MLP)/CSRP3 at the crossroad between mechanotransduction and autophagy. Cell Death & Disease. 6:e1940. doi:10.1038/cddis.2015.308.

Rasola, A., and P. Bernardi. 2011. Mitochondrial permeability transition in Ca^{2+}-dependent apoptosis and necrosis. Cell Calcium. 50:222–233. doi:10.1016/j.ceca.2011.04.007.

Rauniyar, N., and J. R. Yates. 2014. Isobaric labeling-based relative quantification in shotgun proteomics. J. Proteome Res. 13:5293–5309. doi:10.1021/pr500880b.

Resurreccion, A. V. A. 2004. Sensory aspects of consumer choices for meat and meat products. Meat Science. 66:11–20. doi:10.1016/S0309-1740(03)00021-4.

Ritchie, M. E., B. Phipson, D. Wu, Y. Hu, C. W. Law, W. Shi, and G. K. Smyth. 2015. limma powers differential expression analyses for RNA-sequencing and microarray studies. Nucleic Acids Res. 43:e47–e47. doi:10.1093/nar/gkv007.

Rodrigues, J. V., and C. M. Gomes. 2012. Mechanism of superoxide and hydrogen peroxide generation by human electron-transfer flavoprotein and pathological variants. Free Radical Biol. Med. 53:12–19. doi:10.1016/j.freeradbiomed.2012.04.016.

Rodrigues, R. T. de S., M. L. Chizzotti, C. E. Vital, M. C. Baracat-Pereira, E. Barros, K. C. Busato, R. A. Gomes, M. M. Ladeira, and T. da S. Martins. 2017. Differences in beef quality

between Angus (Bos taurus taurus) and Nellore (Bos taurus indicus) cattle through a proteomic and phosphoproteomic approach. PLOS ONE. 12:e0170294.

Rosa, A. F., C. T. Moncau, M. D. Poleti, L. D. Fonseca, J. C. C. Balieiro, S. L. E. Silva, and J. P. Eler. 2018. Proteome changes of beef in Nellore cattle with different genotypes for tenderness. Meat Sci. 138:1–9. doi:10.1016/j.meatsci.2017.12.006.

Ross, A., C. Brunius, O. Chevallier, G. Dervilly, C. Elliott, Y. Guitton, J. E. Prenni, O. Savolainen, L. Hemeryck, N. H. Vidkjær, N. Scollan, S. L. Stead, R. Zhang, and L. Vanhaecke. 2021. Making complex measurements of meat composition fast: Application of rapid evaporative ionisation mass spectrometry to measuring meat quality and fraud. Meat Sci. 181:108333. doi:10.1016/j.meatsci.2020.108333.

Rydström, J. 2006. Mitochondrial NADPH, transhydrogenase and disease. BBA-Bioenergetics. 1757:721–726. doi:10.1016/j.bbabio.2006.03.010.

Sadrzadeh, S. M., E. Graf, S. S. Panter, P. E. Hallaway, and J. W. Eaton. 1984. Hemoglobin. A biologic fenton reagent. J. Biol. Chem. 259:14354–14356.

Samali, A., J. Cai, B. Zhivotovsky, D. P. Jones, and S. Orrenius. 1999. Presence of a pre-apoptotic complex of pro-caspase-3, Hsp60 and Hsp10 in the mitochondrial fraction of Jurkat cells. The EMBO J. 18:2040–2048. doi:10.1093/emboj/18.8.2040.

Sawano, S., K. Oza, T. Murakami, M. Nakamura, R. Tatsumi, and W. Mizunoya. 2020. Effect of gender, rearing, and cooking on the metabolomic profile of porcine muscles. Metabolites. 10:10. doi:10.3390/metabo10010010.

Sayd, T., M. Morzel, C. Chambon, M. Franck, P. Figwer, C. Larzul, P. Le Roy, G. Monin, P. Chérel, and E. Laville. 2006. Proteome analysis of the sarcoplasmic fraction of pig semimembranosus muscle: Implications on meat color development. J. Agric. Food Chem. 54:2732–2737. doi:10.1021/jf052569v.

Schönfeld, P., and L. Wojtczak. 2012. Brown adipose tissue mitochondria oxidizing fatty acids generate high levels of reactive oxygen species irrespective of the uncoupling protein-1 activity state. BBA-Bioenergetics. 1817:410–418. doi:10.1016/j.bbabio.2011.12.009.

Scopes, R. K. 1974. Measurement of protein by spectrophotometry at 205 nm. Anal. Biochem. 59:277–282. doi:10.1016/0003-2697(74)90034-7.

Searle, B. C., M. Turner, and A. I. Nesvizhskii. 2008. Improving sensitivity by probabilistically combining results from multiple MS/MS search methodologies. J. Proteome Res. 7:245–253. doi:10.1021/pr070540w.

Seifert, E. L., C. Estey, J. Y. Xuan, and M.-E. Harper. 2010. Electron transport chain-dependent and -independent mechanisms of mitochondrial H_2O_2 emission during long-chain fatty acid oxidation. J. Biol. Chem. 285:5748–5758. doi:10.1074/jbc.M109.026203.

Seko, Y., T. Fujimura, H. Taka, R. Mineki, K. Murayama, and R. Nagai. 2004. Hypoxia followed by reoxygenation induces secretion of cyclophilin A from cultured rat cardiac myocytes. Biochem. Bioph. Res. Co. 317:162–168. doi:10.1016/j.bbrc.2004.03.021.

Seyfert, M., R. A. Mancini, M. C. Hunt, J. Tang, C. Faustman, and M. Garcia. 2006. Color stability, reducing activity, and cytochrome c oxidase activity of five bovine muscles. J. Agric. Food Chem. 54:8919–8925. doi:10.1021/jf061657s.

Shackelford, S. D., T. L. Wheeler, M. K. Meade, J. O. Reagan, B. L. Byrnes, and M. Koohmaraie. 2001. Consumer impressions of tender select beef. J. Anim. Sci. 79:2605–2614. doi:10.2527/2001.79102605x.

Shadforth, I. P., T. P. Dunkley, K. S. Lilley, and C. Bessant. 2005. i-Tracker: For quantitative proteomics using iTRAQ™. BMC Genomics. 6:145. doi:10.1186/1471-2164-6-145.

Shen, Q.W., W. J. Means, S. A. Thompson, K. R. Underwood, M. J. Zhu, R. J. McCormick, S. P. Ford, and M. Du. 2006a. Pre-slaughter transport, AMP-activated protein kinase, glycolysis, and quality of pork loin. Meat Sci. 74:388–395. doi:10.1016/j.meatsci.2006.04.007.

Shen, Q.W., W. J. Means, K. R. Underwood, S. A. Thompson, M. J. Zhu, R. J. McCormick, S. P. Ford, M. Ellis, and M. Du. 2006b. Early Post-mortem AMP-Activated Protein Kinase (AMPK) Activation leads to phosphofructokinase-2 and -1 (PFK-2 and PFK-1) phosphorylation and the development of pale, soft, and exudative (PSE) conditions in porcine longissimus muscle. J. Agric. Food Chem. 54:5583–5589. doi:10.1021/jf060411k.

Shiio, Y., and R. Aebersold. 2006. Quantitative proteome analysis using isotope-coded affinity tags and mass spectrometry. Nat. Protoc. 1:139–145. doi:10.1038/nprot.2006.22.

Shirley, K. L., D. W. Beckman, and D. J. Garrick. 2008. Inheritance of pulmonary arterial pressure in Angus cattle and its correlation with growth. J. Anim. Sci. 86:815–819. doi:10.2527/jas.2007-0270.

Siendones, E., S. SantaCruz-Calvo, A. Martín-Montalvo, M. V. Cascajo, J. Ariza, G. López-Lluch, J. M. Villalba, C. Acquaviva-Bourdain, E. Roze, M. Bernier, R. de Cabo, and P. Navas. 2014. Membrane-bound CYB5R3 is a common effector of nutritional and oxidative stress response through FOXO3a and Nrf2. Antioxid. Redox Sign. 21:1708–1725. doi:10.1089/ars.2013.5479.

Sierra, V., and M. Olivan. 2013. Role of mitochondria on muscle cell death and meat tenderization. Recent Pat. Endocr. Metab. Immune Drug Discov. 7:120–129. doi:10.2174/1872214811307020005. 2148&volume=7&issue=2&spage=120

Smith, G. C., K. E. Belk, J. N. Sofos, J. D. Tatum, and S. N. Williams. 2000. Economic implications of improved color stability in beef. Antioxidants in muscle foods: nutritional strategies to improve quality. 397–426.

Smith, J. B. 2001. Peptide sequencing by edman degradation. In: eLS. American Cancer Society.

Smyth, M. S., and J. H. J. Martin. 2000. x Ray crystallography. Mol Pathol. 53:8–14.

Soupene, E., and F. A. Kuypers. 2008. Mammalian long-chain acyl-CoA synthetases. Exp. Biol. Med. (Maywood). 233:507–521. doi:10.3181/0710-MR-287.

Stenmark, K. R., M. E. Yeager, K. C. El Kasmi, E. Nozik-Grayck, E. V. Gerasimovskaya, M. Li, S. R. Riddle, and M. G. Frid. 2013. The adventitia: essential regulator of vascular wall structure and function. Annu. Rev. Physiol. 75:23–47. doi:10.1146/annurev-physiol-030212-183802.

Su, Z., A. Yao, I. Zubair, K. Sugishita, M. Ritter, F. Li, J. J. Hunter, K. R. Chien, and W. H. Barry. 2001. Effects of deletion of muscle LIM protein on myocyte function. Am. J. Physiol-Heart C. 280:H2665–H2673. doi:10.1152/ajpheart.2001.280.6.H2665.

Subbaraj, A. K., Y. H. B. Kim, K. Fraser, and M. M. Farouk. 2016. A hydrophilic interaction liquid chromatography–mass spectrometry (HILIC–MS) based metabolomics study on colour stability of ovine meat. Meat Sci. 117:163–172. doi:10.1016/j.meatsci.2016.02.028.

Suman, S. P., C. Faustman, S. L. Stamer, and D. C. Liebler. 2006. Redox instability induced by 4-hydroxy-2-nonenal in porcine and bovine myoglobins at pH 5.6 and 4 °C. J. Agric. Food Chem. 54:3402–3408. doi:10.1021/jf052811y.

Suman, S. P., C. Faustman, S. L. Stamer, and D. C. Liebler. 2007. Proteomics of lipid oxidation-induced oxidation of porcine and bovine oxymyoglobins. Proteomics. 7:628–640. doi:10.1002/pmic.200600313.

Suman, S. P., and P. Joseph. 2013. Myoglobin chemistry and meat color. Annu. Rev. Food Sci. T. 4 (2013) 79–99. 4:79–99. doi:10.1146/annurev-food-030212-182623.

Sundararaman, A., U. Amirtham, and A. Rangarajan. 2016. Calcium-oxidant signaling network regulates AMPK activation upon matrix-deprivation. J. Biol. Chem. 291:14410–14429. doi:10.1074/jbc.M116.731257.

Suzuki, J., Z.-G. Jin, D. F. Meoli, T. Matoba, and B. C. Berk. 2006. Cyclophilin A is secreted by a vesicular pathway in vascular smooth muscle cells. Circ. Res. 98:811–817. doi:10.1161/01.RES.0000216405.85080.a6.

Suzuki, K., H. Shioura, S. Yokota, K. Katoh, S. Roh, F. Iida, T. Komatsu, N. Syoji, H. Sakuma, and S. Yamada. 2017. Search for an index for the taste of Japanese Black cattle beef by panel testing and chemical composition analysis. Anim. Sci. J. 88:421–432. doi:10.1111/asj.12663.

Szklarczyk, D., A. L. Gable, D. Lyon, A. Junge, S. Wyder, J. Huerta-Cepas, M. Simonovic, N. T. Doncheva, J. H. Morris, P. Bork, L. J. Jensen, and C. von Mering. 2019. STRING v11: protein–protein association networks with increased coverage, supporting functional discovery in genome-wide experimental datasets. Nucleic Acids Res. 47:D607–D613. doi:10.1093/nar/gky1131.

Takakura, Y., T. Sakamoto, S. Hirai, T. Masuzawa, H. Wakabayashi, and T. Nishimura. 2014. Characterization of the key aroma compounds in beef extract using aroma extract dilution analysis. Meat Sci. 97:27–31. doi:10.1016/j.meatsci.2014.01.002.

Tamura, Y., S. Iwatoh, K. Miyaura, Y. Asikin, and M. Kusano. 2022. Metabolomic profiling reveals the relationship between taste-related metabolites and roasted aroma in aged pork. LWT. 155:112928. doi:10.1016/j.lwt.2021.112928.

Tang, J., C. Faustman, T. A. Hoagland, R. A. Mancini, M. Seyfert, and M. C. Hunt. 2005. Postmortem oxygen consumption by mitochondria and its effects on myoglobin form and stability. J. Agric. Food Chem. 53:1223–1230. doi:10.1021/jf048646o.

Tang, Z., M. Iqbal, D. Cawthon, and W. G. Bottje. 2002. Heart and breast muscle mitochondrial dysfunction in pulmonary hypertension syndrome in broilers (Gallus domesticus). Comp. Biochem. Phys. A. 132:527–540. doi:10.1016/S1095-6433(02)00005-3.

Tasdemir, E., M. C. Maiuri, L. Galluzzi, I. Vitale, M. Djavaheri-Mergny, M. D'Amelio, A. Criollo, E. Morselli, C. Zhu, F. Harper, U. Nannmark, C. Samara, P. Pinton, J. M. Vicencio, R. Carnuccio, U. M. Moll, F. Madeo, P. Paterlini-Brechot, R. Rizzuto, G. Szabadkai, G. Pierron, K. Blomgren, N. Tavernarakis, P. Codogno, F. Cecconi, and G. Kroemer. 2008. Regulation of autophagy by cytoplasmic p53. Nat. Cell Biol. 10:676–687. doi:10.1038/ncb1730.

Théron, L., T. Sayd, C. Chambon, A. Vénien, D. Viala, T. Astruc, A. Vautier, and V. Santé-Lhoutellier. 2019. Deciphering PSE-like muscle defect in cooked hams: A signature from the tissue to the molecular scale. Food Chem. 270:359–366. doi:10.1016/j.foodchem.2018.07.081.

Tijare, V. V., F. L. Yang, V. A. Kuttappan, C. Z. Alvarado, C. N. Coon, and C. M. Owens. 2016. Meat quality of broiler breast fillets with white striping and woody breast muscle myopathies. Poultry Sci. 95:2167–2173. doi:10.3382/ps/pew129.

Turrens, J. F., and A. Boveris. 1980. Generation of superoxide anion by the NADH dehydrogenase of bovine heart mitochondria. Biochem. J. 191:421–427. doi:10.1042/bj1910421.

Vakifahmetoglu-Norberg, H., A. T. Ouchida, and E. Norberg. 2017. The role of mitochondria in metabolism and cell death. Biochem. Bioph. Res. Co. 482:426–431. doi:10.1016/j.bbrc.2016.11.088.

Vaseva, A. V., N. D. Marchenko, K. Ji, S. E. Tsirka, S. Holzmann, and U. M. Moll. 2012. p53 opens the mitochondrial permeability transition pore to trigger necrosis. Cell. 149:1536–1548. doi:10.1016/j.cell.2012.05.014.

Vásquez-Vivar, J., B. Kalyanaraman, and M. C. Kennedy. 2000. Mitochondrial aconitase is a source of hydroxyl radical. An electron spin resonance investigation. J. Biol. Chem. 275:14064–14069. doi:10.1074/jbc.275.19.14064.

Veit, H. P., and R. L. Farrell. 1978. The anatomy and physiology of the bovine respiratory system relating to pulmonary disease. Cornell Vet. 68:555–581.

Vervliet, T. 2018. Ryanodine receptors in autophagy: Implications for neurodegenerative Diseases? Front. Cell. Neurosci. 12. doi:10.3389/fncel.2018.00089.

Wang, L.-L., L. Han, X.-L. Ma, Q.-L. Yu, and S.-N. Zhao. 2017a. Effect of mitochondrial apoptotic activation through the mitochondrial membrane permeability transition pore on yak meat tenderness during postmortem aging. Food Chem. 234:323–331. doi:10.1016/j.foodchem.2017.04.185.

Wang, L.-L., Q.-L. Yu, L. Han, X.-L. Ma, R.-D. Song, S.-N. Zhao, and W.-H. Zhang. 2018. Study on the effect of reactive oxygen species-mediated oxidative stress on the activation of mitochondrial apoptosis and the tenderness of yak meat. Food Chem. 244:394–402. doi:10.1016/j.foodchem.2017.10.034.

Wang, X, H. Gu, W. Huang, J. Peng, Y. Li, L. Yang, D. Qin, K. Essandoh, Y. Wang, T. Peng, and G.-C. Fan. 2016a. Hsp20-mediated activation of exosome biogenesis in cardiomyocytes improves cardiac function and angiogenesis in diabetic mice. Diabetes. db151563. doi:10.2337/db15-1563.

Wang, X, A. K. Pandey, M. K. Mulligan, E. G. Williams, K. Mozhui, Z. Li, V. Jovaisaite, L. D. Quarles, Z. Xiao, J. Huang, J. A. Capra, Z. Chen, W. L. Taylor, L. Bastarache, X. Niu, K. S. Pollard, D. C. Ciobanu, A. O. Reznik, A. V. Tishkov, I. B. Zhulin, J. Peng, S. F. Nelson, J. C. Denny, J. Auwerx, L. Lu, and R. W. Williams. 2016b. Joint mouse–human phenome-wide association to test gene function and disease risk. Nat. Commun. 7:10464. doi:10.1038/ncomms10464.

Wang, X., B. Zingarelli, M. O′Connor, P. Zhang, A. Adeyemo, E. G. Kranias, Y. Wang, and G.-C. Fan. 2009. Overexpression of Hsp20 prevents endotoxin-induced myocardial dysfunction and apoptosis via inhibition of NF-κB activation. J. Mol. Cell. Cardiol. 47:382–390. doi:10.1016/j.yjmcc.2009.05.016.

Wang, Z., P. Shang, Q. Li, L. Wang, Y. Chamba, B. Zhang, H. Zhang, and C. Wu. 2017b. iTRAQ-based proteomic analysis reveals key proteins affecting muscle growth and lipid deposition in pigs. Scientific Reports. 7:46717. doi:10.1038/srep46717.

Ward, C. E., A. Trent, and J. L. Hildebrand. 1995. Consumer perceptions of lamb compared with other meats. Sheep and goat research journal (USA).

Watanabe, A., G. Kamada, M. Imanari, N. Shiba, M. Yonai, and T. Muramoto. 2015. Effect of aging on volatile compounds in cooked beef. Meat Sci. 107:12–19. doi:10.1016/j.meatsci.2015.04.004.

Wei, Y., Y. Jinchuan, L. Yi, W. Jun, W. Zhongqun, and W. Cuiping. 2013. Antiapoptotic and proapoptotic signaling of cyclophilin A in endothelial cells. Inflammation. 36:567–572. doi:10.1007/s10753-012-9578-7.

Weidenhaupt, M., P. Rossi, C. Beck, H.-M. Fischer, and H. Hennecke. 1996. Bradyrhizobium japonicum possesses two discrete sets of electron transfer flavoprotein genes:fixA, fixB andetfS, etfL. Arch. Microbiol. 165:169–178. doi:10.1007/BF01692858.

van de Wiel, D. F. M., and W. L. Zhang. 2007. Identification of pork quality parameters by proteomics. Meat Sci. 77:46–54. doi:10.1016/j.meatsci.2007.04.017.

Wilkins, M. R., C. Pasquali, R. D. Appel, K. Ou, O. Golaz, J.-C. Sanchez, J. X. Yan, A. A. Gooley, G. Hughes, I. Humphery-Smith, K. L. Williams, and D. F. Hochstrasser. 1996. From proteins to proteomes: Large scale protein identification by two-dimensional electrophoresis and amino acid analysis. Nat. Biotech. 14:61–65. doi:10.1038/nbt0196-61.

Williams, J. L., J. K. Bertrand, I. Misztal, and M. Łukaszewicz. 2012. Genotype by environment interaction for growth due to altitude in United States Angus cattle. J. Anim. Sci. 90:2152–2158. doi:10.2527/jas.2011-4365.

Wither, M., M. Dzieciatkowska, T. Nemkov, P. Strop, A. D'Alessandro, and K. C. Hansen. 2016. Hemoglobin oxidation at functional amino acid residues during routine storage of red blood cells. Transfusion. 56:421–426. doi:10.1111/trf.13363.

Wolf, S., C. Haase-Kohn, and J. Pietzsch. 2011. S100A2 in cancerogenesis: a friend or a foe? Amino Acids. 41:849–861. doi:10.1007/s00726-010-0623-2.

Wu, W., X.-G. Gao, Y. Dai, Y. Fu, X.-M. Li, and R.-T. Dai. 2015. Post-mortem changes in sarcoplasmic proteome and its relationship to meat color traits in M. semitendinosus of Chinese Luxi yellow cattle. Food Res. Int. 72:98–105. doi:10.1016/j.foodres.2015.03.030.

Wu, W., Q.-Q. Yu, Y. Fu, X.-J. Tian, F. Jia, X.-M. Li, and R.-T. Dai. 2016. Towards muscle-specific meat color stability of Chinese Luxi yellow cattle: A proteomic insight into post-mortem storage. J. Proteomics. 147:108–118. doi:10.1016/j.jprot.2015.10.027.

Xanthoudakis, S., S. Roy, D. Rasper, T. Hennessey, Y. Aubin, R. Cassady, P. Tawa, R. Ruel, A. Rosen, and D. W. Nicholson. 1999. Hsp60 accelerates the maturation of pro-caspase-3 by upstream activator proteases during apoptosis. EMBO J. 18:2049–2056. doi:10.1093/emboj/18.8.2049.

Xiong, W., Zhenxuan Deng, Y. Tang, Zhenwei Deng, and M. Li. 2018. Downregulation of KMT2D suppresses proliferation and induces apoptosis of gastric cancer. Biochem. Bioph. Res. Co 504:129–136. doi:10.1016/j.bbrc.2018.08.143.

Yan, L.-J., R. L. Levine, and R. S. Sohal. 1997. Oxidative damage during aging targets mitochondrial aconitase. PNAS. 94:11168–11172. doi:10.1073/pnas.94.21.11168.

Yan, L.-J., and R. S. Sohal. 1998. Mitochondrial adenine nucleotide translocase is modified oxidatively during aging. P. Natl. Acad. Sci. USA 95:12896–12901. doi:10.1073/pnas.95.22.12896.

Yang, S. C., G. E. Yu, J. Ha, S. Kwon, J. H. Hwang, D. H. Park, D. G. Kang, T. W. Kim, H. C. Park, S. M. An, and C. W. Kim. 2018. Association between an electron transfer flavoprotein alpha subunit polymorphism (rs321948383) and the meat quality of Berkshire pigs. J Appl. Anim. Res. 46:1169–1173. doi:10.1080/09712119.2018.1481856.

Yates, J. R., C. I. Ruse, and A. Nakorchevsky. 2009. Proteomics by mass spectrometry: Approaches, advances, and applications. Annu. Rev. Biomed. Eng. 11:49–79. doi:10.1146/annurev-bioeng-061008-124934.

Yin, F., H. Sancheti, and E. Cadenas. 2012. Mitochondrial thiols in the regulation of cell death pathways. Antioxid. Redox Sign. 17:1714–1727. doi:10.1089/ars.2012.4639.

Yin, M. C., C. Faustman, J. W. Riesen, and S. N. Williams. 1993. α-tocopherol and ascorbate delay oxymyoglobin and phospholipid oxidation in vitro. J. Food Sci. 58:1273–1276. doi:10.1111/j.1365-2621.1993.tb06164.x.

Yin, S., C. Faustman, N. Tatiyaborworntham, R. Ramanathan, N. B. Maheswarappa, R. A. Mancini, P. Joseph, S. P. Suman, and Q. Sun. 2011. Species-specific myoglobin oxidation. J. Agric. Food Chem. 59:12198–12203. doi:10.1021/jf202844t.

Yu, Q., X. Tian, L. Shao, X. Li, and R. Dai. 2019. Targeted metabolomics to reveal muscle-specific energy metabolism between bovine longissimus lumborum and psoas major during early postmortem periods. Meat Sci. 156:166–173. doi:10.1016/j.meatsci.2019.05.029.

Yu, Q., X. Tian, L. Shao, L. Xu, R. Dai, and X. Li. 2018. Label-free proteomic strategy to compare the proteome differences between longissimus lumborum and psoas major muscles during early postmortem periods. Food Chem. 269:427–435. doi:10.1016/j.foodchem.2018.07.040.

Yu, Q., W. Wu, X. Tian, M. Hou, R. Dai, and X. Li. 2017a. Unraveling proteome changes of Holstein beef M. semitendinosus and its relationship to meat discoloration during post-mortem storage analyzed by label-free mass spectrometry. J. Proteomics. 154:85–93. doi:10.1016/j.jprot.2016.12.012.

Yu, Q., W. Wu, X. Tian, F. Jia, L. Xu, R. Dai, and X. Li. 2017b. Comparative proteomics to reveal muscle-specific beef color stability of Holstein cattle during post-mortem storage. Food Chem. 229:769–778. doi:10.1016/j.foodchem.2017.03.004.

Zapata, I., H. N. Zerby, and M. Wick. 2009. Functional proteomic analysis predicts beef tenderness and the tenderness differential. J. Agric. Food Chem. 57:4956–4963. doi:10.1021/jf900041j.

Zhai, C., K. Peckham, K. E. Belk, R. Ramanathan, and M. N. Nair. 2019. Carbon chain length of lipid oxidation products influence lactate dehydrogenase and NADH-dependent metmyoglobin reductase activity. J. Agric. Food Chem. 67:13327–13332. doi:10.1021/acs.jafc.9b05634.

Zhai, C., S. P. Suman, M. N. Nair, S. Li, X. Luo, C. M. Beach, B. N. Harsh, D. D. Boler, A. C. Dilger, and D. W. Shike. 2018. Supranutritional supplementation of vitamin E influences mitochondrial proteome profile of post-mortem longissimus lumborum from feedlot heifers. S. Afr. J. Anim. Sci. 48:1140–1147.

Zhang, J., M. Li, Q. Yu, L. Han, and Z. Ma. 2019a. Effects of lysosomal–mitochondrial apoptotic pathway on tenderness in post-mortem bovine longissimus muscle. J. Agric. Food Chem. 67:4578–4587. doi:10.1021/acs.jafc.9b00894.

Zhang, M., D. Wang, X. Xu, and W. Xu. 2019b. Comparative proteomic analysis of proteins associated with water holding capacity in goose muscles. Food Res. Int. 116:354–361. doi:10.1016/j.foodres.2018.08.048.

Zhang, Q., H.-G. Lee, J.-A. Han, E. B. Kim, S. K. Kang, J. Yin, M. Baik, Y. Shen, S.-H. Kim, K.-S. Seo, and Y.-J. Choi. 2010. Differentially expressed proteins during fat accumulation in bovine skeletal muscle. Meat Sci. 86:814–820. doi:10.1016/j.meatsci.2010.07.002.

Zhang, R., A. B. Ross, M. J. Y. Yoo, and M. M. Farouk. 2021a. Use of Rapid Evaporative Ionisation Mass Spectrometry fingerprinting to determine the metabolic changes to dry-aged lean beef due to different ageing regimes. Meat Sci. 181:108438. doi:10.1016/j.meatsci.2021.108438.

Zhang, R., A. B. Ross, M. J. Y. Yoo, and M. M. Farouk. 2021b. Metabolic fingerprinting of in-bag dry- and wet-aged lamb with rapid evaporative ionisation mass spectroscopy. Food Chem. 347:128999. doi:10.1016/j.foodchem.2020.128999.

Zhang, T., C. Chen, K. Xie, J. Wang, and Z. Pan. 2021c. Current State of Metabolomics Research in Meat Quality Analysis and Authentication. Foods. 10:2388. doi:10.3390/foods10102388.

Zhong, B., Z. Hu, J. Tan, T. Lu, Q. Lei, C. Chen, and L. Zeng. 2015. Hsp20 Protects against oxygen-glucose deprivation/reperfusion-induced golgi fragmentation and apoptosis through Fas/FasL pathway. Oxidative Med. Cell. Longev. doi:10.1155/2015/606934.

Zhu, C., D. L. Hu, Y. Q. Liu, Q. J. Zhang, F. K. Chen, X. Q. Kong, K. J. Cao, J. S. Zhang, and L. M. Qian. 2011. Fabp3 inhibits proliferation and promotes apoptosis of embryonic myocardial cells. Cell Biochem. Biophys. 60:259–266. doi:10.1007/s12013-010-9148-2.

Zieske, L. R. 2006. A perspective on the use of iTRAQ^{TM} reagent technology for protein complex and profiling studies. J. Exp. Bot. 57:1501–1508. doi:10.1093/jxb/erj168.

Zuo, H., L. Han, Q. Yu, Z. Guo, J. Ma, M. Li, H. La, and G. Han. 2018. Proteomic and bioinformatic analysis of proteins on cooking loss in yak longissimus thoracis. Eur. Food Res. Technol. 244:1211–1223. doi:10.1007/s00217-018-3037-0.

Zuo, H., L. Han, Q. Yu, K. Niu, S. Zhao, and H. Shi. 2016. Proteome changes on water-holding capacity of yak longissimus lumborum during postmortem aging. Meat Sci. 121:409–419. doi:10.1016/j.meatsci.2016.07.010.

APPENDIX A – The performance of each machine learning algorithm and data reduction combination in each tissue type using I-Knife REIMS data

Appendix A 1. I-Knife REIMS age classification by using fat tissue, lean tissue, and patty

Appendix A 2. I-Knife REIMS diet classification by using fat tissue, lean tissue, and patty

Appendix A 3. I-Knife REIMS gender classification by using fat tissue, lean tissue, and patty

Appendix A 4. I-Knife REIMS flavor intensity level classification by using fat tissue, lean tissue, and patty

Appendix A 5. I-Knife REIMS flavor intensity acceptance classification by using fat tissue, lean tissue, and patty

Appendix A 6. I-Knife REIMS flavor acceptance classification by using fat tissue, lean tissue, and patty

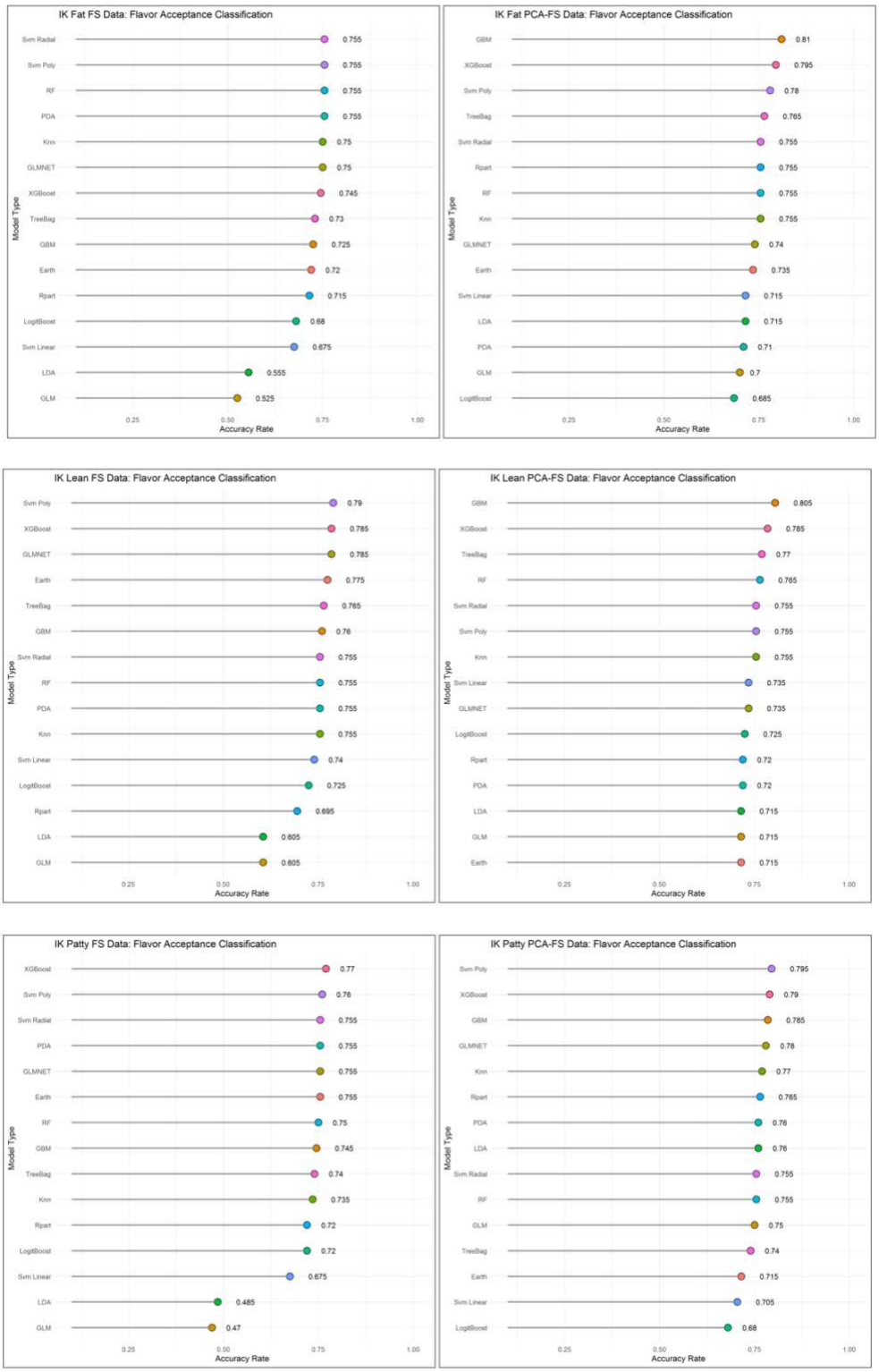

Appendix A 7. I-Knife REIMS off flavors presence classification by using fat tissue, lean tissue, and patty

Appendix A 8. I-Knife REIMS overall acceptance classification by using fat tissue, lean tissue, and patty

APPENDIX B – The performance of each machine learning algorithm and data reduction combination using I-Knife and Meat Probe REIMS data

Appendix B 1. Age classification by patty using I-Knife and Meat Probe REIMS data

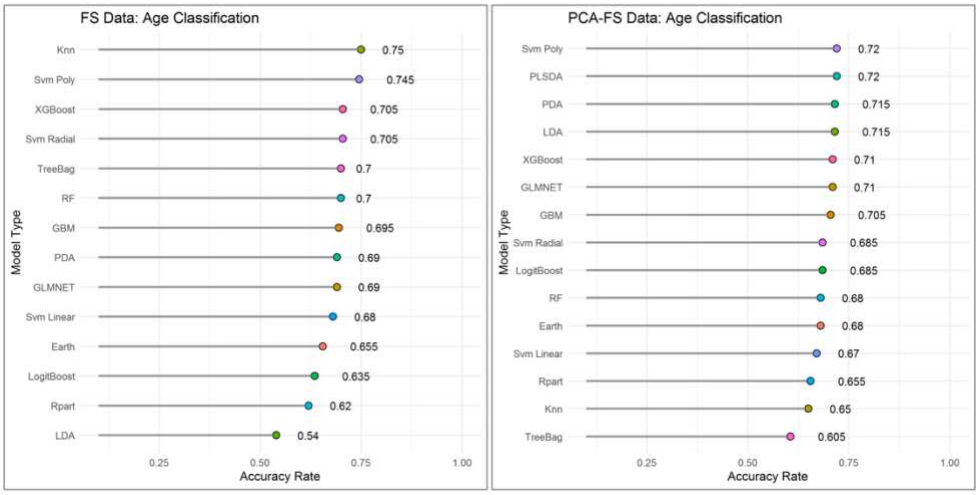

I-Knife

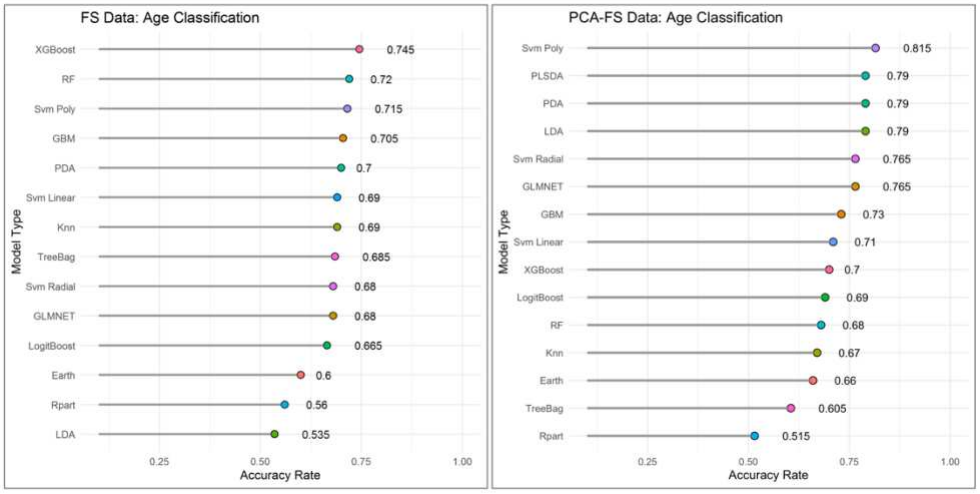

Meat Probe

Appendix B 2. Diet classification by patty using I-Knife and Meat Probe REIMS data

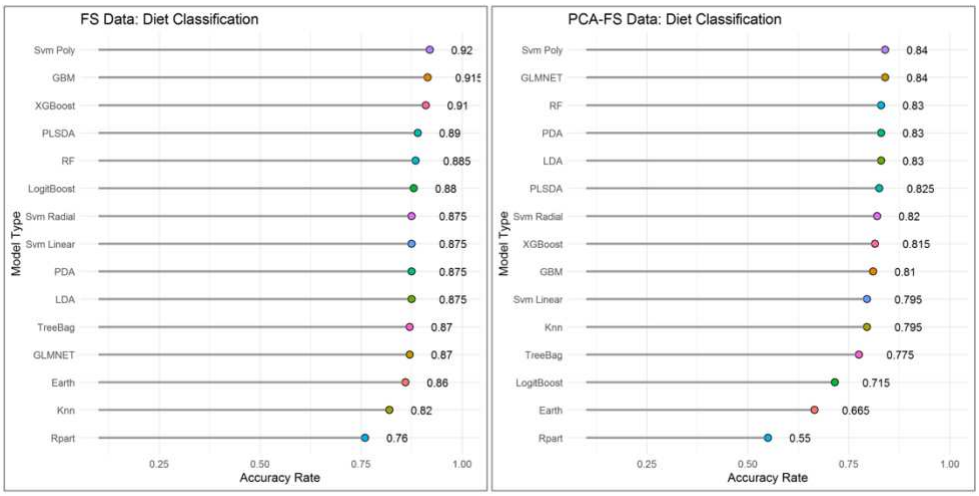

I-Knife

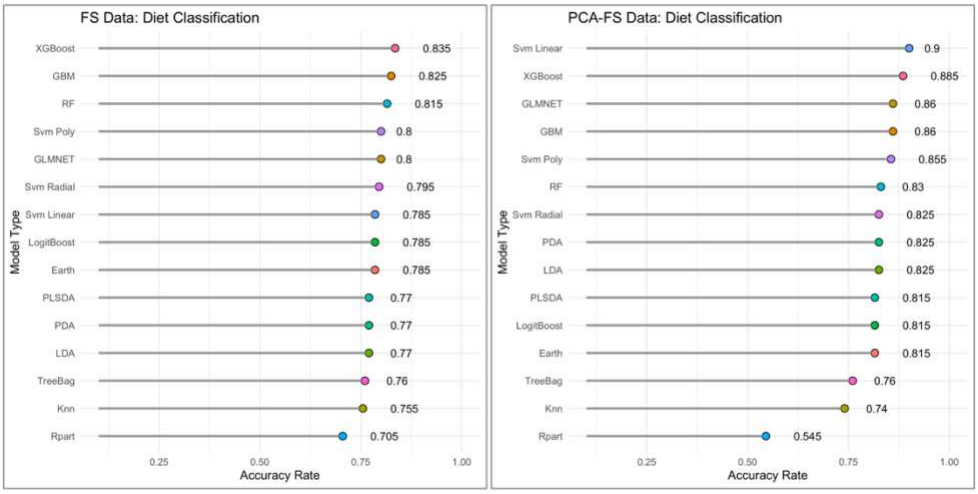

Meat Probe

Appendix B 3. Gender classification by patty using I-Knife and Meat Probe REIMS data

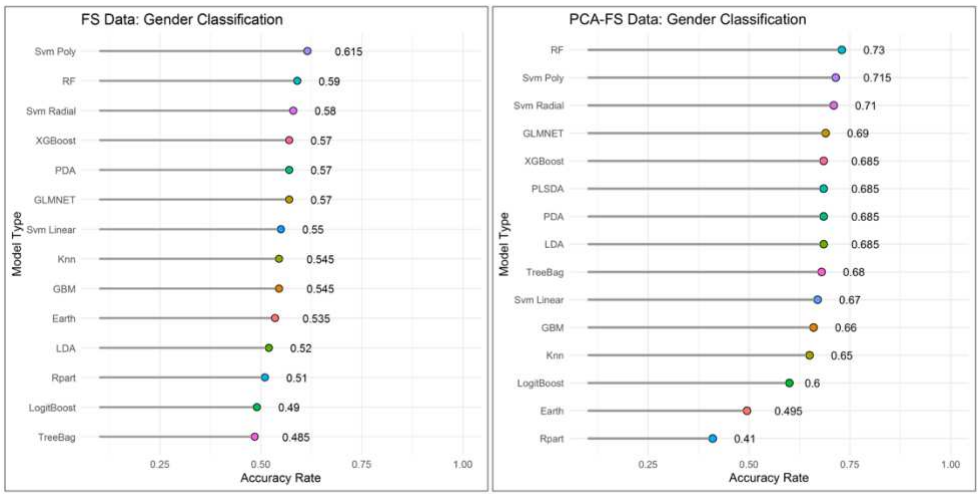

I-Knife

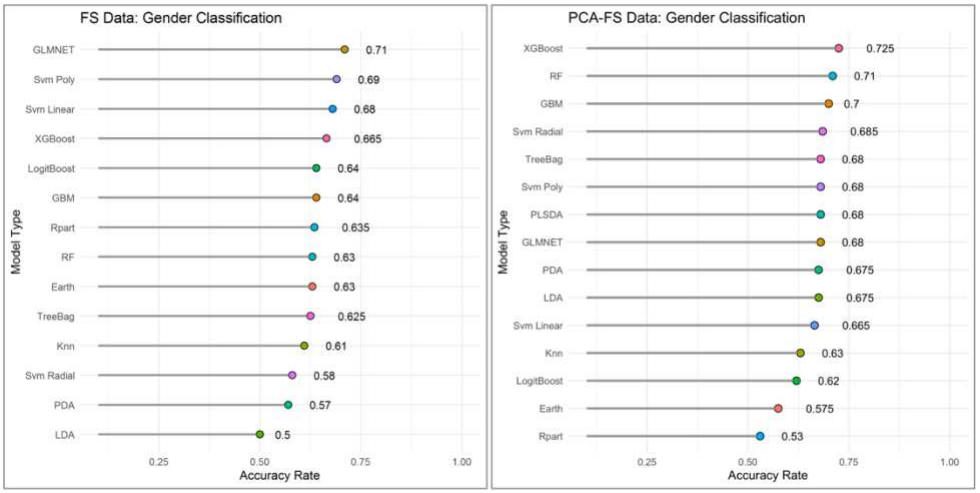

Meat Probe

Appendix B 4. Flavor intensity level classification by patty using I-Knife and Meat Probe REIMS data

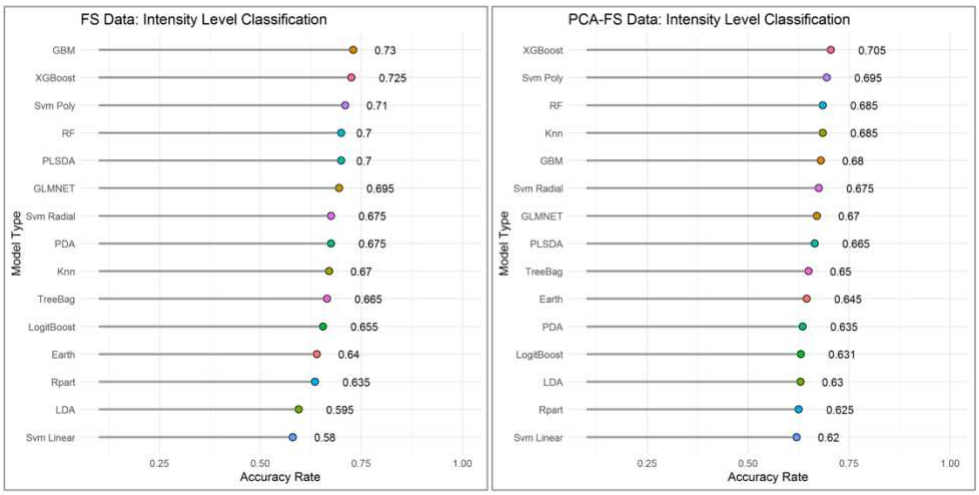

I-Knife

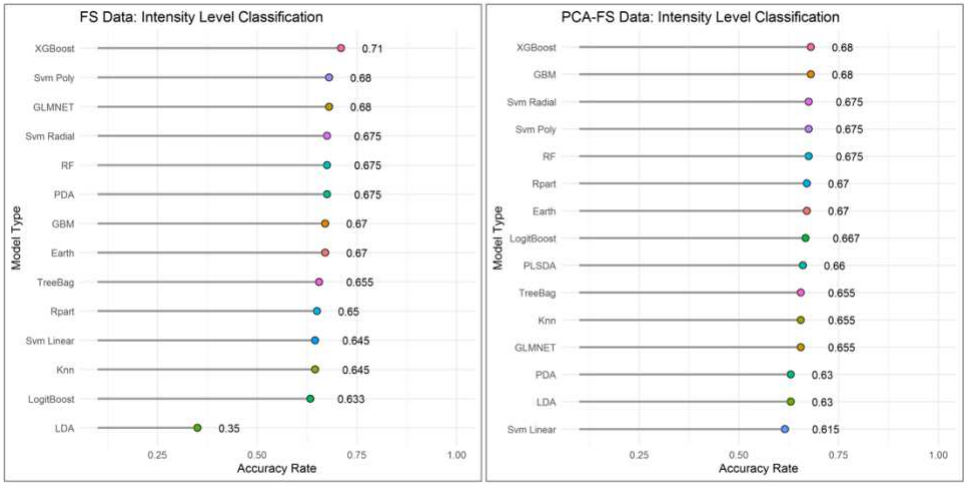

Meat Probe

Appendix B 5. Flavor intensity acceptance classification by patty using I-Knife and Meat Probe REIMS data

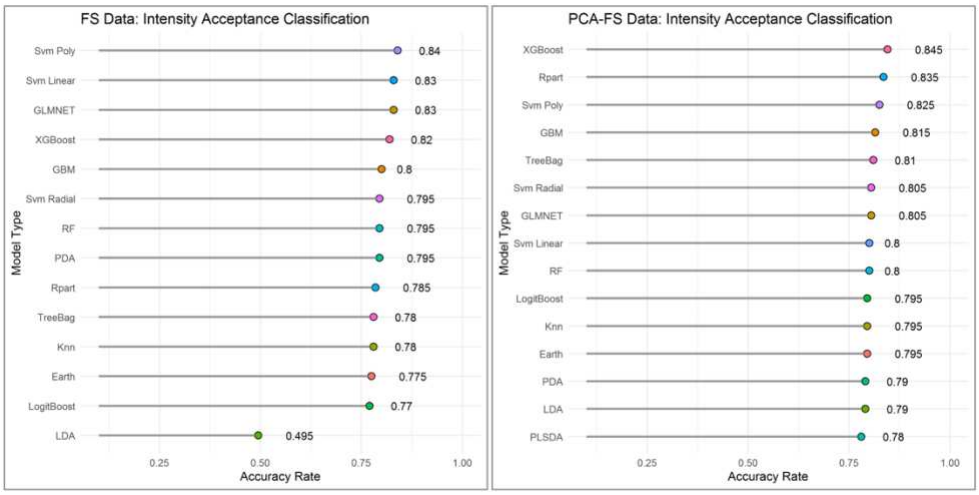

I-Knife

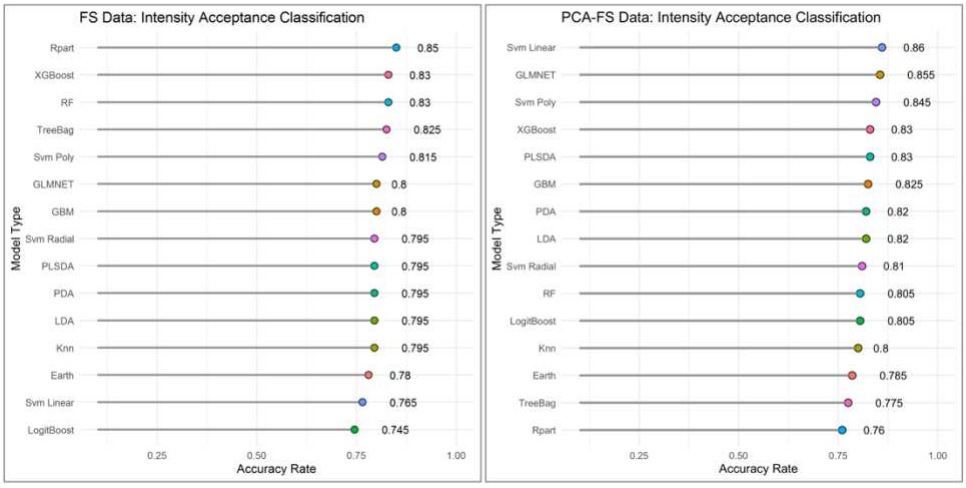

Meat Probe

Appendix B 6. Flavor acceptance classification by patty using I-Knife and Meat Probe REIMS data

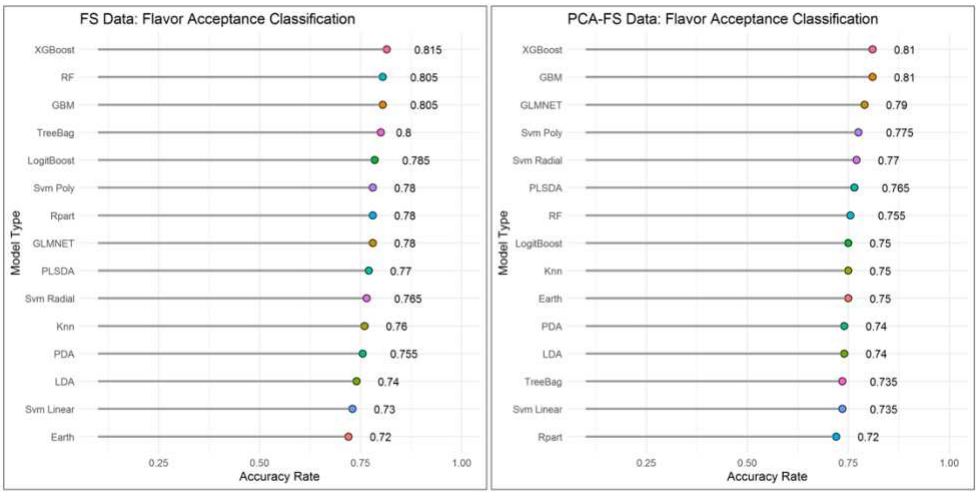

I-Knife

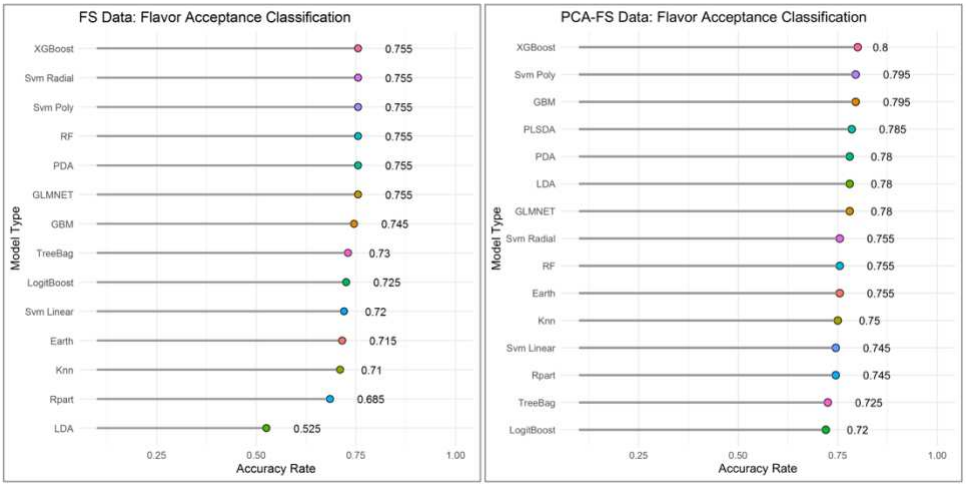

Meat Probe

Appendix B 7. Off flavors presence classification by patty using I-Knife and Meat Probe REIMS data

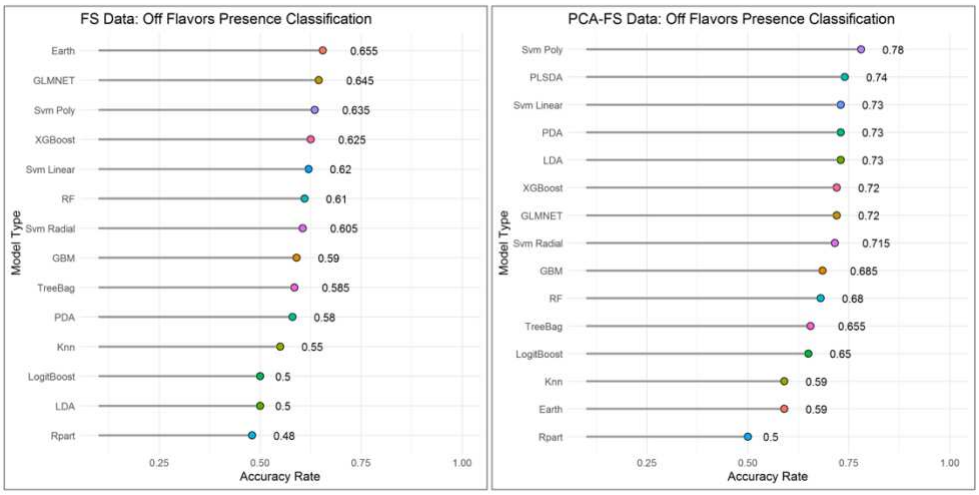

I-Knife

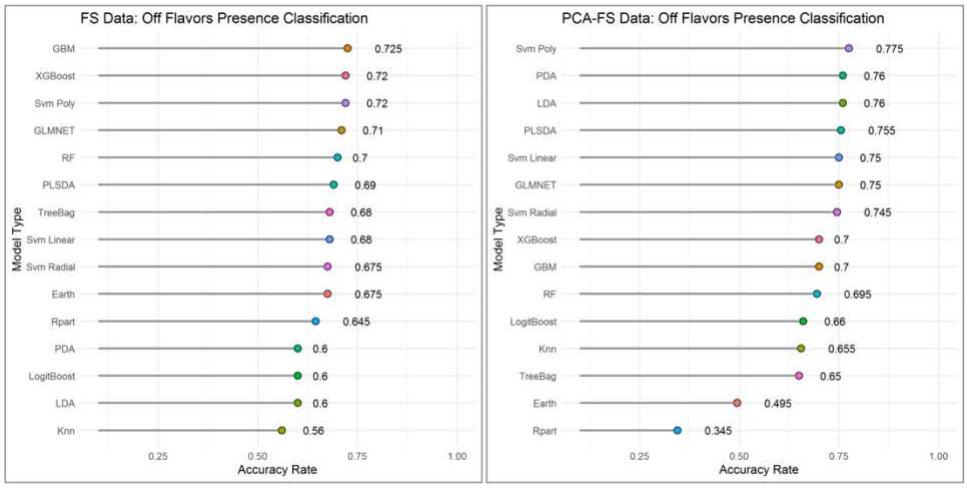

Meat Probe

Appendix B 8. Overall acceptance classification by patty using I-Knife and Meat Probe REIMS data

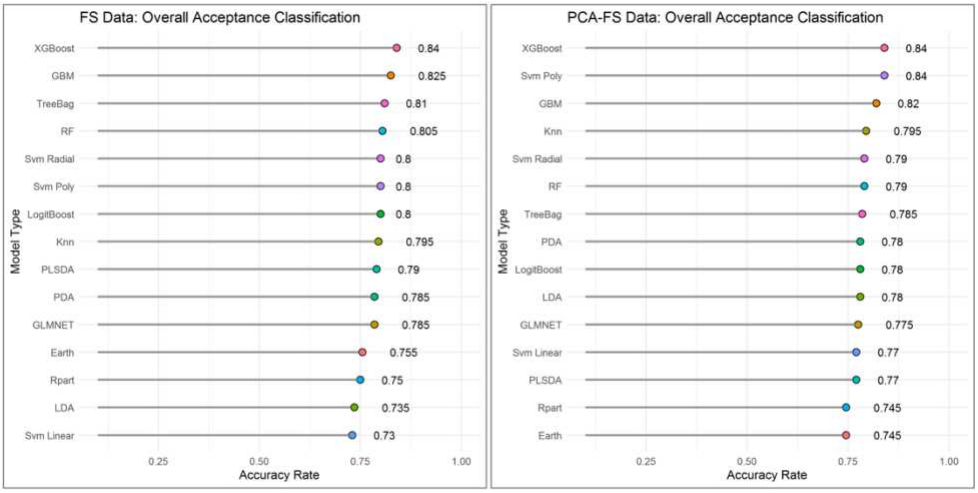

I-Knife

Meat Probe